HIGHWAY RESEARCH RECORD

Number 360 | Frost Action and Drainage
7 Reports

Subject Areas

23 Highway Drainage
61 Exploration-Classification (Soils)
62 Foundations (Soils)
63 Mechanics (Earth Mass)
64 Soil Science

HIGHWAY RESEARCH BOARD
DIVISION OF ENGINEERING NATIONAL RESEARCH COUNCIL
NATIONAL ACADEMY OF SCIENCES—NATIONAL ACADEMY OF ENGINEERING

WASHINGTON, D.C. 1971

ISBN 0-309-01974-5

Price: $2.60

Available from

Highway Research Board
National Academy of Sciences
2101 Constitution Avenue
Washington, D.C. 20418

SPONSORSHIP OF THIS RECORD

GROUP 2—DESIGN AND CONSTRUCTION OF TRANSPORTATION FACILITIES
John L. Beaton, California Division of Highways, chairman

Committee on Subsurface Drainage
Glen L. Martin, Department of Civil Engineering and Engineering Mechanics, Montana State University, Bozeman, chairman
Reginald A. Barron, Mike Bealey, Paul J. Brudy, Harry R. Cedergren, Hsai-Yang Fang, Kenneth F. Ferrari, David S. Gedney, John G. Hendrickson, Jr., W. R. Lovering, Alfred W. Maner, Lyndon H. Moore, William B. Nern, Carl I. Olsen, Travis W. Smith, W. T. Spencer, R. S. Standley

Committee on Frost Action
Edward Penner, National Research Council of Canada, Ottawa, chairman
Wilbur Dunphy, Jr., L. F. Erickson, Hamilton Gray, Wilbur M. Haas, Frank B. Hennion, Alfreds R. Jumikis, Chester W. Kaplar, Miles S. Kersten, Clyde N. Laughter, A. E. Matthews, George W. McAlpin, Paul S. Otis, R. G. Packard, Harold R. Peyton, C. K. Preus, Alex Rutka, R. D. Shumway, Arthur L. Straub, Willis H. Taylor, Jr., Wayne G. Williams

Committee on Environmental Factors Except Frost
William G. Weber, Jr., Pennsylvania Department of Highways, chairman
Richard G. Ahlvin, L. J. Bartelli, T. Allan Haliburton, Delbert L. Lacey, A. E. Matthews, L. T. Norling, Arthur L. Straub, H. C. S. Thom, Thomas H. Thornburn

John W. Guinnee, Highway Research Board staff

The sponsoring committee is identified by a footnote on the first page of each report.

FOREWORD

This RECORD will be of primary interest to engineers and researchers who are involved with the underlying problems associated with roadway failures. A few of the many ramifications of the frost problem are covered in the first 4 papers. Akili describes the stress-strain behavior of a clayey silt and a clay as evidenced by a brittle fracture or plastic deformation. His study leads to a conclusion that the liquid water in the thin-film form controls the reaction. Wang and Roderick enhance the basic knowledge of frost-action reinforcing concepts that frost heave and ice segregation are dependent on the initial (compacting) moisture, soil texture, and dry density. Laba studied the reactions of a sand-ice system subjected to temperature change below freezing. Jumikis contributes influence values for the 3-dimensional disturbance distribution for a heated rectangular structure on permafrost. All of these expand our knowledge of frost action in soils.

The remaining 3 papers are directed toward moisture problems in soils and bases in roadway structures. Haliburton, reporting on a 6-year study, gives recommendations regarding staged construction, geometric profile, shoulders, drainage, subbase, base, surfacing, and subgrade testing in relation to prevention of swell through proper consideration of the moisture problem. Healy and Long describe the construction and laboratory and field testing of a prefabricated drain concept using synthetic cloth and a channelized drainage core. McLean and Krizek describe the application of a finite-element method solution of a steady-state gravity flow to the design of subsurface drains for a depressed highway profile.

CONTENTS

STRESS-STRAIN BEHAVIOR OF FROZEN FINE-GRAINED SOILS

Waddah Akili, The College of Petroleum and Minerals, Dhahran, Saudi Arabia

The objective of this experimental study was to investigate the effect of below-freezing temperature, constant axial deformation rates, and soil type on the stress-strain behavior and strength of frozen fine-grained soils. Two soils were selected for this investigation: a highly plastic clay and a clayey silt. Samples were cored out of statically compacted soil cakes and were quickly frozen. Average molding densities and average molding water contents of test samples fell on the wet side of optimum conditions determined by standard Proctor curves of compaction. Constant axial deformation rate tests were carried out on frozen samples at -1, -5, -9, and -22 C, and at different constant axial deformation rates. Two types of stress-strain behavior were exhibited; the brittle type was associated with the clayey silt, and the plastic type was associated with the clay. Results also show a strong dependency of ultimate strength (peak strength) derived from stress-strain curves on temperature for both soils tested. Ultimate strength is also shown to depend on deformation rate. The inference may be drawn that the amount of liquid water present as a thin film between solid and ice surfaces and the ratio of liquid water to ice in a frozen soil are responsible for ice cementation bonds. These bonds in turn control the stress-strain behavior and the ultimate strength of frozen soils.

•IT HAS BEEN SHOWN that engineering properties, such as creep behavior, strength, and thermal properties, of frozen soils are temperature dependent (1, 2, 3, 4, 5). When temperature dips below freezing, the phase composition of water in fine-grained soils changes accordingly. Part of the available water turns into ice, whereas the rest remains as supercooled water.

The amount of unfrozen water in a frozen soil, its nature, and its equilibrium side by side with ice depend primarily on temperature, mineralogy and particle gradation, water content, and molding conditions of the wet soil. Different soils have different phase compositions at a given subzero temperature, and this composition changes appreciably with the lowering of temperature (6). The ratio of frozen to unfrozen water appears to depend on temperature history, salt concentration in the water (2), and lowest temperature reached during freezing (6).

Many theories have been formulated regarding the mechanisms responsible for the presence of unfrozen water in frozen soils. Williams (7, 8) states that capillarity and suction properties of the soil are the cause of the unfrozen water. Others (9) explain it in terms of the oriented water structure. The least structured water freezes first. Additional cooling freezes lesser amounts of water. A film of water, although very thin, exists at the ice-particle interface at very low temperatures. This film, in particular, and the unfrozen water, in general, seem to have significant effect on stress-strain behavior and strain-time behavior of frozen soils. Vialov (5) postulates that strength and deformation of frozen soils are controlled by cohesive bonds resulting from cementation by ice. Such cementing is the result of the bonds between the ice crystals and the mineral particles that are separated by a film of unfrozen water. This type of bond is very unstable because it changes with any variation in the temperature field. Under the

Sponsored by Committee on Frost Action.

influence of a load, the ice cementation bonds break up, and partial melting of ice occurs. The water film, which increases because of phase change of ice, moves from zones of high stress to zones of smaller stress where it refreezes in time.

To provide information on the stress-strain behavior of frozen fine-grained soils required that constant axial deformation rate tests be carried out on identically molded samples of a plastic clay soil and a clayey silt soil at several subzero temperatures and at different deformation rates. The test results indicate that stress-strain curves of the frozen samples differ in shape depending on soil type, test temperature, and axial deformation rate. The data show convincingly that ultimate strength derived from strain curves depends strongly on temperature and moderately on axial deformation rate.

TABLE 1
CHARACTERISTICS OF 2 SOILS

Characteristic	Sault Ste. Marie Clay	Lafayette Clayey Silt
Liquid limit	60	24
Plastic limit	25	17
Plasticity index	35	7
Specific gravity	2.79	2.69
Gradation, percentage finer		
2 mm	100	100
0.06 mm	90	92
0.002 mm	60	8

EXPERIMENTAL PROGRAM

Soils Studied

The 2 soils selected for this investigation were a red plastic clay obtained from Sault Ste. Marie, Michigan, and a tan glacial clayey silt obtained from a location near Lafayette, Indiana. The Sault Ste. Marie clay was used previously by the author (1). The characteristics of both soils are given in Table 1. The mineral contents of the clay are illite, vermiculite, and chlorite. Illite and quartz are predominant in the clayey silt. The compaction moisture-density relations obtained by using the standard Proctor test are shown in Figure 1.

The major difference between the soils selected is the degree of plasticity and particle gradation. When mixed with sufficient water, the clay soil behaves like putty, whereas the clayey silt has no apparent plasticity when worked by hand.

Molding of Test Samples

The clay and the clayey silt were allowed to air-dry. Then they were processed by crushing and sieving until they passed the No. 40 sieve. Distilled water was added to the air-dried soil in predetermined quantities according to the desired molding conditions. Vigorous periodic hand mixing of the moistened soil ensured even water content distribution prior to molding. The prepared soil was statically compacted in a 12-in. diameter mold specially made for this investigation.

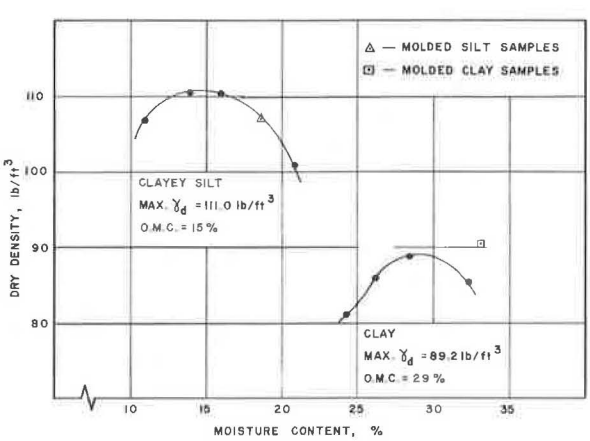

Figure 1. Moisture-density relations determined by using the standard Proctor compaction test.

In the molding process, a predetermined weight of the soil-water mix was placed evenly in the large cylindrical mold (12 in. in diameter and 6 in. high) and was subjected to static load by using a Tinus-Olsen loading machine. The desirable axial load was applied to the wet soil in the mold through a plunger and was maintained constant for a period of about 10 min until desirable density was reached. The

compacted soil cake was taken out of the mold, sliced into 21 pieces, wrapped individually in aluminum foil, and covered with wax pending later use. Cylindrical test samples were prepared as needed from the waxed pieces by punching a cylindrical mold through covered pieces with a hand press (Fig. 2). The cylindrical soil cores were taken out of the split mold (1.3 in. in diameter) and trimmed to the desired height. This coring process was selected over trimming with a soil lathe because of its ease in producing samples with identical cross sections, which are difficult to obtain when the trimming method is used.

Figure 2. Compacted soil piece in wax (left), cylindrical split mold with soil core in it (center), and trimmed sample in a rubber membrane with Lucite disks on top and bottom (right).

The method described in the foregoing permitted preparation of good cylindrical samples with no surface cracks or cavities. It is believed that the structure of the molded samples is the flocculated type associated with an edge-to-face particle arrangement as a result of the static method of compaction applied. Molded samples fell on the wet side of the standard Proctor curve of compaction (Fig. 1) for both soils. Dry densities and water contents of individual samples were within 2 percent of the average density and average water content of all samples used in this investigation.

Sample Preparation and Freezing

The molded soil samples were weighed and measured. Their initial water content was determined. Lucite disks were placed on each end of the cylindrical samples with specially prepared friction reducers to minimize end friction during deformation of samples. The friction reducers consisted of a perforated sheet of aluminum foil coated with a thin layer of silicone grease and covered with a polyethelene sheet on the top and bottom. Rubber membranes were placed over samples with tightly fitting rubber bands placed around the Lucite disks, thereby preventing any loss in moisture prior to or during testing. Samples were then placed in a pan filled with water and were stored at ambient temperature for a period of about 2 weeks before freezing to minimize thixotropic effects.

Test samples were mounted in a triaxial cell, secured in place on the pedestal of the cell, and quickly frozen by filling the cell with a coolant. The coolant, a mixture of ethylene glycol and water, circulated around the cell at a constant temperature by pumping the coolant through a low-temperature bath. All test samples were cooled 3 C below test temperature, then warmed up to test temperature, and left to reach equilibrium for at least 12 hours before they were tested. Freezing of cylindrical samples begins on the surface and progresses inward. Water in large spaces freezes first, and the ice-water interface will extend into smaller spaces and channels until faced with too small a space to allow ice to grow. There the water in the space will remain supercooled as long as the temperature of the sample is constant.

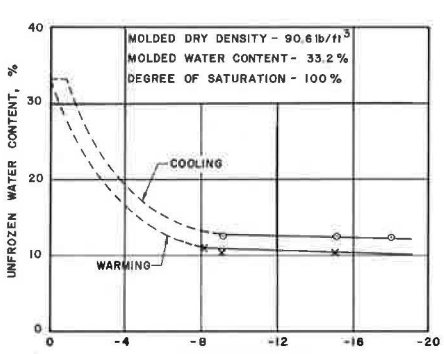

Figure 3. Unfrozen water content versus temperature for Sault Ste. Marie clay.

A sample warmed from a colder temperature to a test temperature will have more moisture frozen than a duplicate sample that is cooled to test temperature. Figure 3 shows the variation of unfrozen water content with temperature for a typical molded sample of Sault Ste. Marie clay. This was determined by the calorimetric method similar to the procedure used by Lovell (6). Reproducibility of calorimetric

results for the clayey silt, used in this investigation, was poor and therefore is not reported here.

Equipment and Testing

The triaxial cell, with the sample mounted in it, was immersed in a circular tank filled with a mixture of ethylene glycol and water (Fig. 4), which was maintained at a constant temperature by circulating it through an adjacent cold temperature bath. Temperature fluctuations near sample were less than ±0.05 C because of delayed temperature response in the triaxial cell as compared to larger variations in the cold temperature bath. Constant axial deformation rates were applied to the loading ram of the triaxial cell by using a variable speed mechanical loading system. Axial loads were measured with a load cell mounted on top of the loading ram and connected to an automatic recorder. Loads were recorded with an accuracy close to ±2 lb. Uniaxial deformations were determined by means of a linear variable differential transformer connected to a strip chart recorder. LVDT readings were checked occasionally with a 0.0001 in. per division dial gage mounted on the triaxial cell and were substituted for chart readings whenever power fluctuations in line affected the accuracy of such readings. The recorder used a 10-in. wide strip of paper that permitted accurate measurement of sample deformation and served as a permanent record of the test.

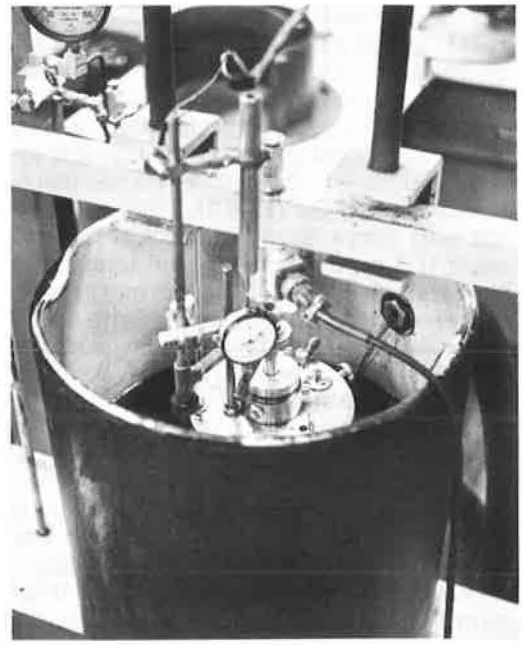

Figure 4. Triaxial cell in tank with coolant circulating.

EXPERIMENTAL RESULTS

Constant axial deformation rate tests were carried out on frozen cylindrical soil samples of clay and clayey silt at several temperatures below freezing. Deformation rates were maintained constant by means of a variable speed mechanical loading system. A summary of the characteristics of the 2 soils used is given in Table 1. Results of the constant axial deformation rate tests are presented in 2 groups according to the soil type.

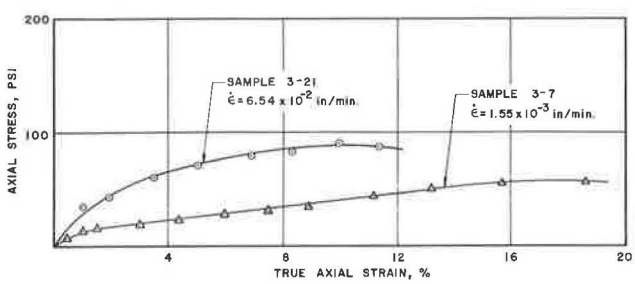

Figure 5. Typical stress-strain curves at -1 C for Sault Ste. Marie clay.

Clay Samples

Typical stress-strain curves for identically prepared and frozen Sault Ste. Marie clay samples deformed at constant deformation rates are shown in Figures 5, 6, 7, and 8. The average molded dry density and average molding water content were 90.6 lb/ft^3 and 33.2 percent respectively. Test temperatures were -1 C (Fig. 5), -5 C (Fig. 6), -9 C (Fig. 7), and -22 C (Fig. 8). At each temperature 2 tests are shown, one for deformation at a

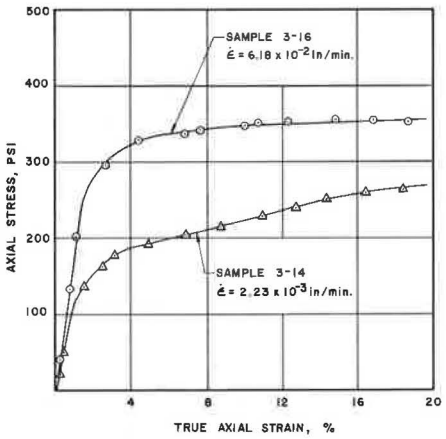

Figure 6. Typical stress-strain curves at –5 C for Sault Ste. Marie clay.

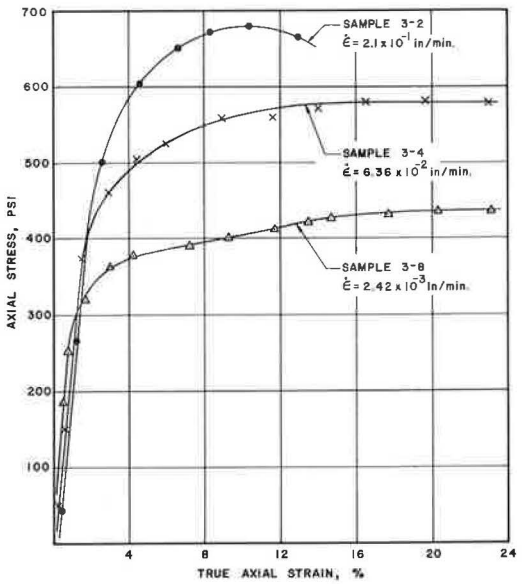

Figure 7. Typical stress-strain curves at –9 C for Sault Ste. Marie clay.

fast rate and one for deformation at a relatively slow rate, except that for temperature -9 C (Fig. 7) 3 different rates of deformation are shown. Tests shown in Figure 9 were conducted at approximately the same rate of deformation. Thus, different stress-strain curves (Fig. 9) reflect the effect of temperature alone on the stress-strain behavior.

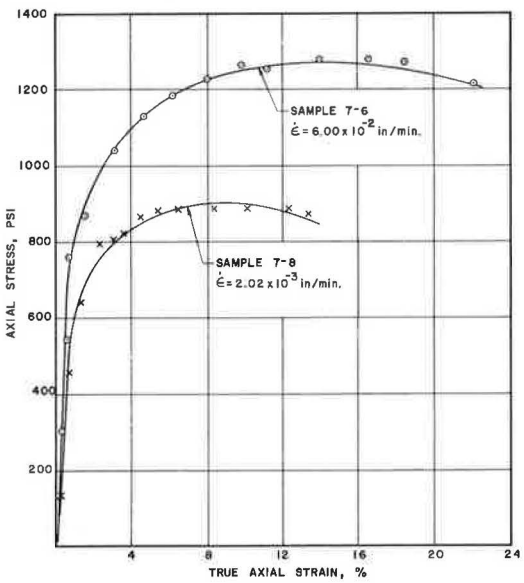

Figure 8. Typical stress-strain curves at –22 C for Sault Ste. Marie clay.

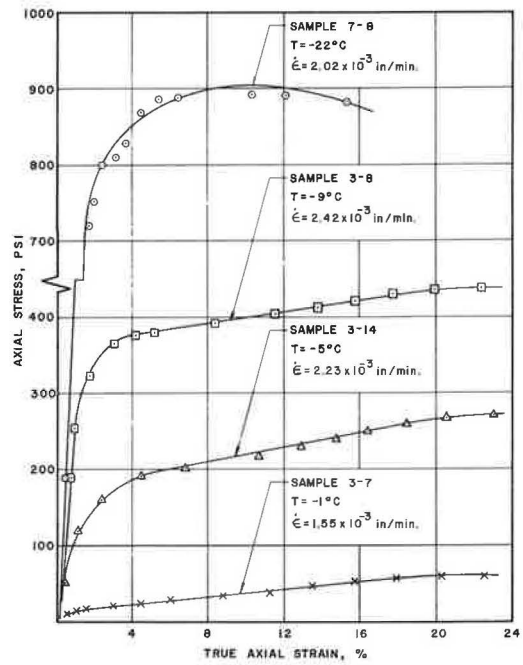

Figure 9. Stress-strain curves at different subzero temperatures and approximately constant axial deformation rate for Sault Ste. Marie clay.

Data shown in Figures 5, 6, 7, 8, and 9 reveal the following:

1. The stress-strain behavior differs depending on the deformation rate. The initial part of these curves at a particular temperature does not seem to be affected by deformation rates. This is the so-called elastic part of the stress-strain diagram that would correspond to expulsion of air present in the sample and to elastic changes in the crystal lattice of the ice and mineral particles. The major portion of this strain is recoverable when load is lifted.
2. The effect of deformation rate becomes well pronounced when samples begin to deform plastically. This is observed in all samples at all temperatures. It is apparent that the faster the deformation rate is, the higher the ultimate strength reached by the sample will be.
3. At relatively slow rates, samples appear to gain resistance to deformation (such as sample 3-14 in Fig. 6 and sample 3-8 in Fig. 7) while deforming plastically. This is a strain-hardening phenomenon that was not observed at -22 C. Samples that deformed slowly at -1, -5, and -9 C kept flowing under load, and ultimate strength, once reached, was almost constant the remainder of the test duration. No fracture or sudden failure resulted in the preceding samples in comparison with samples deformed at -22 C where sudden failure took place on all samples strained at this temperature. It appears that samples deformed at -9 C and higher exhibit considerable viscous flow especially close to the melting point of ice (-1 C), whereas samples deformed at -22 C were less viscous and more brittle.

Clayey Silt Samples

Typical stress-strain curves for identically prepared and frozen clayey silt samples deformed at constant deformation rates are shown in Figures 10 and 11. The average molded dry density and average molding water content were 107 lb/ft^3 and 18.6 percent respectively. Samples 5-10, 5-5, and 5-13 shown in Figure 10 were deformed at constant temperature (-5 C) but at varying deformation rates, indicating that the faster the rate of deformation was, the higher the ultimate strength was. Samples 5-13 and 5-17 reflect the effect of different temperatures (-5 and -1 C) at identical deformation rates. The following observations can be made for the clayey silt soil:

1. The elastic portion of the stress-strain curves appears to be smaller than that of the highly plastic clay at comparable

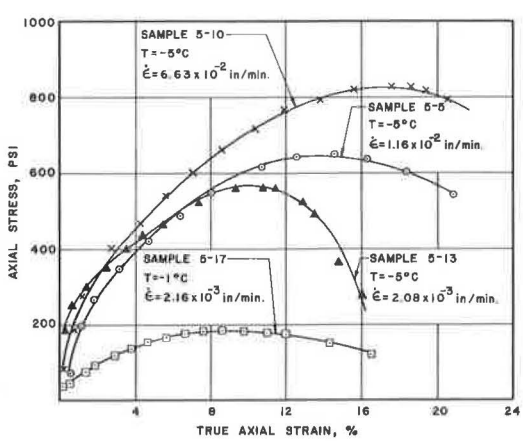

Figure 10. Stress-strain curves at –1 C, –5 C, and different axial deformation rates for Lafayette clayey silt.

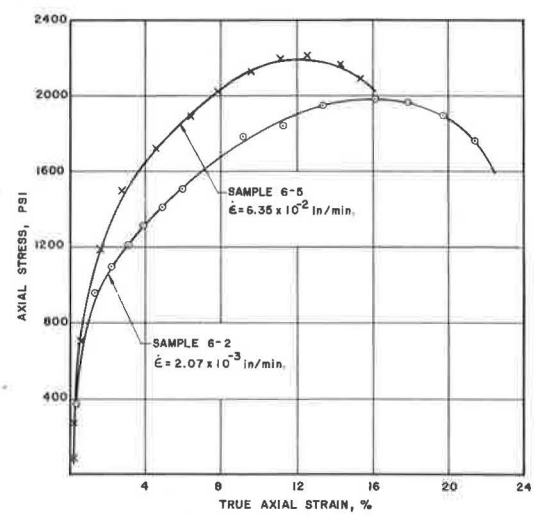

Figure 11. Typical stress-strain curves at –22 C for Lafayette clayey silt.

temperatures and deformation rates. Deformed samples exhibit well-pronounced stress-strain curves with well-defined peaks.

2. Samples deformed at rates and temperatures comparable with those of the clay soil samples reach peak strength at smaller strains. All samples fail by sudden rupture shortly after peak strength has been reached, except at -1 C where some viscous flow has been exhibited.

3. Most of the samples tested in this category demonstrated definite failure surfaces with an approximate angle of 60 deg in the major principal plane.

DISCUSSION OF RESULTS

Based on the experimental data presented, it seems possible to distinguish between the behavior of those samples that deformed and failed shortly after deformation in a brittle fashion and those samples that deformed rather excessively with no visible fracture or sudden failure, which is referred to here as plastic failure. The first type of deformation and failure was exhibited by the clayey silt, except at a high temperature (-1 C), and the latter type was exhibited by the plastic clay, except when the temperature was too low (-22 C) or the deformation rate was too large (2.1×10^{-1} in./min).

When a sample fails in a brittle fashion, the inference may be drawn that the ice cementation bonds between ice crystals and mineral particles have been overcome and destroyed completely. On the other hand, in a plastic type of failure these bonds seem to stretch permitting mineral particles to slide past one another and to rotate from their initial positions so that bonds are preserved and the material remains intact. The extent to which particles can rotate or slide past one another is dependent on the amount of liquid water and on the ratio of liquid water to ice present in a sample. The liquid water exists as a film of variable thickness between solid and ice surfaces. The thickness of this film depends strongly on temperature and soil type.

Ultimate strength values derived from stress-strain curves shown in Figures 5 through 11 as a function of test temperature at constant rates of deformation are shown in Figure 12. The linear variations shown are meant to be used in a relative sense. Both soils exhibit strong dependency of ultimate strength on temperature. For example, the approximate ratio of ultimate strength at -22 C to that at -5 C was 3.6 to 1 for the clayey silt and 3.3 to 1 for the clay soil at the same deformation rate of 2.1×10^{-3} in./min.

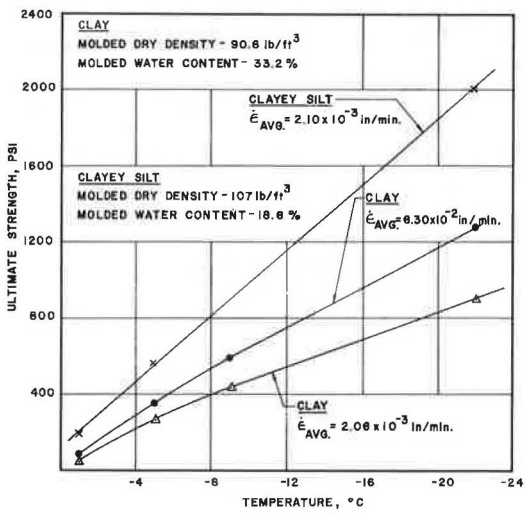

Figure 12. Ultimate strength derived from stress-strain curves versus subzero temperature for Sault Ste. Marie clay and Lafayette clayey silt.

Both soils have shown moderate deformation rate effect (Fig. 12); that is, the strength increases with increasing deformation rates. For example, the ultimate strength of the clay soil increases approximately 30 percent as the axial deformation rate increases from 2.06×10^{-3} in./min to 6.30×10^{-2} in./min. This is a rate increase of the order of 33 times.

CONCLUSIONS

In this investigation, constant axial deformation rate tests were carried out on identically molded and frozen cylindrical soil samples in an attempt to gain information concerning the effects of soil type, subzero temperature, and axial deformation rates on the stress-strain behavior of frozen fine-grained soils. From the results of the testing, the following conclusions have been drawn:

1. Two types of stress-strain behavior have emerged—a brittle type associated

with low plasticity soils (clayey silt) and a plastic type of failure associated with high plasticity soils (clay);

2. Low plasticity soils exhibit plastic behavior when temperature is relatively high (-1 C), and high plasticity soils exhibit brittle behavior when temperature is relatively low (-22 C) or when axial deformation rates are rather fast (0.21 in./min) or when both occur;

3. Ultimate strength derived from stress-strain curves depends strongly on temperature, and, based on molding conditions and soils used here, seems to increase about 3-1/2 times as the temperature decreases from -5 C to -22 C;

4. Ultimate strength depends moderately on deformation rate and increases by 30 percent when deformation rate increases from about 0.002 to 0.063 in./min; and

5. Data in this investigation suggest that it is primarily the amount of liquid water and the ratio of liquid water to ice present in a frozen soil matrix that control its stress-strain behavior and its ultimate strength.

ACKNOWLEDGMENTS

The author acknowledges and is grateful for the support provided by the National Science Foundation for this investigation. This paper is a portion of the research work on creep and strength of frozen soils carried out at Drexel University, Philadelphia, Pennsylvania. Further appreciation is extended to the College of Petroleum and Minerals, Dhahran, Saudi Arabia, for its support and encouragement.

REFERENCES

1. Akili, W. On the Stress-Creep Relationship for a Frozen Clay Soil. Materials Research and Standards, No. 1, Vol. 10, 1970.
2. Andersland, O. B., and Akili, W. Stress Effect on Creep Rates of a Frozen Clay Soil. Geotechnique, No. 1, Vol. 17, 1967.
3. Leonards, G. A., and Andersland, O. B. The Clay Water System and the Shearing Resistance of Clays. Proc. Research Conf. on Shear Strength of Cohesive Soils, ASCE, 1960.
4. Young, R. Research on Fundamental Properties and Characteristics of Frozen Soils. Proc. of First Canadian Conf. on Permafrost, Tech. Memo. 76, Ottawa, Jan. 1963.
5. Vialov, S. S. Mechanisms of Rheological Processes. In The Strength and Creep of Frozen Soils and Calculations for Ice-Soil Retaining Structures (Vialov, S. S., ed.), U.S. Army Cold Regions Research and Engineering Laboratory, Translation 76, 1961, Chap. 2.
6. Lovell, C. W. Temperature Effects on Phase Composition and Strength of Partially Frozen Soil. HRB Bull. 168, 1957, pp. 74-95.
7. Williams, P. J. Specific Heats and Unfrozen Water Content of Frozen Soils. Proc. First Canadian Conf. on Permafrost, Tech. Memo. 76, Ottawa, Jan. 1963.
8. Williams, P. J. Unfrozen Water Content of Frozen Soils and Soil Moisture Suction. Geotechnique, No. 2, Vol. 14, 1964.
9. Grim, R. E. Clay-Water System. In Clay Mineralogy, 2nd Ed., McGraw-Hill, 1968.

FROST BEHAVIOR OF COMPACTED SOILS

Mian-Chang Wang, University of Rhode Island; and
Gilbert L. Roderick, University of Wisconsin

The frost behavior of compacted soils subjected to a unidirectional penetration of freezing temperature from the top under a temperature gradient of 20 F/6 in. was studied. The results indicated that rate and maximum depth of freezing temperature penetration, water content increase, frost heave, and development of ice segregation were dependent greatly on soil texture compositions and compaction conditions including initial degree of saturation, molding moisture content, and dry density. Although sand size content was constant, increasing the clay size content (smaller than 0.002 mm) decreased frost heave, average water content increase, size of ice lenses, and depth to ice front. In general, decreasing the dry density only decreased the rate of frost penetration and increased the amount of water content increase and total heave. However, frost heave of Providence silt compacted by using standard AASHO compaction increased as molding moisture content increased regardless of the change in dry density. Frost heave increased linearly with average water content increase. The rate of increase, for a constant degree of saturation, increased as percentage of fines decreased.

•FREEZING causes volume to increase in soils because of volume expansion of interstitial water and formation of ice lenses in the soils. Frost heaving in soils may result in engineering problems and failures in hydraulic structures, highway pavements, and buildings. Because of the detrimental effects of frost action, considerable progress has been made in clarifying the mechanism of frost action in soils (1-7), in understanding the factors affecting frost action (8-13), and in developing techniques for handling frost-susceptible soils (13-16).

Frost action is a dynamic unsteady-state process, the nature of which is complex and involves a number of variables that are strongly interrelated. Because the intensity of frost action depends on so many factors that are indeterminate, it is almost impossible to predict the amount of frost heave in a soil under field conditions by means of laboratory tests and available theory. However, the relative potential for frost heave to occur in any soil could be estimated by studying the various factors that aid in its development.

This study was, therefore, undertaken to investigate the effect of a number of factors, such as molding moisture content, initial degree of saturation, dry density, and soil texture, on the frost behavior of compacted soils. The frost behavior that was studied included depth and rate of frost penetration, moisture migration due to freezing, frost heaving, and development of ice segregation.

APPARATUS, MATERIALS, AND TEST PROCEDURE

Tests were conducted by measuring temperature, overall heave, and final moisture content and by observing the development of ice segregation in test specimens subjected to a unidirectional penetration of freezing temperature under a temperature gradient of 25 F at the top and 45 F at the bottom of the 6-in. high test specimens. The testing

Sponsored by Committee on Frost Action and presented at the 50th Annual Meeting.

apparatus included a cold chest, a galvanometer and thermocouples, dial gages, and an X-ray machine. A detailed description of the apparatus is given in the Appendix; a schematic view of the test setup is shown in Figure 1.

Five soil specimens were tested simultaneously. Overall heave and final moisture content were determined for all test specimens. Soil temperature readings were taken only from the specimen located at the center of the group, and observation of ice segregation was made only for the specimen located at the front left side.

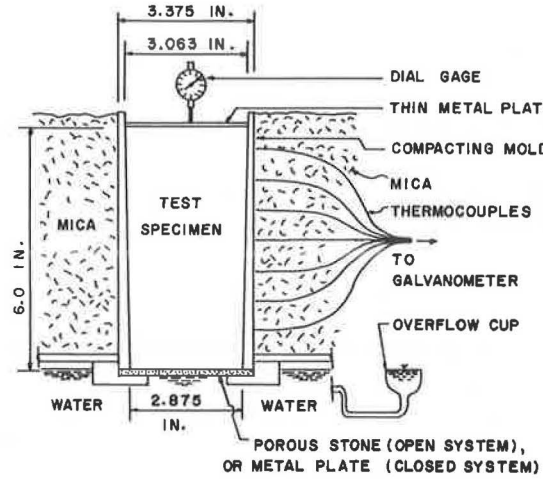

Figure 1. Schematic view of test setup.

Three test soils were used: Providence silt and 2 mixtures of Providence silt with different amounts of commercial Ca-montmorillonite plus sand-sized particles. One mixture had 21 percent Ca-montmorillonite plus 4 percent sand, and the other had 57 percent Ca-montmorillonite plus 10 percent sand by weight. The index properties of the 3 test soils are given in Table 1; the distribution of grain sizes are shown in Figure 2.

Test specimens were compacted by using a drop-weight compaction machine manufactured by Soiltest, Inc. The device had a drop weight of 15 lb for striking the top piston of the compaction mold. The drop height for the weight was controlled by a clip arrangement on the shaft guide.

The compaction molds, having inside diameters of 2.875 in. at the bottom and 3.063 in. at the top and a height of 6 in., were made of 2-5/6 in. (inside diameter) by 1/4 in. thick Lucite cylinders. The reason for using inside-tapered cylinders was to reduce wall friction or resistance to heaving. Damage due to compaction was prevented by confining the Lucite cylinder in a steel mold having an inside diameter exactly equal to the outside dimension of the Lucite cylinder.

The test specimens were compacted in 3 equal layers. Without the soil specimen being extruded from the Lucite mold, the specimen was capped with aluminum foil to prevent moisture evaporation and was then installed in the test chamber for at least 24 hours. Temperature in the test chamber at this stage was controlled at 45 F for the purpose of simulating field ground temperature.

Immediately following installation of the thermal insulation system and the heave- and temperature-measuring systems, testing was started by regulating the temperature

TABLE 1

INDEX PROPERTIES OF TEST SOILS

Test Number	Test Soil	Specific Gravity	Liquid Limit	Plastic Limit (%)	Plasticity Index	Texture Composition[a] Clay (%)	Silt (%)	Sand (%)
1	Providence silt	2.75	28.0	24.0	4.0	9	54	37
2	Providence silt + 21% Ca-montmorillonite + 4% sand	2.74	35.2	24.5	10.7	13	50	37
3	Providence silt + 57% Ca-montmorillonite + 10% sand	2.71	46.8	26.0	20.8	23	40	37

[a]According to International Society of Soil Science Classification System: clay size, < 0.002 mm; silt size, 0.002 to 0.02 mm; sand size, 0.02 to 2.0 mm.

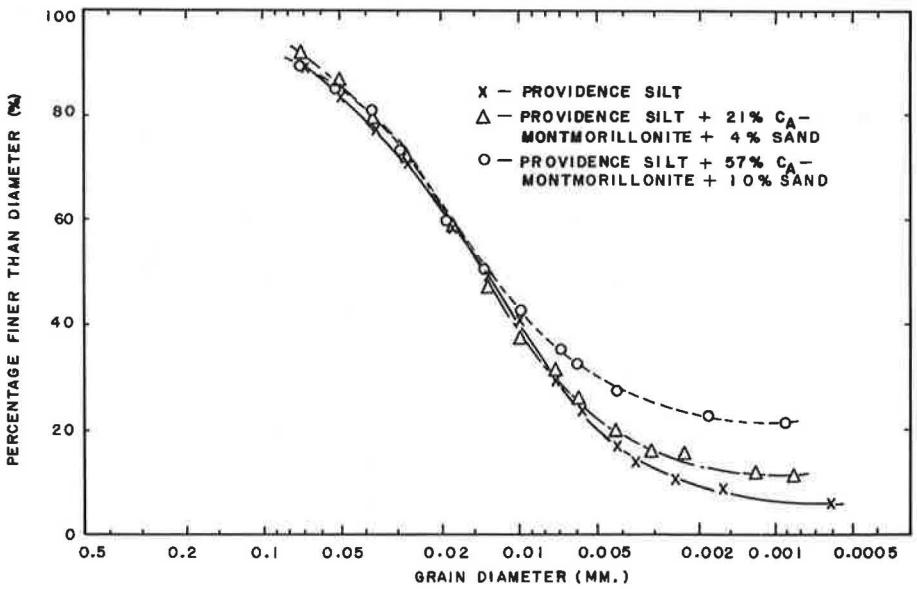

Figure 2. Distribution of grain sizes in soils investigated.

at the top of the test specimens to 25 F and by keeping the temperature at the bottom of test specimens constant at 45 F. Both 25 F and 45 F temperatures were used respectively at the top and the bottom of the test specimens throughout all tests. During testing, soil temperature readings were taken at total elapsed time intervals, such as 1, 2, 3, 5, 7, 15, and 30 hours, whereas overall heave determination and ice segregation observations were made every 24 hours. All tests were terminated after 5 days.

EXPERIMENTAL RESULTS AND DISCUSSION

Soil Temperature

Because of the unidirectional penetration of subfreezing temperature from the top of the test specimens, soil temperature at a certain depth decreases with increasing time of freezing. Typical curves for the variation of the soil temperature at different depths with freezing time for the compacted Providence silt in both closed and open systems are shown in Figures 3 and 4 respectively. It is seen that the slopes of the curves decrease as freezing time increases, implying that the soil temperature at any depth drops at a rate that decreases as freezing time increases because of the decreasing temperature gradient associated with increasing freezing time. In addition, because the curves are nearly parallel to each other, the rate of soil temperature change is nearly independent of the depth. The supply of excess water from the bottom of the test specimens in the open system causes a slower rate of cooling in the open system than in the closed system, as shown in Figure 5.

Effect of dry density on the rate of freezing temperature penetration, under a degree of saturation of 60 percent, is shown in Figure 6. Figure 6 also shows the following:

1. The effect of dry density was insignificant in the closed system; in the open system, the higher the dry density was, the deeper the freezing temperature penetration was.
2. At early stages of freezing, the rate of freezing temperature penetration in the open system was nearly a constant regardless of the magnitude of dry density; the rate in the open system was slower than that in the closed system because of the effect of additional water supply.

During the freezing process, the only sources of heat supply were moisture transport and the latent heat of fusion of the water in the soil. The moisture transport is

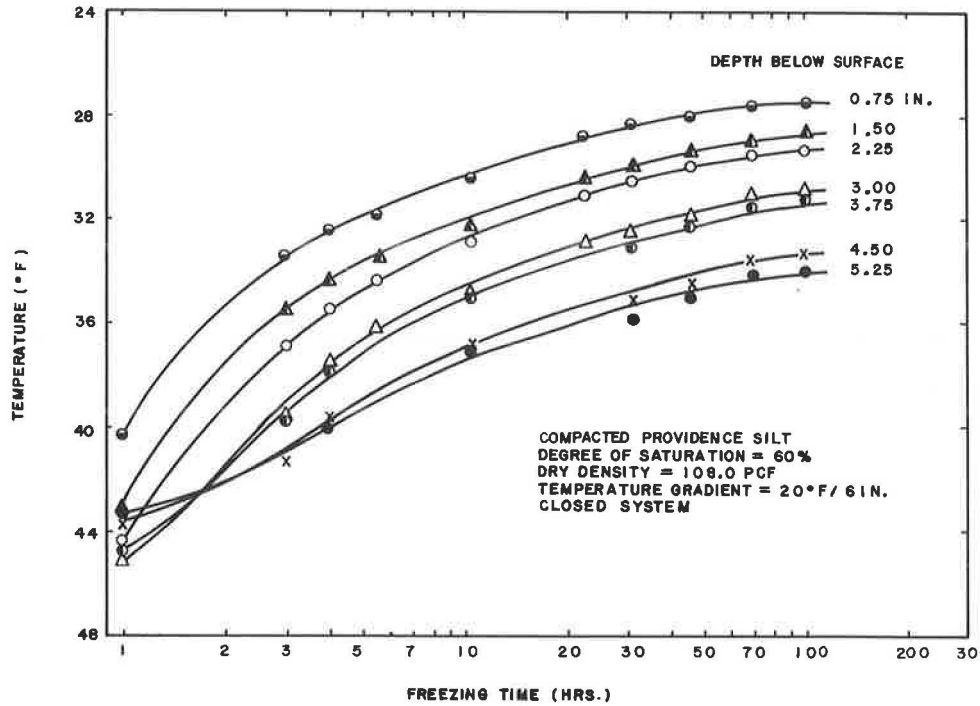

Figure 3. Variation of temperature at different depths with freezing time for Providence silt in closed system.

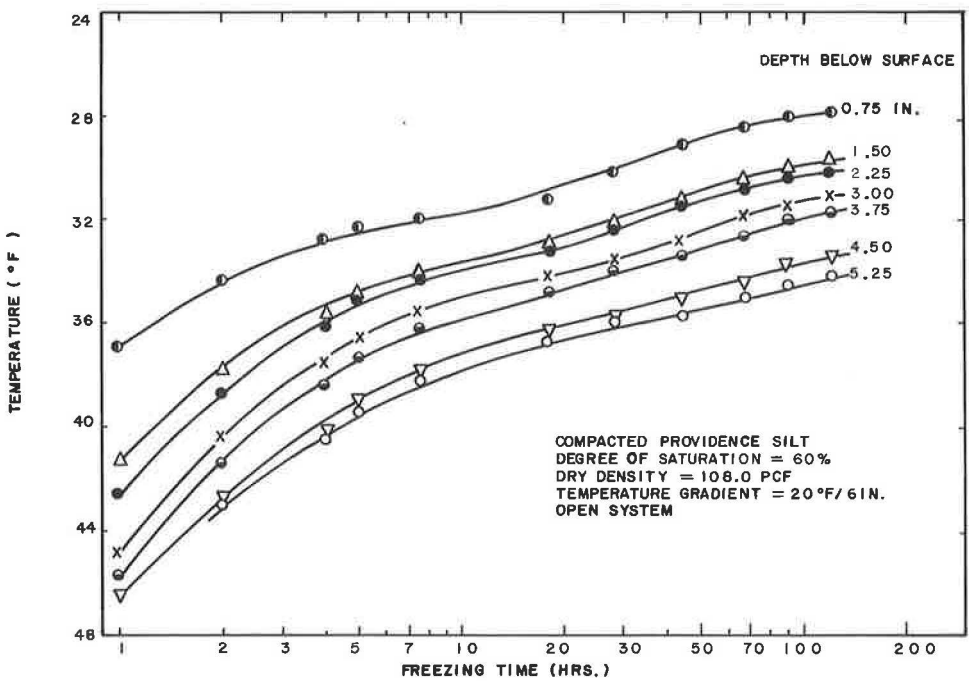

Figure 4. Variation of temperature at different depths with freezing time for Providence silt in open system.

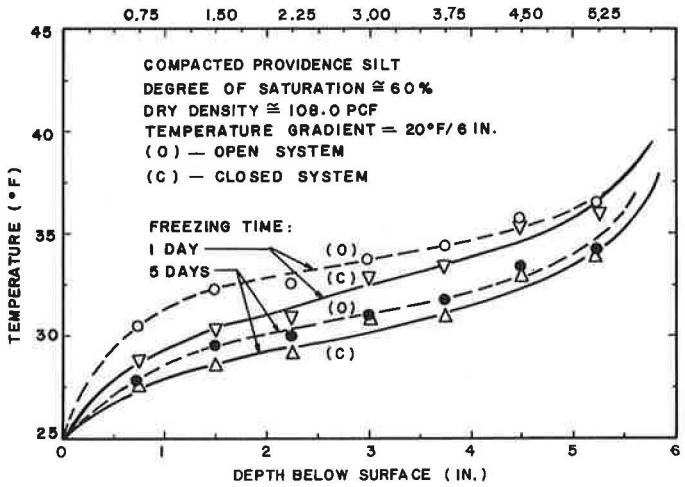

Figure 5. Soil temperature distribution with depth.

caused by the pressure deficiency at the ice front. The pressure deficiency is a measure of the matrix and osmotic potentials. Because the variation of osmotic potential for the conditions under study is generally considered to be negligible (17), the pressure deficiency reflects essentially the matrix potential. The matrix potential is a function of water content, and change in water content is directly influenced by the rate of ice lens growth that, in turn, is controlled by the external temperature gradient and the physical properties of the soil. For a given external temperature gradient,

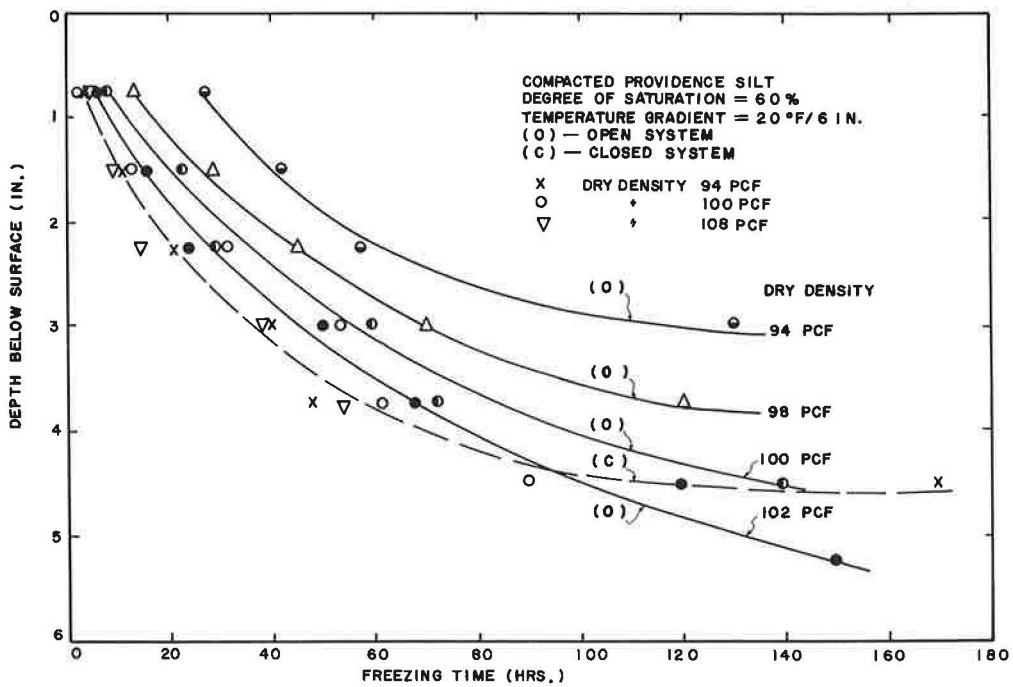

Figure 6. Penetration of 32 F temperature as a function of freezing time for a constant degree of saturation in both open and closed systems.

therefore, the pressure gradient would be directly related to the physical properties of the soil including the composition of the soil and the state of the soil mass with regard to soil moisture content, density, and the like. According to Darcy's law, the amount of water flow is directly proportional to the soil permeability and the pressure gradient. It follows that the soil property is the only essential factor controlling the amount of moisture transfer, as long as the external temperature gradient is a constant. For a constant degree of saturation, a lower dry density results in a higher void ratio and leads to a higher amount of moisture transfer. Consequently, a lower dry density gives a larger amount of moisture transfer to raise the soil temperature and impede the penetration of freezing temperature.

Latent heat depends only on the amount of water in a unit volume of soil. The lower the dry density is, under a constant degree of saturation, the higher the amount of water in a unit volume of soil will be, and, accordingly, the higher the latent heat will be. From the combination of these 2 effects (i.e., a large amount of moisture transport and a high value of the latent heat of fusion), it is therefore obvious that the depth to which the freezing temperature can penetrate is less for low dry density.

The negligible effect of dry density on the rate of freezing temperature penetration in the closed system, as indicated by the experimental results, probably illustrates that the effect of the latent heat of fusion on the rate of temperature penetration is relatively less significant than the effect of excess water supply, at least for the conditions investigated. Temperature increase due to the dissipation of the latent heat of fusion of soil moisture for the range of dry densities studied was computed. It was found that the difference in temperature increase between the largest and smallest dry densities (i.e., 108 pcf and 92 pcf) was not more than 1 F. Therefore, the results did not show appreciably the effect of dry density on the rate of freezing temperature penetration in the closed system.

Figure 7 shows the effect of degree of saturation on the rate of freezing temperature penetration. It is seen that, under a constant dry density, the rate of freezing temperature penetration increased as the degree of saturation decreased regardless of the

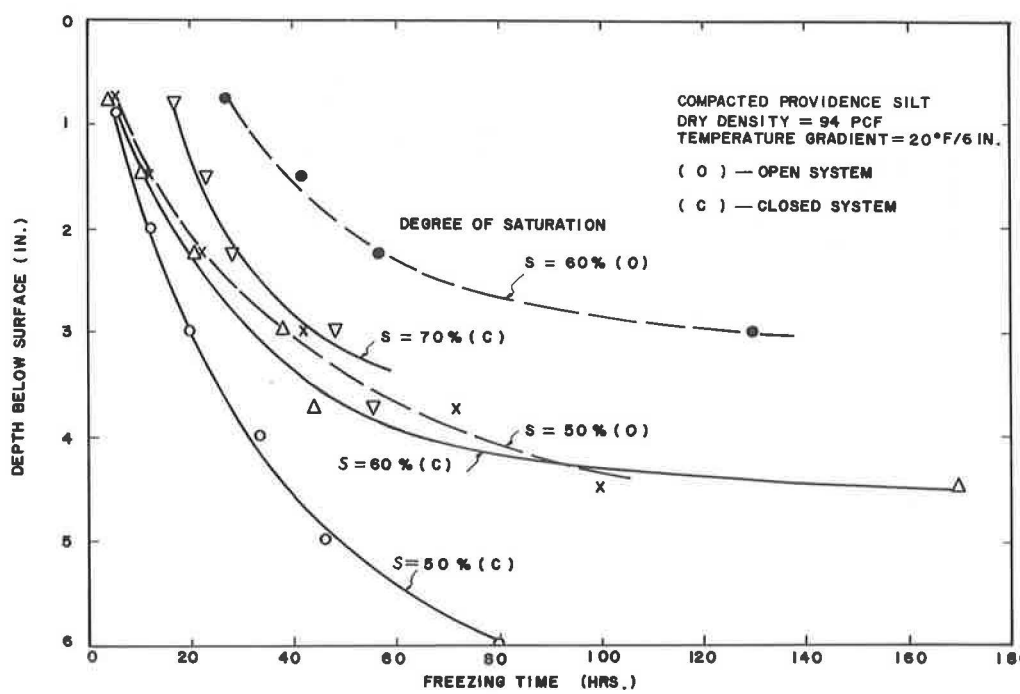

Figure 7. Penetration of 32 F temperature as a function of freezing time for a constant dry density in both open and closed systems.

nature of the testing system. This is as would be expected because a high degree of saturation, under a constant dry density, gives high moisture content that increases not only the amount of latent heat of fusion but also the soil permeability. Both of these factors favor raising soil temperature and impeding freezing temperature penetration. It is also seen that, with all other factors being equal, the depth to which the freezing temperature penetrates within a constant freezing time was greater in the closed system than in the open system.

The effect of soil texture on the rate of freezing temperature penetration is shown in Figures 8 and 9. Figure 8 shows the variation of temperature at midheight of the test specimens with time. It is seen that the rate of temperature variation with time approached zero sooner for the soil sample containing a higher percentage of the fraction smaller than 0.002 mm. Figure 9 shows that, among the 3 soils tested, the greatest depth to which the freezing temperature could penetrate decreased as content of fine fraction increased. In addition, the rate of frost penetration increased as the percentage of fine fraction increased, at least to a depth of 2.25 in. Below a depth of 2.25 in., however, the rate tended to decrease as the content of fines increased.

The percentage of fine fraction in a soil mass is an important consideration because the pore size decreases as this percentage increases. Under a constant degree of saturation and dry density, the consequence of reduction in pore size is to lower the freezing point of the pore water and to decrease the amount of pore water that can move freely without the influence of particle surface forces. As a result, the soil with higher content of fine fraction would be subject to a rapid frost penetration. The reason for the experimental results shown in Figure 9 is not fully understood, but the slower rate of frost penetration at a depth greater than 2.25 in. for the soil containing a higher percentage of fines might be due to retardation resulting from some factors such as excess water supply from the bottom of the test specimens. The results of the final water content measurements shown in Figure 10 could be used to support, at least

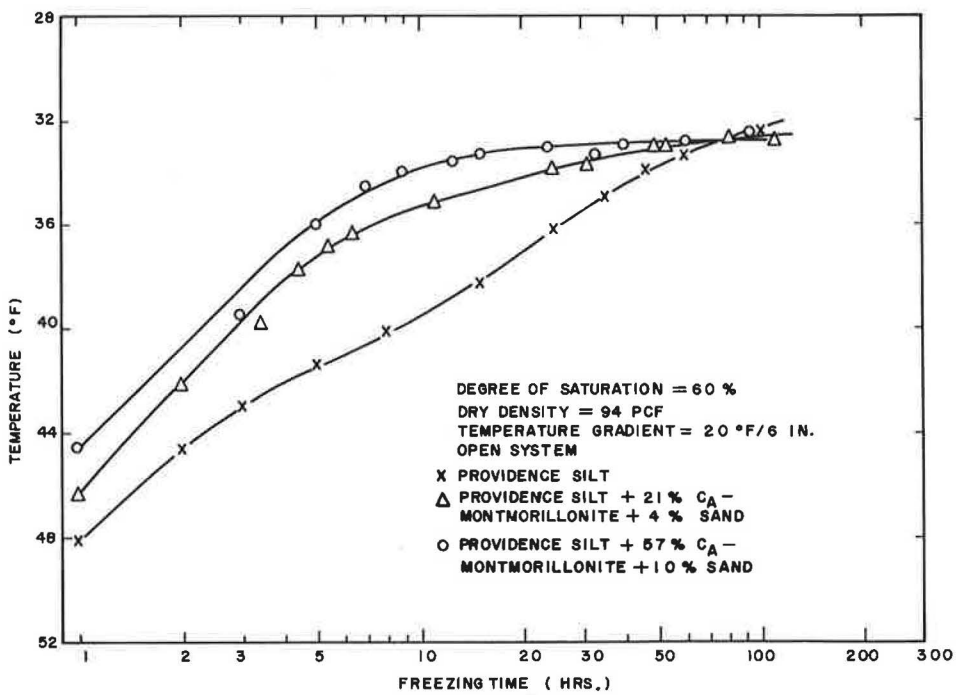

Figure 8. Variation of temperature at midheight of test specimens with time for different soil textures in open system.

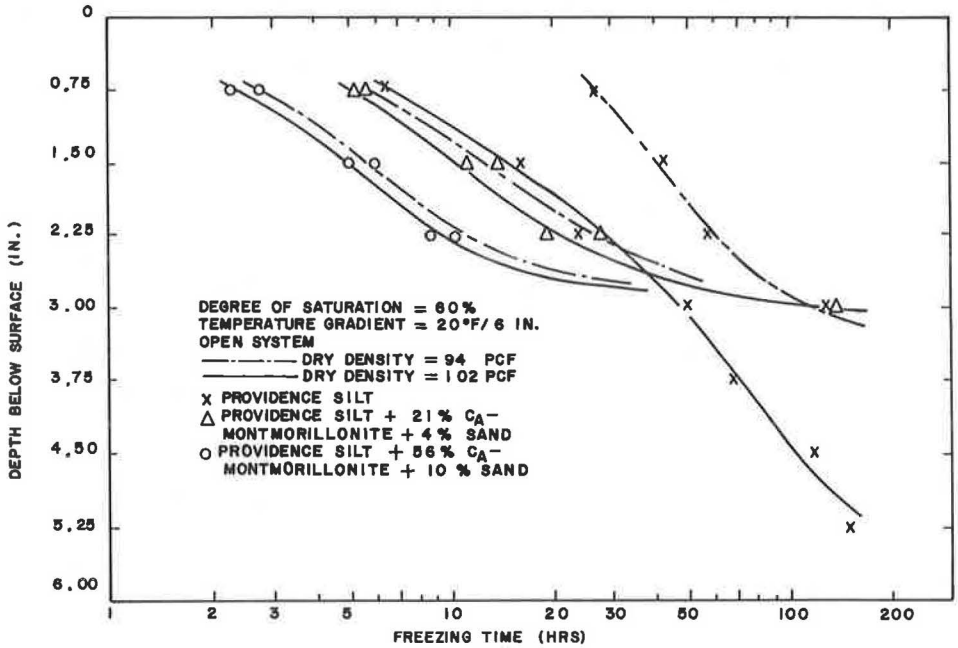

Figure 9. Penetration of 32 F temperature as a function of freezing time for different soil textures in open system.

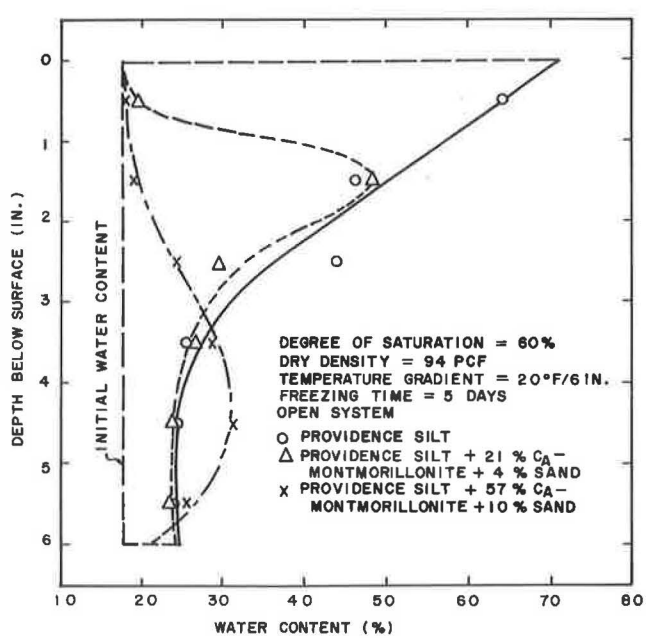

Figure 10. Final water content distribution with depth for different soil textures in open system.

partly, the reason. Figure 10 shows that the distribution of final water contents was such that the maximum height supplied by the excess water decreased as the content of fine particles increased.

Final Water Content

The water content distribution of test specimens, after having been frozen for 5 days, was determined by splitting the specimen into 6 horizontal segments of equal length. In general, the final water content distribution for compacted Providence silt decreased as depth below the surface increased, as shown in Figure 11. Because there was neither moisture evaporation from the top nor water supply from the bottom in the closed system, the average final water content should be equal to the initial water content; that is, the moisture increase in the upper portion should be equal to the moisture decrease in the lower portion of the test specimen. In the open system, because of the excess water supply from the bottom, the average final water content was always larger than the initial water content. In addition, the water content increase in the top 1 in. of the test specimen was considerably larger than the average overall increase.

The water content increase (i.e., the difference between the final and initial water contents) in the top 1 in. of the test specimens varied appreciably with varying molding conditions. Figures 12 and 13 show that the water content increase at the top was greater as molding water content increased but smaller as dry density increased regardless of the nature of the test system. The effect of degree of saturation on the water content increase at the top appeared to be less significant in the closed system than in the open system. The reason might be that, as has been pointed out before, the rate of moisture migration is directly proportional to the permeability of the soil, and the soil permeability is closely related to the degree of saturation. In the closed system, the moisture increase at the top resulted entirely from moisture migrating from the bottom portion. Because most of the moisture transportable under a given external temperature gradient had migrated by the time the test was completed, the effect of degree of saturation on the rate of moisture migration could not be reflected appreciably on the test results. In the open system, the portion of moisture increase due to

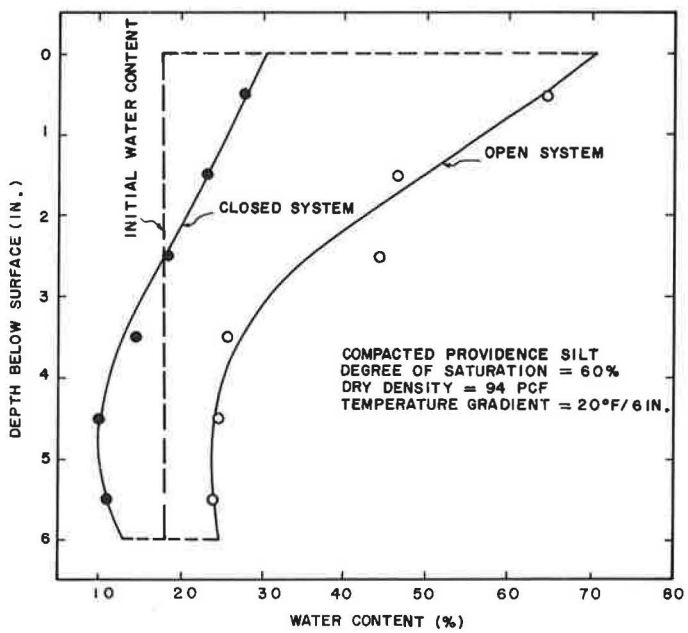

Figure 11. Typical final water content distributions with depth.

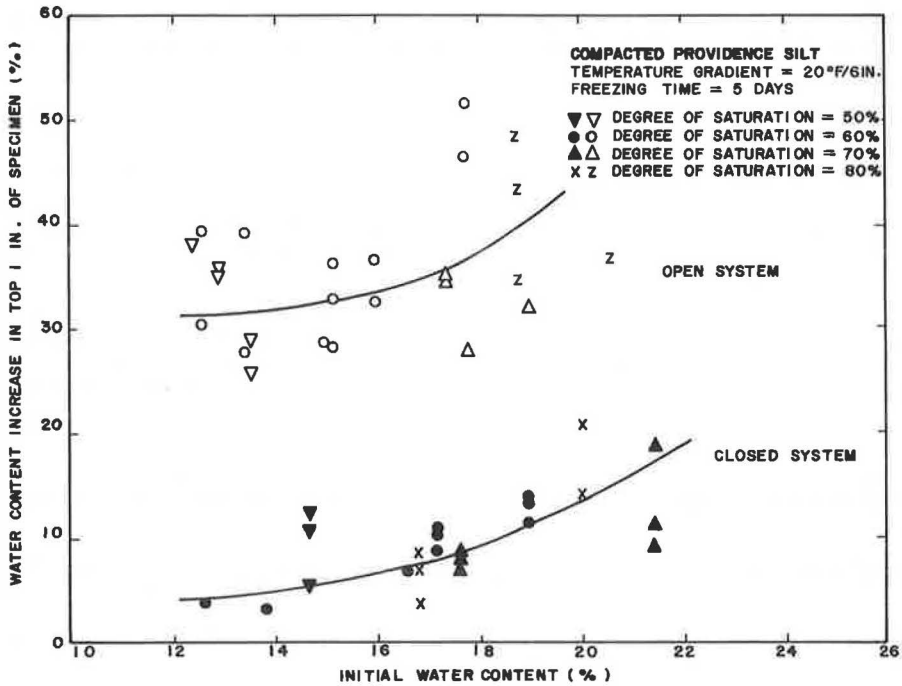

Figure 12. Influence of initial water content on water content increase in top 1 in. of test specimens for Providence silt.

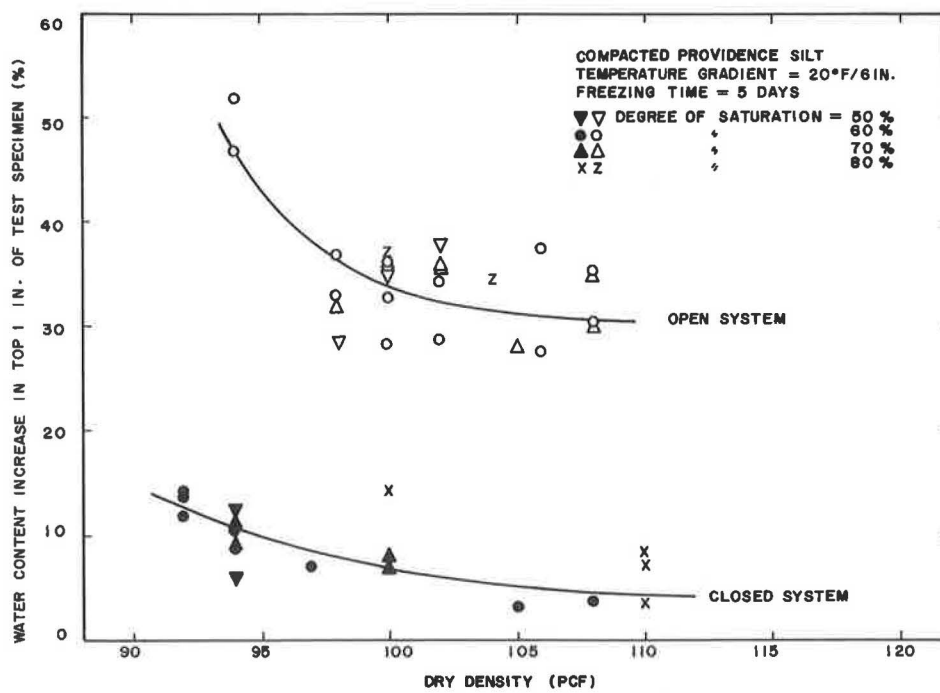

Figure 13. Influence of dry density on water content increase in top 1 in. of test specimens for Providence silt.

excess water supply from the bottom varied with various degrees of saturation and resulted in different amounts of moisture increase at the end of the test. However, no definite trend was obtained to indicate the consequent effect of the degree of saturation.

The general feature of final water content distribution with depth changed significantly with changing soil textures. It was found that the depth at which the maximum final water content occurred increased as the percentage of fine fraction smaller than clay size (0.002 mm) increased. Typical curves of the distribution are shown in Figure 10. The difference may be attributed to the effect of pore size. Because decreasing pore size increases the energy required to cause the same amount of water flow, the height at which the maximum moisture content occurs increases as pore size increases, that is, as fine content decreases. Following the same reasoning, we can conclude that the average overall water content increase would be less as fine-grain content increased.

Frost Heave

Test results show that considerably less heaving developed in the closed system than in the open system. Some specimens in the closed system even showed shrinkage or contraction that resulted from consolidation within the lower portion of the test specimens because of soil moisture that migrated to the upper portion.

Variation of heaving with freezing time was such that the slope of the curves decreased rapidly as duration of freezing increased and eventually approached almost a constant value. The maximum slopes, which were equivalent to the maximum rate of heave, increased as dry density increased, as shown in Figure 14.

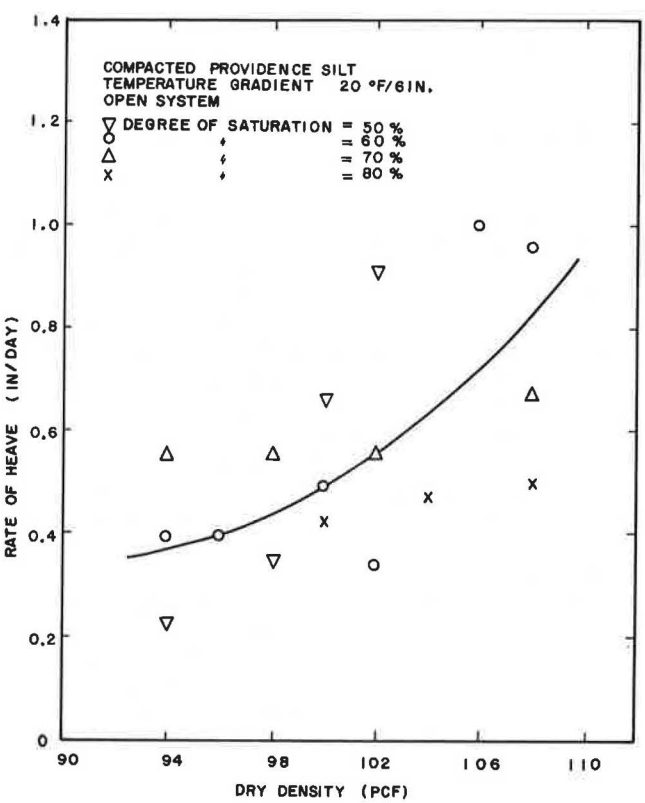

Figure 14. Maximum rate of heave versus dry density for Providence silt.

An increase in the rate of frost heave with an increase in dry density, however, does not necessarily imply that the overall heaving would follow the same trend. Instead, Figure 15 shows that, within the range of conditions investigated, for a given degree of saturation, total heave decreased linearly as dry density increased. The slope of the lines increased as degree of saturation increased. Also, for a given dry density, the higher the degree of saturation is, the higher the heaving rate will be. Figure 15 also shows that total heave increased as molding moisture content increased for a constant dry density, and increased as degree of saturation increased.

The effect of compaction on frost heaving should be a combined effect of molding moisture content, dry density, degree of saturation, and the like. A standard AASHO compaction curve, shown in Figure 15, illustrates that, for the conditions under investigation, frost heave always increased as molding water content increased no matter how the dry density varied. This implies

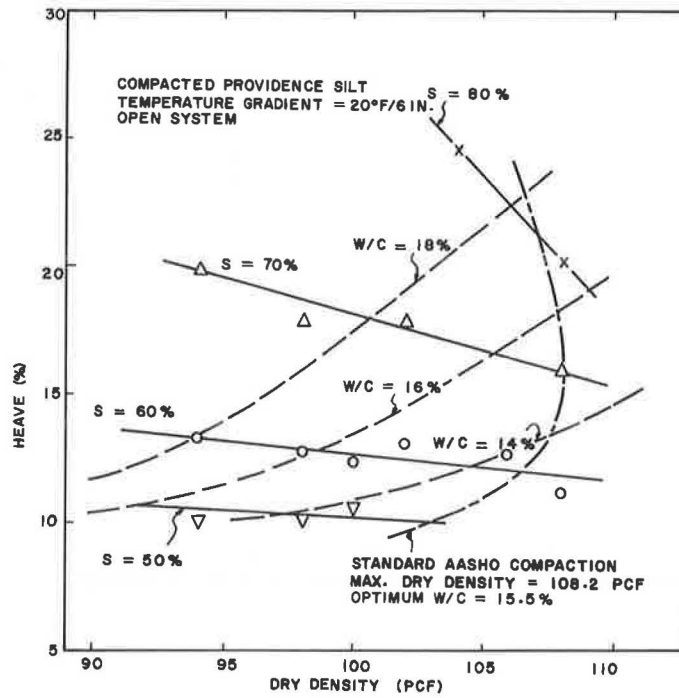

Figure 15. Total heave as a function of dry density.

that the effect of dry density was masked by the combined effect of molding water content and degree of saturation.

Figure 16 shows the difference in the rate of heaving for different soil textures compacted at the same dry density and degree of saturation. It is noted that increasing the fine grain fraction (smaller than 0.002 mm) decreased the rate of heaving. In addition, the intensity of heaving decreased as the percentage of fine fraction increased.

Total heave was plotted versus average water content increase for various degrees of saturation in Providence silt and in various soil textures with 60 percent degree of saturation, as shown in Figure 17. Total heave increased almost linearly with greater average water content increase. The higher the degree of saturation was, for a given water content increase, the higher the heave was. This could be expected because the higher the degree of saturation was, the smaller the pore size for a constant moisture content was, or the larger the volume of pore water was for a constant dry density. The smaller pore size would give greater volume expansion under the same moisture increase, whereas the larger volume of pore water would make the formation of bigger ice lenses possible. Consequently, for a given amount of water content increase, heave increased as the degree of saturation increased.

A marked difference in the slopes of the linear relationships for different soil textures is noted (Fig. 17). The higher the content of fines is (smaller than 0.002 mm), the smaller the slope will be. The test results may emphasize the effect of the size of ice lenses on the overall volume change of the test specimens because, as will be seen later, it was observed from the X-ray radiograph that the thickness of ice layers was different for different contents of fine-grain fraction, which was thicker for the soil having less clay-size content.

Ice Segregation

Development of ice segregation in the test specimens was studied by using an X-ray radiograph and by directly observing ice lenses by splitting the specimens

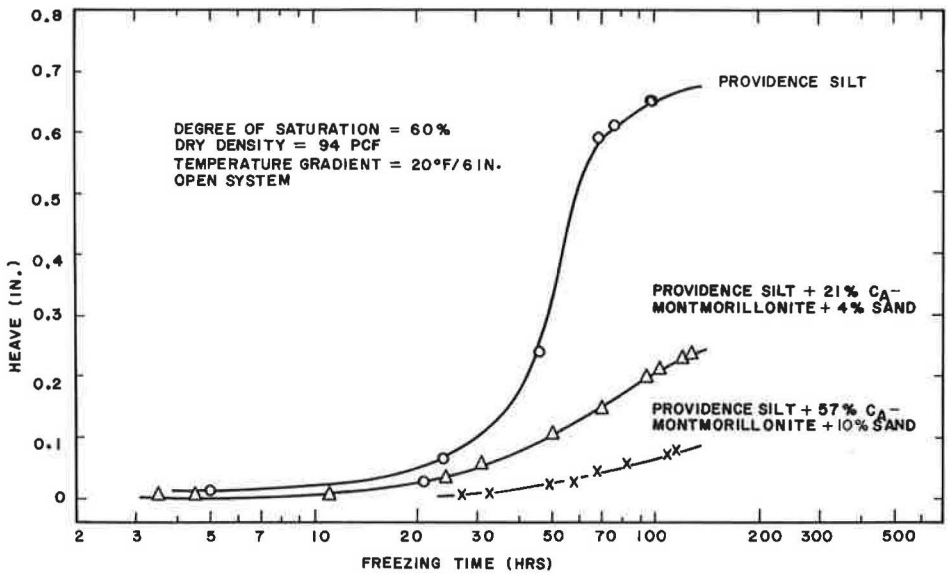

Figure 16. Variation of total heave with freezing time for different soil textures.

longitudinally. The X-ray radiographs were taken immediately before the test and every 24 hours during testing. It was found that, in general, the size of ice lenses was much smaller in the closed system than in the open system and that in the open system ice lenses decreased in size as percentage of fines increased.

Depth to the ice front was measured directly from the radiographs. The depth increased at freezing time increased at a gradually decreasing rate, as shown in Figure 18. Penetration of the ice front approached a maximum sooner in the closed system than in the open system; the maximum penetration by the end of testing was smaller in the closed system than in the open system. In the open system, the depth to the ice front increased as the degree of saturation increased while dry density was constant, and increased as dry density decreased while degree of saturation was constant. Depth to the ice front was smaller for the soil samples containing higher percentages of fines.

SUMMARY AND CONCLUSIONS

The frost behaviors of 3 soils compacted by using various compaction conditions were studied by means of a unidirectional penetration of freezing temperature under a temperature gradient of 20 F/6 in. (25 and 45 F at top and bottom respectively of 6-in. high test specimens). The results of this study have presented a more complete picture of the influence of factors on the frost behavior of compacted soils. It is believed that recognition of the importance of the many factors controlling frost action may aid in the selection of appropriate compaction conditions and in the improvement of methods in engineering practice for predicting the effects of frost action. From the results of this study, the following summary and conclusions appear warranted:

Freezing Temperature Penetration

1. The rate of freezing temperature (32 F) penetration decreased as freezing time increased but was faster in the closed system than in the open system.
2. Under a constant degree of saturation, the rate and the maximum depth of freezing temperature penetration increased as dry density increased in the open system; however, the effect of dry density was insignificant in the closed system.

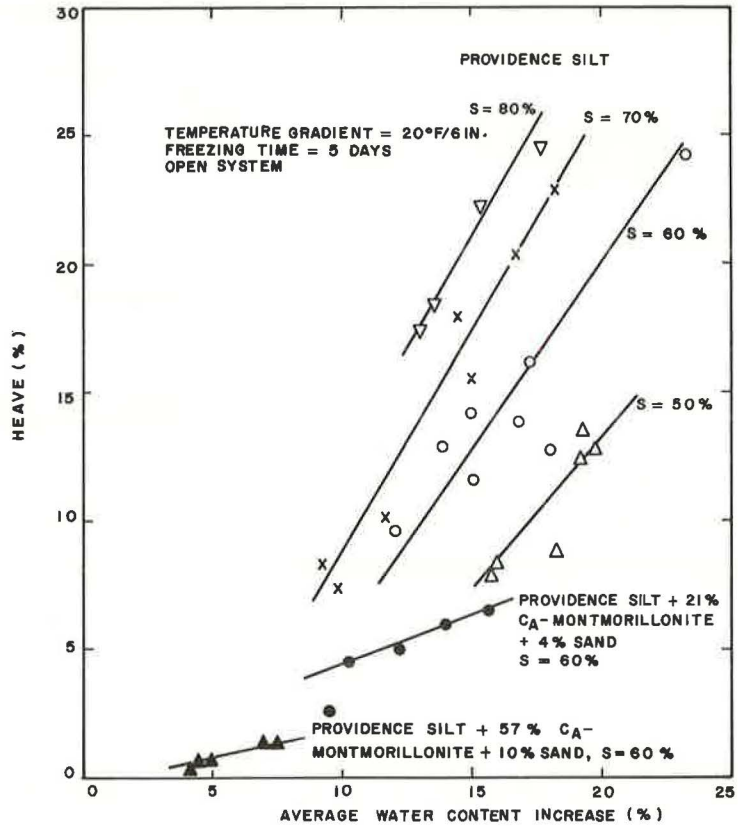

Figure 17. Relationship between total heave and average water content increase.

3. Under a constant dry density, the rate of freezing temperature penetration increased as degree of saturation decreased.

4. For the particular test conditions used, the rate of frost penetration increased above a depth of 2.25 in. as the content of grains smaller than clay size (0.002 mm) increased. Below a depth of 2.25 in., the rate tended to decrease as the content of fines increased.

Final Water Content

5. Although other factors were equal, there was a greater water content increase in the top 1 in. of the test specimens respectively as molding moisture content increased, dry density decreased, or content of fine fraction smaller than clay size decreased.

6. The final water content distribution with depth for various soil textures was such that the depth at which the maximum occurred increased as percentage of fines increased.

Frost Heave

7. Increasing dry density increased the maximum rate of frost heaving but decreased linearly the total heave for a constant degree of saturation. The higher the degree of saturation was, the larger the amount of heave was.

8. Frost heave of soils that were compacted by using a constant compaction effort (e.g., standard AASHO compaction) increased as molding moisture content increased no matter how the dry density changed.

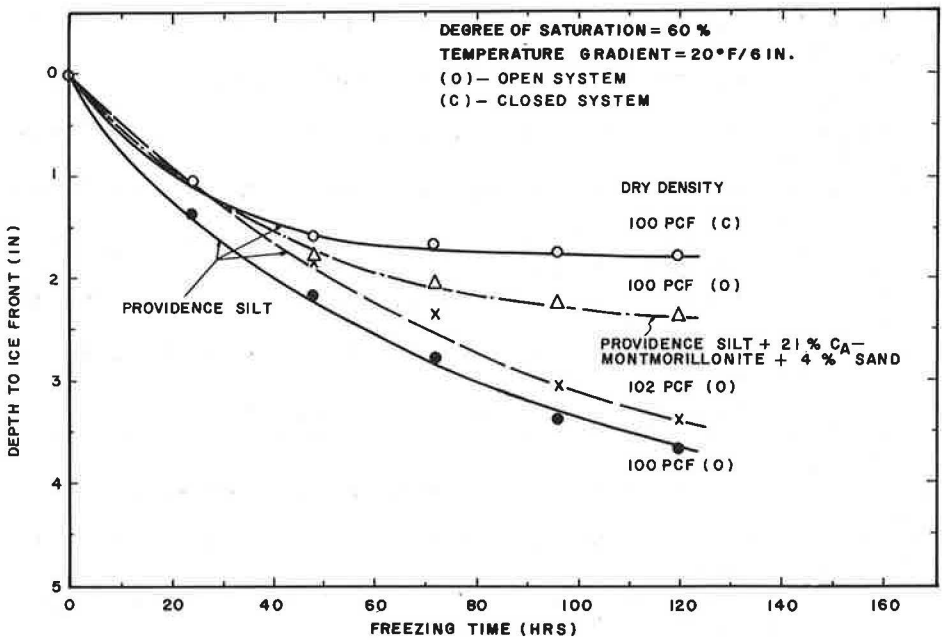

Figure 18. Penetration of ice front with freezing time.

9. Even though the content of sand size was kept constant, frost heave decreased as clay size content increased, i.e., as silt size content decreased.

10. Within the conditions investigated, observations were made of linear relationships between total heave and average water content increase for Providence silt compacted at various degrees of saturation and for different soil textures under a constant degree of saturation.

Ice Segregation

11. Larger ice lenses and greater depth of ice front penetration were given by the open system than by the closed system. Furthermore, in the open system, the size of ice lenses and the thickness of ice layer decreased as percentage of fines increased.

ACKNOWLEDGMENT

The writers are grateful to the following: Water Resources Research Center, U.S. Department of the Interior, for support of this research; David Ding-Jung Pang and Jsung-teh Sung for conducting the testing program; Milton T. Huston, Soil Mechanics Laboratory, University of Rhode Island, for assistance in the development of testing apparatus; and James K. Mitchell, University of California at Berkeley, for reviewing the manuscript. The drawings were prepared by Wen-hsiung Chen.

REFERENCES

1. Taber, S. Frost Heaving. Jour. of Geology, Vol. 37, No. 1, 1929.
2. Taber, S. The Mechanism of Frost Heaving. Jour. of Geology, Vol. 38, 1930.
3. Beskow, G. Soil Freezing and Frost Heaving With Special Application to Roads and Railroads, 1935. Osterberg, J. O., tr., Northwestern Univ., 1947.
4. Martin, R. T. Rhythmic Ice Banding in Soil. HRB Bull. 218, 1959, pp. 11-23.
5. Penner, E. Soil Moisture Movement During Ice Segregation. HRB Bull. 135, 1956, pp. 109-118.

6. Penner, E. Soil Moisture Tension and Ice Segregation. HRB Bull. 168, 1957, pp. 50-64.
7. Penner, E. The Mechanism of Frost Heaving in Soils. HRB Bull. 225, 1959, pp. 1-22.
8. Casagrande, A. Discussion on Frost Heaving. HRB Proc., Vol. 11, Pt. 1, 1932, pp. 168-172.
9. Penner, E. The Importance of Freezing Rate in Frost Action in Soils. Proc. ASTM, Vol. 60, 1960.
10. Haley, J. F., and Kaplar, C. W. Cold-Room Studies of Frost Action in Soils. HRB Spec. Rept. 2, 1952, pp. 246-267.
11. Haley, J. F. Cold-Room Studies of Frost Action in Soils, A Progress Report. HRB Bull. 71, 1953, pp. 1-18.
12. Linell, K. A., and Kaplar, C. W. The Factor of Soil and Material Type in Frost Action. HRB Bull. 225, 1959, pp. 81-128.
13. Frost Action in Soils, A Symposium. HRB Spec. Rept. 2, 1952, 385 pp.
14. Lambe, T. W. Modification of Frost-Heaving of Soils With Additives. HRB Bull. 135, 1956, pp. 1-23.
15. Tsytovich, N. A. Bases and Foundations on Frozen Soils. HRB Spec. Rept. 58, 1960, 93 pp.
16. Winn, H. F. Frost Action in Stabilized Soil Mixtures. HRB Proc., Vol. 18, Pt. 1, 1938, pp. 264-290.
17. Richards, L. A., and Wadleigh, C. H. Soil Physical Conditions and Plant Growth. Academic Press, N.Y., 1952, Chap. 3.

APPENDIX

DESCRIPTION OF TEST APPARATUS

Cold Chest

A refrigerator having an inside dimension approximately 23 in. wide by 13.5 in. long by 31 in. high was used to control temperature within the test chamber. The size of the test chamber was large enough to accommodate 5 test specimens. The test specimens, contained in Lucite cylinders, were separated with granular insulation, a commercial mica, so that freezing temperature could only penetrate unidirectionally from the top of the test specimens. Plates of Styrofoam were place against the door of the cold chest to retain the commercial mica and also to prevent both freezing temperature and outside temperature from penetrating laterally into the bottom of the test chamber.

The temperature at the bottom of the test chamber was kept uniform and constant at 45 F by means of water circulated by a pump. The level of the circulating water was so controlled by an overflow cup set outside of the refrigerator that it was just in touch with the bottom of the test samples. Besides controlling the temperature, the circulating water also served as a constant groundwater table as in the field condition. This simulated groundwater table could be used to supply additional water during freezing when a porous stone was set underneath the soil samples. The testing system in this case is called the open system. Whenever the closed system was desired (i.e., no excess water supply), the porous stone was replaced by a thin metal plate.

Temperature-Measuring System

The temperature-measuring system was composed of copper-constantan thermocouples and a readout unit for measuring soil temperature as well as the air and water temperatures in the test chamber. The readout unit was a reflecting type of galvanometer, manufactured by the Leeds and Northrup Company, No. 2436-b. The measuring instrument had a sensitivity of 0.1 microamperes per scale division and a system resistance of 35 ohms. The complete assembly was set beside the refrigerator so that readings could be taken without disturbing the test chamber temperature.

Among 5 test soil specimens, only the one at the center of the group was used to measure soil temperature. The thermocouples were connected to the test soil specimen at intervals of 0.75 in. through the height of the specimen so that the rate of temperature penetration could be measured directly (Fig. 1). The holes on the Lucite cylinder for the thermocouples were staggered about the circumference of the cylinder.

Volume Change Measuring System

Dial gages reading to 0.001 in. were used to measure uniaxial heaving or shrinking of the test samples. The dial gages were fastened on horizontal rods that, in turn, were fixed on the wall of the test chamber. A thin metal plate was set between the dial gage and the test specimen to ensure a smooth surface and also to prevent the evaporation of soil moisture. A light, controlled by a switch located outside the refrigerator, was used to light the test chamber so that gage readings could be taken more easily. All readings could be taken through the transparent door of the refrigerator without disturbing the testing process.

X-Ray Machine

The X-ray machine was a modified medical X-ray unit manufactured by the Picker X-Ray Corporation. It was operated with a voltage of 80 kilovolts and a current of 15 milliamperes. For observation of the development of ice segregation, X-ray radiographs were taken every 24 hours for the sample located at the front left side of the group.

VISCOELASTIC PROPERTIES OF A LATERALLY CONFINED SAND-ICE SYSTEM SUBJECTED TO TEMPERATURE INCREASE

J. T. Laba, Associate Professor of Civil Engineering, University of Windsor, Windsor, Ontario

A frozen sand-ice layer, when subjected to a temperature rise, will exert pressure against confining boundaries. The magnitude of this pressure can be measured and recorded in the form of a pressure-time curve. The sand-ice system closely resembles a viscoelastic material, and its time-dependent behavior under applied pressure can be compared to the behavior of the viscoelastic model. Subjecting the theoretical model to loading conditions equal to actual pressures exerted by a sand-ice layer and measured experimentally made it possible to study both the viscous (plastic) flow and elastic strain in a frozen soil layer. Furthermore, applying viscoelastic model analogy to the investigated frozen sand-ice layer, which was radially restrained and subjected to a uniform temperature increase, made it possible to derive equations for initial modulus of elasticity of a frozen sand layer, effect of temperature increase on the modulus of elasticity, time-dependent coefficient of viscosity of a frozen sand-ice layer, and time-dependent functions of elastic strain and plastic (creep) strain.

•THE MAGNITUDE of the lateral thrust exerted by a frozen sand layer on rigid confining boundaries and caused by uniform temperature increase was discussed elsewhere by the author (1). Two different sands were used in the foregoing experimental investigation. Sand No. 1 was a crushed uniform sand from Ottawa, Illinois (uniformity coefficient 1.5), whereas sand No. 2 was a natural well-graded sand from Paris, Ontario (uniformity coefficient 3.8). The grain-size distributions are shown in Figure 1. The soil specimens tested (4 in. high and 9-5/8 in. in diameter) were composed of sand and a variety of ice contents. The horizontal strain in the frozen sand was measured by means of BLH Type A-9 bonded resistance strain gages embedded in the sand. The test method used consisted of zeroing the strain bridge with the frozen soil at a constant initial temperature and then raising the soil temperature at a desired rate while simultaneously applying and measuring the resisting radial pressure required to prevent the soil-ice system from expanding.

The pressure σ exerted by the frozen sand layer was found to be a function of 5 variables: the initial temperature of the frozen layer T_o, the rate of the layer's temperature increase θ, the time of temperature increase t, the initial porosity of the sand n, and the degree of ice saturation S_i.

Based on the experimentally obtained results, 3 general equations were derived for pressure-time curves, for values of maximum pressure developed by a sand-ice layer, and for period of time required by the sand-ice layer to reach its maximum pressure. This research study was accomplished by not introducing the viscoelastic behavior of a sand-ice system but by knowing only the physical soil properties n, S_i, T_o, and θ.

However, applying viscoelastic model analogy to the frozen sand layer and subjecting the theoretical model to loading conditions equal to the actual pressures exerted by the

Sponsored by Committee on Frost Action and presented at the 50th Annual Meeting.

sand-ice system made it possible to study changes occurring in the elastic and plastic strain during the time when the frozen soil layer is subjected to a uniform temperature increase and, therefore, to varying lateral stress. Thus, the object of the investigation presented in this paper is to study the time-dependent behavior of a frozen sand layer subjected to a temperature increase but prevented from expanding by all-round rigid retaining boundaries.

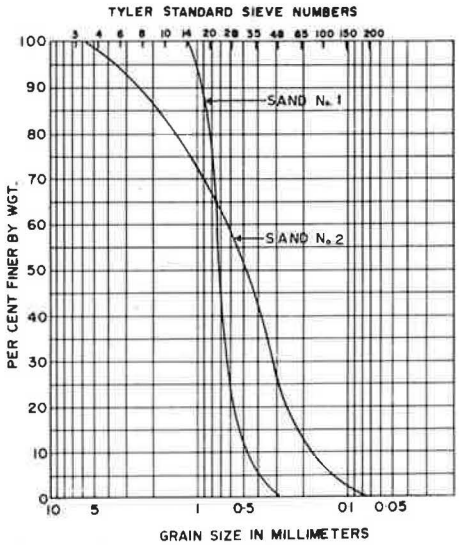

Figure 1. Grain-size distribution.

VISCOELASTIC MODEL ANALOGY

Typical pressure-time curves shown in Figures 2 and 3 clearly indicate the time-dependent behavior of the lateral pressure developed by sand-ice specimens when they are subjected to temperature increase and prevented from expansion by retaining boundaries.

The sand-ice resembles a viscoelastic material, and its behavior under applied pressure can be compared to the behavior of the viscoelastic model (i.e., the Maxwell model), which combines elastic and viscous (plastic) response and shows the appropriate physical picture of the time-dependent material.

Let us assume that the Maxwell model is placed horizontally between 2 rigid walls located a distance L apart (Fig. 4) and that the model is subjected to a uniform temperature increase. Because the rigid walls cannot be moved apart (L is constant), the linear expansion caused by temperature increase will not take place; but, instead, pressure on the confining boundaries will develop. The counteractive pressure provided by retaining walls will, in turn, apply a compressive force on the spring and the dashpot. Under these circumstances, the resultant horizontal linear strain must be zero because

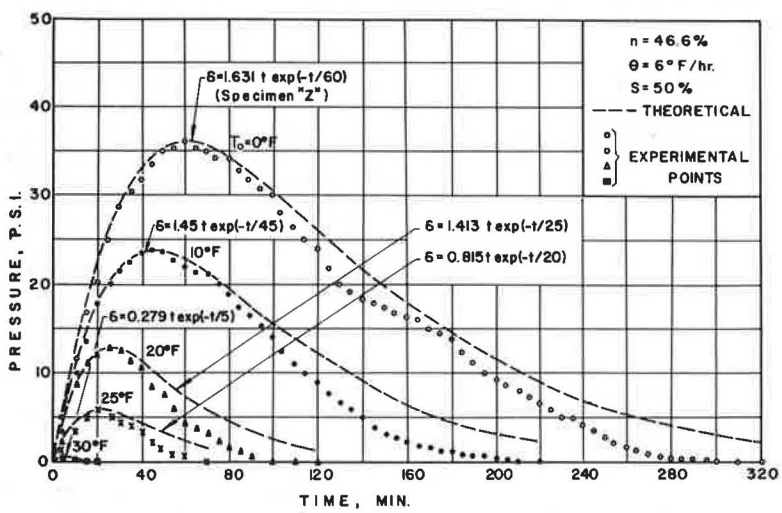

Figure 2. Pressure-time curves for temperature rise of 6 F per hour and 50 percent ice saturation from the indicated initial temperatures.

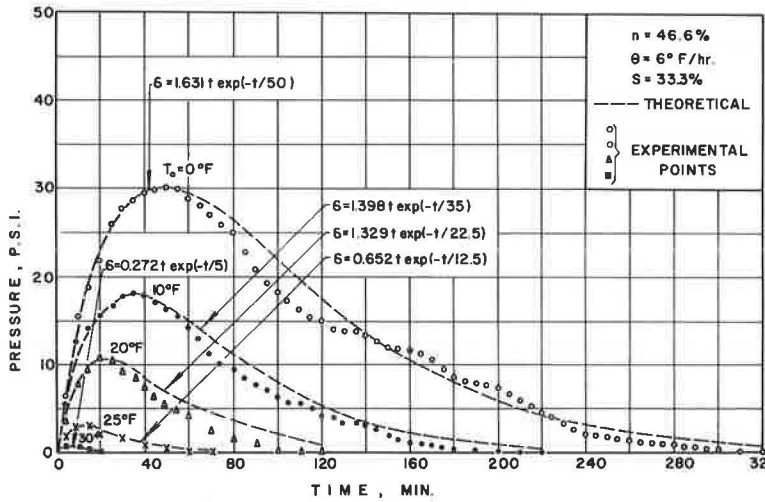

Figure 3. Pressure-time curves for temperature rise of 6 F per hour and 33.3 percent ice saturation from the indicated initial temperatures.

$$\epsilon_T - (\epsilon_{eL} + \epsilon_{pL}) = 0 \qquad (1)$$

where

ϵ_T = strain caused by temperature increase;
ϵ_{eL} = strain in elastic component, spring; and
ϵ_{pL} = strain in viscous element, dashpot.

The analogy between the behavior of the theoretical viscoelastic model and the investigated sand-ice specimens is obvious, if we assume that the elastic behavior of the frozen soil is represented by the action of the spring and the plastic flow (creep) in the ice matrix by the motion of the dashpot.

Each sand-ice specimen tested (1) was circular in shape (diameter = 9-5/8 in.) and during the testing was subjected to a radial stress σ uniformly distributed around its circumference. Because both the sample itself and the external loading were symmetrical around the sample's center, the sample remained perfectly circular in form for the duration of the experiment. If we assume that the sand-ice specimen is a homogeneous and isotropic material (idealization of a sand-ice system with irregular ice crystal orientation), then both the radial and circumferential strains must be uniform and equal throughout the soil sample. It follows that each element, such as N or P shown in Figure 5, will be subjected to biaxial stresses equal in magnitude and that

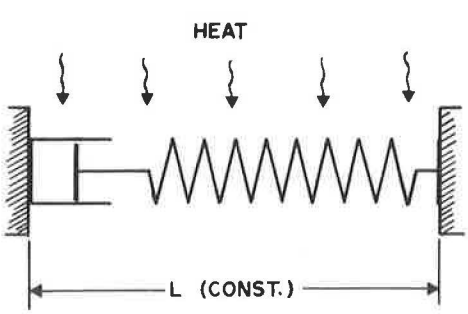

Figure 4. Viscoelastic model.

$$\sigma x = \sigma y = \sigma \qquad (2)$$

where

$\sigma x, \sigma y$ = principal stresses, and
σ = radial stress.

According to the law of elasticity, the value of elastic stress can be expressed as

$$\epsilon_{eL} = \frac{\sigma}{E} \qquad (3)$$

where E is the modulus of elasticity. The plastic deformation may be determined from Newton's law of viscosity (2) as follows:

$$\frac{d\epsilon_{pL}}{dt} = \frac{\sigma}{\eta}$$

or

$$\epsilon_{pL} = \int_0^t \frac{\sigma}{\eta}\, dt \tag{4}$$

where η is the coefficient of viscosity (proportionality). The strain caused by a uniform temperature increase is

$$\epsilon_T = \alpha\theta t \tag{5}$$

where

α = average coefficient of thermal expansion of the material,
θ = rate of sample's temperature increase, and
t = time.

Referring to the stress conditions of element N shown in Figure 5 and combining Eqs. 1, 3, 4, and 5, we have

$$\alpha\theta t = (1-\mu_1)\frac{\sigma_{(t)}}{E_{(t)}} + (1-\mu_2)\int_0^t \frac{\sigma_{(t)}}{\eta_{(t)}}\, dt \tag{6}$$

where

μ_1 = Poisson's ratio in the elastic range;
μ_2 = Poisson's ratio in the plastic range; and
(t) = a subscript, indicating a time-dependent function.

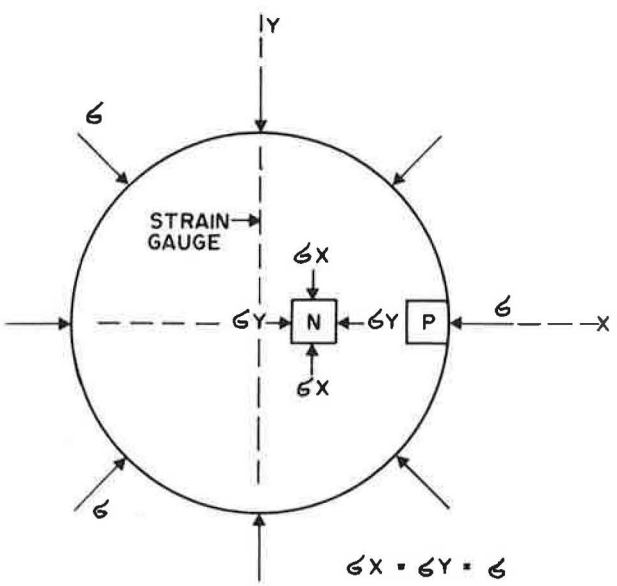

Figure 5. Compressive stresses in sand-ice specimen.

Because at the present time values of μ_1 and μ_2 are not available for frozen sand, Eq. 6 can be written in a different form, for the problem at hand, without including directly Poisson's ratios μ_1 and μ_2.

$$\alpha\theta t = \frac{\sigma_{(t)}}{E'_{(t)}} + \int_0^t \frac{\sigma_{(t)}}{\eta'_{(t)}}\, dt \tag{7}$$

where

$E'_{(t)}$ = modulus of elasticity, expressed as a ratio of equal biaxial stresses to the uniaxial strain; and
$\eta'_{(t)}$ = coefficient of viscosity, expressed as a ratio of equal biaxial stresses to the uniaxial velocity gradient of the plastic flow.

In Eq. 7, only values of $E'_{(t)}$ and $\eta'_{(t)}$ are unknown because the values of $\sigma_{(t)}$ were obtained experimentally and recorded in the form of pressure-time curves. For each pressure-time curve, the relationship between pressure and time can be approximated by Eq. 8 (see the broken lines shown in Figs. 2 and 3).

$$\sigma_{(t)} = A\, t \exp(-t/t_m) \tag{8}$$

where

A = coefficient, psi/min;
t = time, min; and
t_m = time required to reach maximum pressure, min.

From Eq. 8 it follows that

$$\sigma \max = 0.3679\, A\, t_m \tag{9}$$

Because the values of maximum pressure σ max and the required time t_m to reach this pressure were measured for each experiment, it was possible to calculate by using Eq. 10 the corresponding values of the coefficient A.

$$A = \sigma \max / 0.3679\, t_m \tag{10}$$

Combining Eqs. 7 and 8 and differentiating with respect to t gives the following differential equation:

$$\alpha\theta = \frac{d}{dt}\left[\frac{A\, t \exp(-t/t_m)}{E'_{(t)}}\right] + \frac{A\, t \exp(-t/t_m)}{\eta'_{(t)}}$$

or

$$\frac{\alpha\theta \exp(t/t_m)\, E'_{(t)}}{A} = 1 - t/t_m - \frac{\dot{E}'_{(t)}}{E'_{(t)}}\, t + \frac{E'_{(t)}}{\eta'_{(t)}}\, t \tag{11}$$

The modulus of elasticity of a sand-ice specimen, before being subjected to a temperature increase, can be obtained from Eq. 11 by introducing the following boundary conditions. At t = 0, σ = 0, and $E'_{(t)} = E'_o$; therefore,

$$E'_o = A/\alpha\theta \tag{12}$$

where E'_o is the initial modulus of elasticity of a frozen sand.

Substituting $\alpha\theta\, E'_o$ for A in Eq. 11 gives

$$\frac{E'_{(t)}}{E'_o} \exp(t/t_m) = 1 - t/t_m - \frac{\dot{E}'_{(t)}}{E'_{(t)}}\, t + \frac{E'_{(t)}}{\eta'_{(t)}}\, t \tag{13}$$

Temperature Effect on E'_o

Equation 12 shows that E'_o is directly proportional to the coefficient A and inversely proportional to α and θ. Because A itself is a function of T_o, S_i, θ, and n, it can be expected that the modulus of elasticity E'_o of a sand-ice system will also be influenced by the previously mentioned parameters, with the possible exception of θ. Values of A obtained from 15 experiments (sand No. 1, n = 46.6 percent, S_i = 50 percent, θ = 3, 6, and 9 F/hour) and $\alpha = 15 \times 10^{-6}$ per deg F were used to calculate coefficients of elasticity E'_o (Table 1).

Figure 6 shows the relationship between E'_o and the initial soil temperature T_o for 3 rates of temperature increase θ. It can be observed that the modulus of elasticity

decreases as the frozen sand's initial temperature increases. On the other hand, it appears that the rate of temperature increase θ has very little, if any, influence on E_o'. The dispersion in values of E_o' obtained for 3 rates of θ, at the same initial soil temperature T_o, could be caused by instrumental errors and also by the difference in the crystalline structure of the ice matrix formed in the otherwise identical sand-ice specimens.

The relationship between E_o' and T_o shown in Figure 6 can be represented by the following equation:

$$E_o' = 11.3 \times 10^5 - 1{,}030\, T_o^2 \quad \text{in psi} \qquad (14)$$

or less accurately, by the straight-line equation

$$E_o' = (11.3 - 0.2\, T_o) \times 10^5 \quad \text{in psi} \qquad (15)$$

TABLE 1

TEMPERATURE EFFECT ON MODULUS OF ELASTICITY

Rate of Temperature Increase (deg F/min)	Initial Temperature (deg F)	Coefficient (psi/min)	Coefficient of Elasticity E_o ($\times 10^{-5}$ psi)
0.05	0	0.815	10,866
	10	0.718	9,574
	20	0.543	7,240
	25	0.380	5,066
	30	0.136	1,812
0.10	0	1.631	10,874
	10	1.450	9,666
	20	1.413	9,420
	25	0.815	5,434
	30	0.279	1,860
0.15	0	2.718	12,080
	10	2.536	11,270
	20	1.699	7,550
	25	1.411	6,270
	30	0.544	2,418

Note: Sand No. 1, S_i = 50 percent, n = 46.6 percent, and $\alpha = 15 \times 10^{-6}$

Recent literature dealing with the properties of pure ice (3, 4, 5) supports the observations that were made on sand-ice specimens and that indicate that the elastic modulus of ice decreases as ice temperature increases.

Modulus of Elasticity $E_{(t)}'$ and Coefficient of Viscosity $\eta_{(t)}'$

An analysis of the viscoelastic behavior of the sand-ice system was carried out by using the specimen of sand No. 1, having n = 46.6 percent, S_i = 50 percent, T_o = 0 F, and being subjected to a temperature rise of θ = 0.1 F/min. The selected sample has been called specimen Z, and its pressure-time curves (both experimental and theoretical) are shown in Figure 2. The theoretical (idealized) pressure-time curve computed from Eq. 8 by using the experimentally obtained values of A = 1.631 and t_m = 60 min gives

$$\sigma_{(t)} = 1.631\, t \exp(-t/60) \quad \text{in psi} \qquad (16)$$

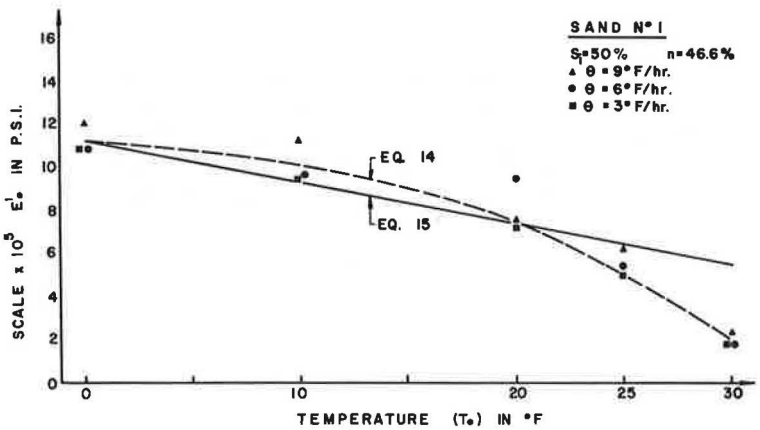

Figure 6. Initial modulus of elasticity versus initial frozen sand temperature.

Before being subjected to a constant rate of temperature increase of θ = 0.1 F/min, the selected soil specimen Z was at the initial temperature of T_o = 0 F and, therefore, had an initial modulus of elasticity $E'_o = 11.3 \times 10^5$ psi (Fig. 6). During the progress of the experiment, the frozen specimen, while uniformly increasing in temperature, was subjected at the same time to a constantly changing stress $\sigma_{(t)}$. Because both the stress and the soil temperature increase Δ T are time dependent, it can therefore be expected that the modulus of elasticity $E'_{(t)}$ of the specimen Z will decrease with time from its maximum value $E'_{(t)} = E'_o$ at t = 0 min, in the same way as the broken curve shown in Figure 6. Equation 14, which indicates the effect of the temperature increase on the initial elastic modulus of the sand-ice system, can be used as a fair approximation of the relationship $E'_{(t)}$ versus time when the independent variable T_o is replaced by $\Delta T = \theta t$. This is because Eq. 14 was derived for the sand-ice system subjected to similar stresses and temperature changes as the specimen being discussed. Therefore, the elastic modulus of the specimen Z at any time after it is subjected to a temperature increase, can be expressed as

$$E'_{(t)} = E'_o - a\,\Delta T^2 = E'_o - b\,t^2 \qquad \text{in psi} \tag{16}$$

where

E'_o = 11.3×10^5 psi;
ΔT = (θt) = increase of soil temperature, deg F;
a = 1,030;
t = time, min; and
b = $(a\theta^2)$ = 10.3

Equation 16 can be open to criticism because it involves some degree of approximation; therefore, 2 additional, less accurate equations for $E'_{(t)}$ are included in the analysis. This will help to evaluate the effect that the changes in function $E'_{(t)}$ will induce on $\eta'_{(t)}$ and also on the magnitude of the plastic strain ϵ_{pL}.

If for purposes of comparison one assumes that the elastic modulus decreases uniformly with time, then

$$E'_{(t)} = E'_o - s_1 \Delta T = E'_o - s\,t \qquad \text{in psi} \tag{17}$$

where

E'_o = 11.3×10^5 psi;
ΔT = (θt) = increase in soil temperature, deg F;
s_1 = 20,000; and
s = (θs_1) = 2,000.

Or, if one assumes that modulus of elasticity is a constant, then

$$E'_{(t)} = E'_o = 11.3 \times 10^5 \qquad \text{in psi} \tag{18}$$

The curves showing the 3 equations for $E'_{(t)}$ are shown in Figure 7. The circular points shown in Figure 7 indicate the effect of temperature increase on the soil's initial modulus of elasticity, when θ = 6 F/hour. The same points are shown in Figure 6 and were obtained from Eq. 12. Substituting in turn Eqs. 16, 17, and 18 for $E'_{(t)}$ into differential Eq. 13 gives the following corresponding functions for coefficient of viscosity $\eta'_{(t)}$ in lb-min/in.^{2}:

$$\eta'_{(t)} = \frac{(E'_o - b\,t^2)\,t}{\dfrac{(E'_o - b\,t^2)\exp(t/t_m)}{E'_o} - \dfrac{2\,b\,t^2}{E'_o - b\,t^2} + t/t_m - 1} \tag{19}$$

$$\eta'_{(t)} = \frac{(E'_o - s\,t)\,t}{\dfrac{(E'_o - s\,t)\exp(t/t_m)}{E'_o} - \dfrac{s\,t}{E'_o - s\,t} + t/t_m - 1} \tag{20}$$

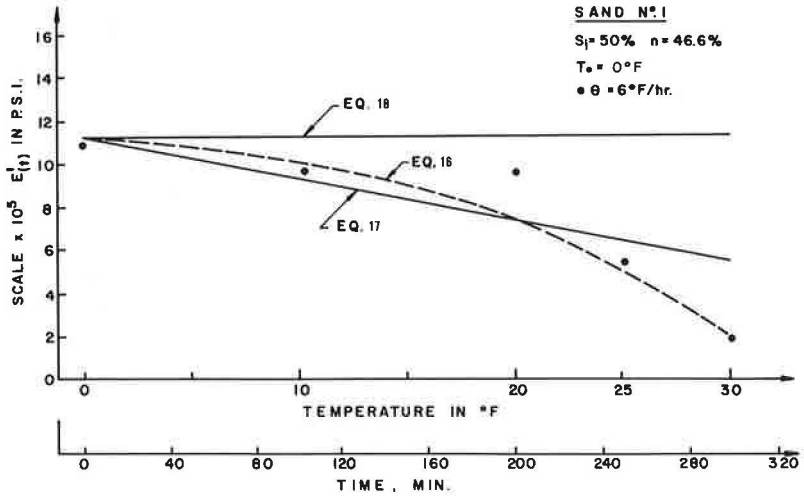

Figure 7. Modulus of elasticity versus time (or temperature) for specimum Z.

$$\eta'_{(t)} = \frac{E'_o\, t}{\exp(t/t_m) + t/t_m - 1} \tag{21}$$

where

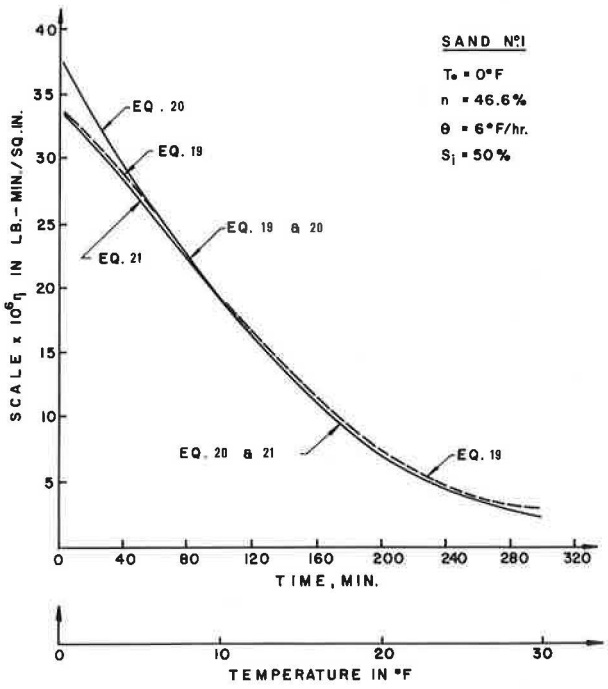

Figure 8. Coefficient of viscosity versus time (or temperature) for specimen Z.

E'_o = 11.3×10^5 psi,
b = 10.3,
s = 2,000, and
t_m = 60 min.

The curves showing the values of $\eta'_{(t)}$ for specimen Z obtained from Eqs. 19, 20, and 21 are shown in Figure 8.

It can be observed that the curves showing the 3 different functions of $\eta'_{(t)}$ are practically identical, except during the first 60 min when the curve representing Eq. 20 indicates larger values for the coefficient of viscosity than the remaining two. On the other hand, there is no significant difference at any time between the corresponding values of $\eta'_{(t)}$ from either Eq. 19 or Eq. 21, even though each equation was derived from a different function of $E'_{(t)}$. The reason for this is that the increase in the difference between the 2 functions of $E'_{(t)}$, represented by Eq. 16 and Eq. 18 (Fig. 7), changes rather slowly during the first hour after the experiment has begun. After this time, the influence of $E'_{(t)}$ on $\eta'_{(t)}$ appears to be negligible.

This leads to the conclusion that, for all practical purposes, the coefficient of viscosity $\eta'_{(t)}$ of the specimen Z, during the time when the confined frozen sand sample is subjected to a constant rate of temperature increase from 0 to 30 F, can be expressed satisfactorily by Eq. 21, which is the simplest of the 3 equations introduced.

Elastic Strain ϵ_{eL} and Plastic Deformation (Creep) ϵ_{pL}

If the functions defining the modulus of elasticity and the coefficient of viscosity for the investigated specimen Z are known, the horizontal elastic strain and plastic-viscous deformation can be determined at any time when the specimen is subjected to a temperature increase and hence to varying lateral stress. According to the viscoelastic model analogy, the sum of the elastic and plastic strain, at all times in the frozen specimen, is equal to the strain caused by the uniform rate of warming.

The elastic strain resulting from elastic deformations of the sand-ice system can be calculated for the problem at hand from the following equation:

$$\epsilon_{eL} = \frac{\sigma_{(t)}}{E'_{(t)}} \tag{22}$$

If we substitute for $E'_{(t)}$ the best available function $E'_{(t)} = E'_o - bt^2 = 11.3 \times 10^5 - 10.3\ t^2$, then

$$\epsilon_{eL} = \frac{A\ t \exp(-t/t_m)}{E'_o - bt^2} = \frac{t \exp(-t/60)}{6.928 \times 10^5 - 6.315\ t^2} \quad \text{in in./in.} \tag{23}$$

or, if we assume, for purposes of comparison, that $E'_{(t)}$ is a constant $E'_{(t)} = E'_o = 11.3 \times 10^5$, then

$$\epsilon_{eL} = \frac{A\ t \exp(-t/t_m)}{E'_o} = \frac{t \exp(-t/60)}{6.928 \times 10^5} \quad \text{in in./in.} \tag{24}$$

The plastic-viscous irreversible deformation in specimen Z, resulting from the ice flow and possibly from displacement of sand particles, can be obtained from Eq. 25,

$$\epsilon_{pL} = \int_0^t \frac{\sigma_{(t)}}{\eta'_{(t)}}\, dt = A \int_0^t \frac{t \exp(-t/60)}{\eta'_{(t)}}\, dt \tag{25}$$

or, from the more simple equation,

$$\epsilon_{pL} = \alpha\theta t - \epsilon_{eL} = 1.5 \times 10^{-6}\ t - \epsilon_{eL} \quad \text{in in./in.} \tag{26}$$

Figure 9 shows the relationship between plastic and elastic strain during the period of 300 min when the temperature in the investigated specimen Z increased from 0 to 30 F. It can be seen that, during the first 41 min after the radially confined sand-ice layer is exposed to a temperature change, the plastic component of the horizontal strain increases rapidly but still is smaller than the elastic component. At approximately t = 41.5 min, both strain components are equal, and, after that time, the plastic component representing the accumulative creep (from t = 0 min) of the sand-ice specimen is predominant. The results shown in Figure 9 were obtained by substituting in Eq. 26 $\alpha = 15 \times 10^{-6}$ per deg F for the average coefficient of thermal expansion of specimen Z.

Because ϵ_{eL} is directly proportional to the applied stress σ, the function of ϵ_{eL} resembles in shape the pressure-time curve of specimen Z. Regardless of which of the 2 equations introduced for ϵ_{eL} were used, the maximum elastic strain occurred at time $t = t_m = 60$ min when the specimen was subjected to the largest radial stress (σ max = 36 psi).

It can be noticed that all time-dependent functions, namely the elastic modulus, coefficient of viscosity, plastic strain, and elastic strain, were not extended beyond the time t = 300 min or T = 30 F. At this time, the theoretical pressure-time curve of specimen Z still indicates the existence of some radial pressure, whereas the measured pressure

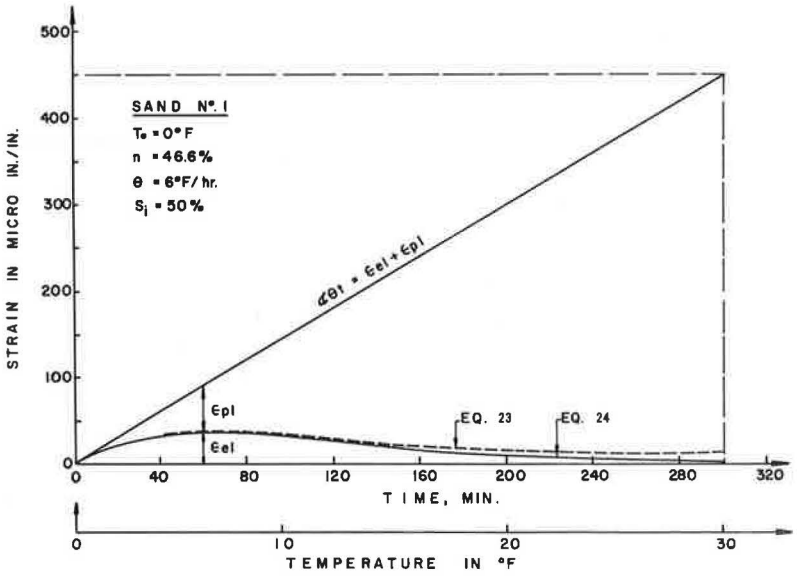

Figure 9. Elastic and plastic strain components versus time (or temperature) for specimen Z.

dropped to zero. The reason for this behavior was that, when the progressively increasing average sample temperature (measured at midheight of the sample) reached 30 F, the top part of the 4-in. thick soil layer was experiencing some thawing of the ice matrix. During the ice-melting process, there was no lateral thrust exerted by the soil-water-ice layer; therefore, the elastic and plastic strains experienced by the sand-ice system ceased to exist.

Figure 9 also shows the comparison between 2 ϵ_{eL}-time curves obtained from Eqs. 23 and 24 respectively. It can be observed that the difference in the magnitude of ϵ_{eL} given by the 2 curves increases progressively with time and reaches its maximum at t = 300 min. However, at that time, not only the difference discussed but also the values of ϵ_{eL} itself obtained from either equation are negligible when compared with the magnitude of the creep sustained by the frozen soil specimen. If a comparison is made at t = 300 min, then from Eqs. 23 and 26 the following values for the elastic and plastic strain are obtained: ϵ_{eL} = 16 μin./in. and ϵ_{pL} = 434 μin./in. On the other hand, the corresponding values obtained from Eqs. 24 and 26 are ϵ_{eL} = 3 μin./in. and ϵ_{pL} = 447 μin./in.

The resulting difference between the 2 functions of ϵ_{eL} has only a small influence on the large magnitude of ϵ_{pL} and, therefore, for all practical purposes the modulus of elasticity $E'_{(t)}$ for specimen Z can be assumed to be the constant value $E'_{(t)} = E'_o$ without the corresponding values of $\eta'_{(t)}$ and also ϵ_{pL} being seriously distorted.

CONCLUSIONS

Based on the preceding discussion, the following conclusions can be drawn:

1. The elastic strain-time curve of a frozen sand layer resembles in shape its pressure-time curve. Maximum elastic strain and maximum pressure occur at the same time. After reaching this time, the elastic strain decreases rapidly and becomes almost negligible when compared with the plastic strain.
2. Plastic (creep) strain in a restrained frozen sand layer commences immediately after the frozen sand is subjected to a temperature increase. This creep strain increases continuously with time, reaching its maximum value just before the ice matrix thaws.

3. For all practical purposes without serious error, the functions of $\eta'_{(t)}$ and ϵ_{pL} can be derived by assuming that the modulus of elasticity of a frozen sand layer subjected to lateral stress and to a uniform temperature increase is constant and equal to the initial modulus of elasticity of the frozen sand layer E'_o.

ACKNOWLEDGMENT

This work was supported by the Department of University Affairs, Ontario, and the National Research Council of Canada.

REFERENCES

1. Laba, J. T. Lateral Thrust in Frozen Granular Soils Caused by Temperature Change. Highway Research Record 304, 1970, pp. 27-37.
2. Tsytovich, N. A. Bases and Foundations on Frozen Soil. HRB Spec. Rept. 58, 1960, 93 pp.
3. Gold, L. W. Some Observations on the Dependence of Strain on Stress for Ice. Can. Jour. Phys., Vol. 36, 1958.
4. Tsytovich, N. A. Basic Mechanics of Freezing, Frozen and Thawing Soils. Academy of Sciences of the USSR. National Research Council of Canada, Technical Translation No. 1239, 1966.
5. Voitkovskii, K. F. The Mechanical Properties of Ice. Izv. Akad. Nauk, SSSR, Am. Met. Soc., Translation AMS-T-R-391, 1960.

THREE-DIMENSIONAL INFLUENCE VALUES OF DISTURBANCE DISTRIBUTION OF TEMPERATURE FROM HEATED STRUCTURES ON PERMAFROST

Alfreds R. Jumikis, College of Engineering, Rutgers University,
The State University of New Jersey

This paper presents temperature influence values and graphs for evaluating and plotting quickly and effectively temperature fields in permafrost beneath heated rectangular structures.

•THE OUTLINE by Lachenbruch (1) of a 3-dimensional temperature distribution in permafrost underneath heated buildings gives a transcendental equation (Eq. 1) for computing the steady-state principle of thermal disturbance T (x, y, z) at any point (x, y, z) in the hemispace underneath an area rectangular in plan whose dimensions are 2a × 2b or to 1 side of the vertical axis of symmetry through the center (x = 0; y = 0) of the rectangle. When a constant temperature T_{const} from a heated building is maintained over a rectangular area on the horizontal boundary surface of the hemispace, namely permafrost, the equation for calculating T in a steady state of heat flow is as follows:

$$T(x, y, z) = \frac{T_{const}}{2\pi} \left\{ \arctan\left[\frac{(x+a)(y+b)}{z\sqrt{z^2 + (x+a)^2 + (y+b)^2}}\right] - \arctan\left[\frac{(x-a)(y+b)}{z\sqrt{z^2 + (x-a)^2 + (y+b)^2}}\right] \right. \quad (1)$$

$$\left. - \arctan\left[\frac{(x+a)(y-b)}{z\sqrt{z^2 + (x+a)^2 + (y-b)^2}}\right] + \arctan\left[\frac{(x-a)(y-b)}{z\sqrt{z^2 + (x-a)^2 + (y-b)^2}}\right] \right\}$$

where

(x, y, z) = coordinates of any point in the hemispace,
2a = long side of rectangle, and
2b = short side of rectangle.

In addition to these 4 arctan terms, there are 8 more algebraic terms involved by extending Boussinesq's theory of elasticity. Tables prepared by the author according to the theory of elasticity (2) render greater influence values than those obtained by Eq. 1.

The temperature values T are to be determined either by analysis or by means of graphical integration, i.e., by constructing a concentric annular grid by gnomonic projections of meridians and parallels of a hemisphere onto its north polar tangent plane as suggested by Lachenbruch (1).

In 1963, Porkhayev (3) also presented an equation similar to Eq. 1 but differently derived for calculating temperature distribution for a 3-dimensional problem for any

Sponsored by Committee on Frost Action.

point in the hemispace. Obviously, Eq. 1 is very cumbersome to use in calculating and plotting temperature fields.

Neither in Lachenbruch's article nor in Prokhayev's paper can any data be found that would facilitate determining and plotting quickly and effectively the temperature fields in soil, namely, permafrost, from constant surface temperature such as that from heated structures.

TEMPERATURE INFLUENCE VALUES

The author prepared tabulations (Tables 1, 2, and 3) and charts (Figs. 1, 2, 3, and 4) of the temperature influence values for the following reasons:

1. Heat-conduction problems in permafrost, especially permafrost thawing (degradation) from heated structures in connection with laying of foundations in the Arctic and Antarctic, are of interest to the disciplines of foundation engineering and thermal soil mechanics;
2. The evaluation of thawing induced by various modifications of the temperature on the ground surface is important in problems of engineering design and logistics; and

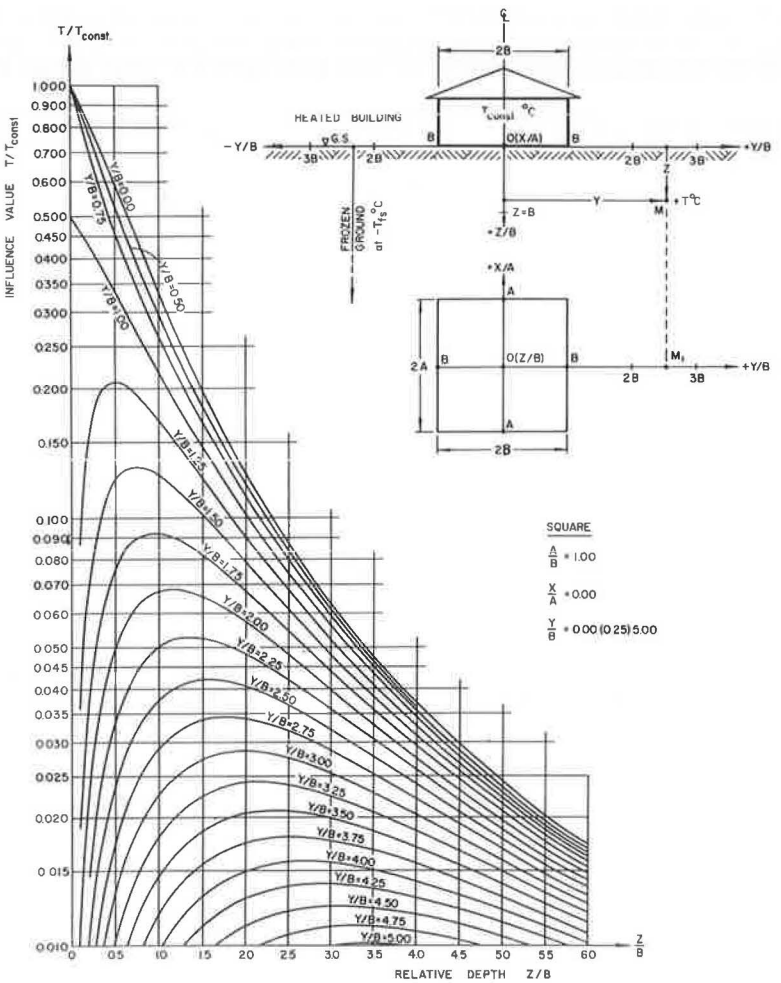

Figure 1. Influence values of distribution of temperature from heated structure structure on permafrost, T/T_{const} and A/B = 1.00.

3. The mathematics for calculating temperature fields should be readily available and accessible to engineers for effective use in the design of structures in permafrost.

The temperature distribution influence values are prepared for a square (Table 1), a rectangle (Table 2), and a strip (Table 3). These tables contain influence values in the form of dimensionless temperature ratios T/T_{const} as functions of relative dimensions a/b and relative coordinates x/a, y/b, z/a, and z/b. (Because the computer prints in capital letters, the tabular designations are given in capital letters, such as A/B, X/A, Y/B, Z/A, and Z/B.) Data given in the tables pertain to temperature fields in the vertical x = 0 planes that pass through the center (x = 0, y = 0) of the rectangles. The tables are prepared for a constant surface temperature of T_{const} = 1 C. For temperatures T_{const} other than 1 C, the tabular influence values must be multiplied by the temperature T_{const} in hand.

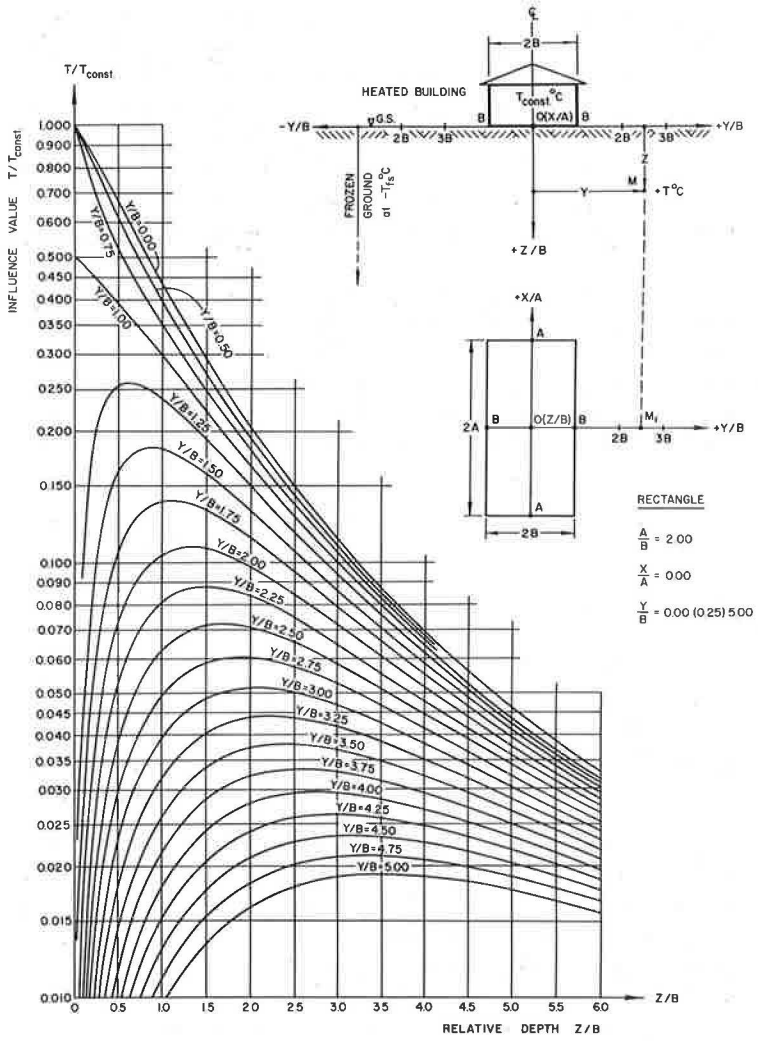

Figure 2. Influence values of distribution of temperature from heated structure on permafrost, T/T_{const} and A/B = 2.00.

TABLE 1

INFLUENCE VALUES OF DISTRIBUTION OF TEMPERATURE FROM HEATED STRUCTURE ON PERMAFROST, T/T_{const} = (Y/B) AND A/B = 1.00

2(A) = FOOTING LENGTH (X-DIRECTION) 2(B) = FOOTING WIDTH (Y-DIRECTION)

A/B= 1.0 X/A= 0.00

Z/B	Y/B										
	0.00	0.25	0.50	0.75	1.00	1.25	1.50	1.75	2.00	2.25	2.50
0.0	1.00000	1.00000	1.00000	1.00000	0.50000	0.00000	0.00000	0.00000	0.00000	0.00000	0.00000
0.1	0.91034	0.90665	0.89157	0.83845	0.46452	0.09029	0.03612	0.01897	0.01138	0.00742	0.00513
0.2	0.82286	0.81596	0.78873	0.70520	0.42970	0.15359	0.06802	0.03673	0.02230	0.01464	0.01016
0.3	0.73948	0.73021	0.69522	0.60313	0.39613	0.18822	0.09318	0.05234	0.03236	0.02144	0.01497
0.4	0.66166	0.65097	0.61252	0.52400	0.36426	0.20337	0.11108	0.06524	0.04125	0.02769	0.01948
0.5	0.59033	0.57909	0.54046	0.46053	0.33442	0.20692	0.12254	0.07528	0.04881	0.03326	0.02363
0.6	0.52591	0.51480	0.47811	0.40614	0.30677	0.20384	0.12867	0.08262	0.05498	0.03809	0.02736
0.7	0.46839	0.45787	0.42428	0.36397	0.28136	0.19707	0.13137	0.08756	0.05981	0.04215	0.03064
0.8	0.41747	0.40781	0.37777	0.32621	0.25817	0.18834	0.13112	0.09051	0.06339	0.04547	0.03346
0.9	0.37264	0.36397	0.33753	0.29362	0.23708	0.17870	0.12897	0.09184	0.06587	0.04807	0.03582
1.0	0.33333	0.32566	0.30264	0.26528	0.21795	0.16877	0.12556	0.09190	0.06739	0.05002	0.03776
1.1	0.29893	0.29221	0.27229	0.24050	0.20064	0.15892	0.12134	0.09101	0.06812	0.05139	0.03928
1.2	0.26883	0.26299	0.24582	0.21873	0.18497	0.14939	0.11664	0.08941	0.06819	0.05225	0.04043
1.3	0.24248	0.23743	0.22266	0.19953	0.17080	0.14030	0.11170	0.08729	0.06774	0.05267	0.04124
1.4	0.21939	0.21503	0.20233	0.18254	0.15798	0.13170	0.10666	0.08481	0.06688	0.05271	0.04175
1.5	0.19911	0.19535	0.18442	0.16745	0.14636	0.12363	0.10166	0.08210	0.06569	0.05245	0.04200
1.6	0.18127	0.17802	0.16861	0.15400	0.13582	0.11609	0.09676	0.07925	0.06427	0.05193	0.04202
1.7	0.16551	0.16271	0.15459	0.14198	0.12625	0.10906	0.09202	0.07633	0.06266	0.05121	0.04185
1.8	0.15157	0.14915	0.14212	0.13121	0.11756	0.10253	0.08746	0.07339	0.06093	0.05033	0.04152
1.9	0.13920	0.13710	0.13101	0.12154	0.10964	0.09645	0.08310	0.07047	0.05913	0.04931	0.04105
2.0	0.12819	0.12636	0.12107	0.11282	0.10242	0.09082	0.07896	0.06761	0.05727	0.04821	0.04046
2.1	0.11836	0.11677	0.11215	0.10494	0.09582	0.08559	0.07503	0.06481	0.05539	0.04703	0.03979
2.2	0.10955	0.10816	0.10412	0.09781	0.08979	0.08073	0.07131	0.06210	0.05352	0.04580	0.03904
2.3	0.10164	0.10043	0.09689	0.09134	0.08426	0.07623	0.06781	0.05949	0.05166	0.04454	0.03824
2.4	0.09452	0.09345	0.09034	0.08545	0.07919	0.07204	0.06450	0.05698	0.04984	0.04327	0.03740
2.5	0.08809	0.08715	0.08440	0.08006	0.07453	0.06815	0.06136	0.05456	0.04805	0.04200	0.03653
2.6	0.08227	0.08144	0.07901	0.07516	0.07024	0.06456	0.05844	0.05228	0.04631	0.04073	0.03563
2.7	0.07698	0.07624	0.07409	0.07069	0.06628	0.06118	0.05568	0.05009	0.04462	0.03947	0.03473
2.8	0.07217	0.07152	0.06960	0.06657	0.06263	0.05805	0.05308	0.04799	0.04299	0.03823	0.03382
2.9	0.06778	0.06720	0.06549	0.06278	0.05925	0.05513	0.05064	0.04600	0.04142	0.03702	0.03291
3.0	0.06377	0.06325	0.06172	0.05930	0.05613	0.05240	0.04833	0.04411	0.03990	0.03584	0.03201
3.1	0.06009	0.05963	0.05826	0.05608	0.05323	0.04986	0.04617	0.04231	0.03844	0.03468	0.03112
3.2	0.05671	0.05630	0.05507	0.05311	0.05053	0.04749	0.04412	0.04060	0.03704	0.03356	0.03024
3.3	0.05361	0.05323	0.05212	0.05036	0.04803	0.04526	0.04220	0.03897	0.03569	0.03247	0.02938
3.4	0.05074	0.05040	0.04940	0.04781	0.04570	0.04318	0.04039	0.03742	0.03441	0.03142	0.02854
3.5	0.04809	0.04779	0.04688	0.04544	0.04352	0.04123	0.03868	0.03596	0.03317	0.03040	0.02772
3.6	0.04564	0.04537	0.04455	0.04323	0.04149	0.03940	0.03706	0.03456	0.03199	0.02942	0.02691
3.7	0.04337	0.04312	0.04238	0.04118	0.03959	0.03769	0.03554	0.03324	0.03086	0.02847	0.02613
3.8	0.04126	0.04103	0.04036	0.03927	0.03782	0.03607	0.03410	0.03198	0.02978	0.02756	0.02537
3.9	0.03930	0.03909	0.03847	0.03748	0.03615	0.03455	0.03274	0.03078	0.02874	0.02668	0.02463
4.0	0.03747	0.03728	0.03672	0.03581	0.03459	0.03312	0.03145	0.02964	0.02775	0.02583	0.02392
4.1	0.03576	0.03559	0.03508	0.03424	0.03313	0.03178	0.03024	0.02856	0.02680	0.02501	0.02322
4.2	0.03417	0.03401	0.03354	0.03278	0.03175	0.03050	0.02908	0.02753	0.02590	0.02423	0.02255
4.3	0.03268	0.03253	0.03210	0.03140	0.03045	0.02930	0.02799	0.02655	0.02503	0.02347	0.02190
4.4	0.03128	0.03115	0.03075	0.03010	0.02923	0.02817	0.02695	0.02562	0.02420	0.02274	0.02127
4.5	0.02997	0.02985	0.02948	0.02888	0.02808	0.02710	0.02597	0.02473	0.02341	0.02205	0.02067
4.6	0.02874	0.02862	0.02829	0.02774	0.02699	0.02608	0.02504	0.02388	0.02265	0.02138	0.02008
4.7	0.02758	0.02747	0.02716	0.02665	0.02597	0.02512	0.02415	0.02307	0.02193	0.02073	0.01951
4.8	0.02649	0.02639	0.02610	0.02563	0.02500	0.02421	0.02331	0.02230	0.02123	0.02011	0.01897
4.9	0.02546	0.02537	0.02510	0.02467	0.02408	0.02335	0.02251	0.02157	0.02056	0.01951	0.01844
5.0	0.02449	0.02441	0.02416	0.02375	0.02321	0.02253	0.02174	0.02087	0.01993	0.01894	0.01793
5.1	0.02358	0.02352	0.02327	0.02289	0.02238	0.02175	0.02101	0.02020	0.01932	0.01839	0.01743
5.2	0.02271	0.02264	0.02242	0.02207	0.02160	0.02101	0.02032	0.01956	0.01873	0.01786	0.01696
5.3	0.02189	0.02182	0.02162	0.02130	0.02085	0.02030	0.01966	0.01894	0.01817	0.01735	0.01650
5.4	0.02111	0.02105	0.02086	0.02056	0.02014	0.01963	0.01903	0.01836	0.01763	0.01686	0.01606
5.5	0.02038	0.02032	0.02014	0.01986	0.01947	0.01899	0.01843	0.01780	0.01711	0.01639	0.01563
5.6	0.01968	0.01962	0.01946	0.01919	0.01883	0.01838	0.01785	0.01726	0.01662	0.01593	0.01522
5.7	0.01901	0.01896	0.01881	0.01856	0.01822	0.01780	0.01730	0.01675	0.01614	0.01549	0.01482
5.8	0.01838	0.01833	0.01819	0.01796	0.01764	0.01724	0.01678	0.01625	0.01568	0.01507	0.01443
5.9	0.01778	0.01774	0.01760	0.01738	0.01709	0.01671	0.01628	0.01578	0.01524	0.01467	0.01406
6.0	0.01721	0.01717	0.01704	0.01684	0.01656	0.01621	0.01579	0.01533	0.01482	0.01427	0.01370
6.1	0.01666	0.01662	0.01651	0.01631	0.01605	0.01572	0.01533	0.01489	0.01441	0.01390	0.01336
6.2	0.01614	0.01611	0.01600	0.01581	0.01557	0.01526	0.01489	0.01448	0.01402	0.01353	0.01302
6.3	0.01565	0.01561	0.01551	0.01534	0.01510	0.01481	0.01447	0.01408	0.01365	0.01318	0.01270
6.4	0.01517	0.01514	0.01504	0.01488	0.01466	0.01439	0.01406	0.01369	0.01328	0.01285	0.01238
6.5	0.01472	0.01469	0.01460	0.01445	0.01424	0.01398	0.01367	0.01332	0.01294	0.01252	0.01208
6.6	0.01429	0.01426	0.01417	0.01403	0.01383	0.01359	0.01330	0.01297	0.01260	0.01221	0.01179
6.7	0.01387	0.01385	0.01376	0.01363	0.01344	0.01321	0.01294	0.01262	0.01228	0.01190	0.01151
6.8	0.01348	0.01345	0.01337	0.01325	0.01307	0.01285	0.01259	0.01229	0.01197	0.01161	0.01123
6.9	0.01310	0.01307	0.01300	0.01288	0.01271	0.01251	0.01226	0.01198	0.01167	0.01133	0.01097
7.0	0.01273	0.01271	0.01264	0.01253	0.01237	0.01217	0.01194	0.01167	0.01138	0.01105	0.01071
7.1	0.01238	0.01236	0.01230	0.01219	0.01204	0.01185	0.01163	0.01138	0.01110	0.01079	0.01046
7.2	0.01205	0.01203	0.01197	0.01186	0.01172	0.01155	0.01133	0.01109	0.01083	0.01053	0.01022
7.3	0.01173	0.01171	0.01165	0.01155	0.01142	0.01125	0.01105	0.01082	0.01056	0.01029	0.00999
7.4	0.01142	0.01140	0.01134	0.01125	0.01112	0.01096	0.01077	0.01056	0.01031	0.01005	0.00977
7.5	0.01112	0.01110	0.01105	0.01096	0.01084	0.01069	0.01051	0.01030	0.01007	0.00982	0.00955
7.6	0.01083	0.01082	0.01077	0.01068	0.01057	0.01043	0.01025	0.01006	0.00984	0.00959	0.00934
7.7	0.01056	0.01054	0.01050	0.01042	0.01031	0.01017	0.01001	0.00982	0.00961	0.00938	0.00913
7.8	0.01030	0.01028	0.01023	0.01016	0.01006	0.00992	0.00977	0.00959	0.00939	0.00917	0.00893
7.9	0.01004	0.01003	0.00998	0.00991	0.00981	0.00969	0.00954	0.00937	0.00918	0.00897	0.00874
8.0	0.00979	0.00978	0.00974	0.00967	0.00958	0.00946	0.00932	0.00915	0.00897	0.00877	0.00855

TABLE 2

INFLUENCE VALUES OF DISTRIBUTION OF TEMPERATURE FROM HEATED STRUCTURE ON PERMAFROST, $T/T_{const} = f(Y/B)$ AND A/B = 2.00

2(A) = FOOTING LENGTH (X-DIRECTION) 2(B) = FOOTING WIDTH (Y-DIRECTION)

A/B= 2.0 X/A= 0.00

Z/B	Y/B										
	0.00	0.25	0.50	0.75	1.00	1.25	1.50	1.75	2.00	2.25	2.50
0.0	1.00000	1.00000	1.00000	1.00000	0.50000	0.00000	0.00000	0.00000	0.00000	0.00000	0.00000
0.1	0.92905	0.92496	0.90873	0.85375	0.47752	0.10083	0.04442	0.02541	0.01636	0.01129	0.00817
0.2	0.85941	0.85175	0.82226	0.73515	0.45517	0.17431	0.08439	0.04946	0.03216	0.02231	0.01619
0.3	0.79226	0.78190	0.74368	0.64649	0.43310	0.21843	0.11714	0.07104	0.04690	0.03280	0.02391
0.4	0.72852	0.71646	0.67398	0.57910	0.41143	0.24212	0.14198	0.08950	0.06021	0.04255	0.03122
0.5	0.66883	0.65601	0.61274	0.52550	0.39028	0.25309	0.15962	0.10458	0.07184	0.05139	0.03801
0.6	0.61353	0.60069	0.55893	0.48101	0.36974	0.25625	0.17128	0.11638	0.08169	0.05924	0.04420
0.7	0.56273	0.55039	0.51147	0.44286	0.34990	0.25452	0.17824	0.12517	0.08977	0.06603	0.04975
0.8	0.51634	0.50482	0.46937	0.40938	0.33083	0.24970	0.18160	0.13135	0.09618	0.07177	0.05462
0.9	0.47416	0.46363	0.43182	0.37954	0.31258	0.24293	0.18226	0.13532	0.10105	0.07648	0.05883
1.0	0.43591	0.42643	0.39816	0.35265	0.29517	0.23495	0.18093	0.13747	0.10456	0.08025	0.06237
1.1	0.40128	0.39283	0.36787	0.32825	0.27863	0.22625	0.17813	0.13814	0.10687	0.08313	0.06529
1.2	0.36995	0.36247	0.34051	0.30600	0.26296	0.21719	0.17429	0.13764	0.10817	0.08523	0.06762
1.3	0.34160	0.33501	0.31574	0.28563	0.24815	0.20800	0.16970	0.13621	0.10860	0.08662	0.06942
1.4	0.31595	0.31015	0.29325	0.26695	0.23420	0.19885	0.16462	0.13407	0.10833	0.08739	0.07072
1.5	0.29271	0.28761	0.27280	0.24978	0.22107	0.18986	0.15922	0.13139	0.10746	0.08764	0.07158
1.6	0.27164	0.26716	0.25416	0.23397	0.20873	0.18110	0.15365	0.12830	0.10613	0.08744	0.07205
1.7	0.25251	0.24857	0.23715	0.21941	0.19716	0.17264	0.14800	0.12493	0.10442	0.08686	0.07218
1.8	0.23511	0.23165	0.22161	0.20598	0.18632	0.16450	0.14236	0.12136	0.10242	0.08596	0.07201
1.9	0.21928	0.21623	0.20738	0.19358	0.17617	0.15672	0.13679	0.11767	0.10020	0.08480	0.07159
2.0	0.20483	0.20214	0.19433	0.18213	0.16667	0.14929	0.13133	0.11391	0.09781	0.08344	0.07095
2.1	0.19164	0.18927	0.18235	0.17154	0.15778	0.14222	0.12602	0.11014	0.09530	0.08190	0.07013
2.2	0.17958	0.17747	0.17134	0.16173	0.14946	0.13551	0.12087	0.10639	0.09271	0.08024	0.06916
2.3	0.16852	0.16666	0.16121	0.15265	0.14169	0.12915	0.11590	0.10269	0.09009	0.07848	0.06806
2.4	0.15838	0.15672	0.15187	0.14423	0.13441	0.12313	0.11112	0.09905	0.08744	0.07664	0.06686
2.5	0.14906	0.14758	0.14325	0.13642	0.12761	0.11744	0.10654	0.09550	0.08480	0.07476	0.06558
2.6	0.14048	0.13915	0.13528	0.12917	0.12124	0.11205	0.10215	0.09205	0.08218	0.07285	0.06425
2.7	0.13257	0.13138	0.12791	0.12242	0.11528	0.10696	0.09795	0.08871	0.07960	0.07092	0.06287
2.8	0.12526	0.12420	0.12108	0.11614	0.10970	0.10216	0.09395	0.08547	0.07707	0.06900	0.06145
2.9	0.11851	0.11755	0.11475	0.11029	0.10446	0.09762	0.09013	0.08235	0.07459	0.06709	0.06002
3.0	0.11225	0.11139	0.10886	0.10484	0.09956	0.09333	0.08649	0.07934	0.07217	0.06520	0.05858
3.1	0.10645	0.10567	0.10339	0.09975	0.09495	0.08928	0.08302	0.07645	0.06982	0.06333	0.05714
3.2	0.10106	0.10036	0.09830	0.09499	0.09063	0.08546	0.07973	0.07368	0.06754	0.06150	0.05570
3.3	0.09606	0.09542	0.09354	0.09054	0.08657	0.08185	0.07659	0.07102	0.06533	0.05971	0.05428
3.4	0.09139	0.09081	0.08911	0.08638	0.08276	0.07843	0.07360	0.06846	0.06320	0.05796	0.05287
3.5	0.08704	0.08652	0.08497	0.08247	0.07917	0.07521	0.07076	0.06602	0.06113	0.05625	0.05149
3.6	0.08298	0.08250	0.08109	0.07881	0.07579	0.07215	0.06806	0.06367	0.05914	0.05459	0.05012
3.7	0.07919	0.07875	0.07746	0.07538	0.07260	0.06926	0.06549	0.06143	0.05722	0.05297	0.04879
3.8	0.07564	0.07524	0.07405	0.07215	0.06960	0.06653	0.06305	0.05929	0.05537	0.05140	0.04748
3.9	0.07231	0.07194	0.07086	0.06911	0.06677	0.06394	0.06072	0.05724	0.05359	0.04989	0.04620
4.0	0.06919	0.06885	0.06786	0.06625	0.06409	0.06148	0.05851	0.05527	0.05188	0.04841	0.04496
4.2	0.06350	0.06322	0.06238	0.06101	0.05918	0.05694	0.05439	0.05160	0.04865	0.04561	0.04257
4.4	0.05847	0.05822	0.05751	0.05634	0.05478	0.05286	0.05065	0.04823	0.04566	0.04300	0.04030
4.6	0.05399	0.05378	0.05317	0.05217	0.05082	0.04917	0.04726	0.04515	0.04290	0.04056	0.03817
4.8	0.04999	0.04981	0.04929	0.04843	0.04726	0.04583	0.04417	0.04233	0.04035	0.03828	0.03617
5.0	0.04641	0.04626	0.04580	0.04506	0.04405	0.04280	0.04135	0.03973	0.03799	0.03616	0.03428
5.2	0.04319	0.04306	0.04266	0.04201	0.04113	0.04004	0.03877	0.03735	0.03582	0.03419	0.03252
5.4	0.04029	0.04017	0.03983	0.03926	0.03849	0.03754	0.03642	0.03517	0.03380	0.03236	0.03086
5.6	0.03766	0.03756	0.03726	0.03676	0.03609	0.03524	0.03426	0.03315	0.03194	0.03065	0.02931
5.8	0.03528	0.03519	0.03492	0.03449	0.03389	0.03315	0.03228	0.03129	0.03021	0.02906	0.02786
6.0	0.03311	0.03303	0.03280	0.03241	0.03188	0.03123	0.03045	0.02957	0.02861	0.02758	0.02650
6.2	0.03113	0.03106	0.03086	0.03051	0.03005	0.02946	0.02877	0.02799	0.02713	0.02620	0.02522
6.4	0.02932	0.02926	0.02908	0.02877	0.02836	0.02784	0.02722	0.02652	0.02574	0.02491	0.02403
6.6	0.02767	0.02761	0.02745	0.02718	0.02680	0.02634	0.02578	0.02515	0.02446	0.02371	0.02291
6.8	0.02614	0.02609	0.02595	0.02570	0.02537	0.02495	0.02445	0.02389	0.02326	0.02258	0.02186
7.0	0.02474	0.02470	0.02456	0.02435	0.02405	0.02367	0.02322	0.02271	0.02214	0.02153	0.02087
7.2	0.02345	0.02341	0.02329	0.02309	0.02282	0.02248	0.02208	0.02162	0.02110	0.02054	0.01995
7.4	0.02225	0.02221	0.02211	0.02193	0.02169	0.02138	0.02101	0.02059	0.02013	0.01962	0.01908
7.6	0.02114	0.02111	0.02101	0.02085	0.02063	0.02035	0.02002	0.01964	0.01922	0.01875	0.01826
7.8	0.02011	0.02008	0.01999	0.01985	0.01965	0.01940	0.01910	0.01875	0.01836	0.01794	0.01749
8.0	0.01915	0.01913	0.01905	0.01892	0.01874	0.01851	0.01823	0.01792	0.01756	0.01718	0.01676
8.2	0.01826	0.01824	0.01817	0.01805	0.01788	0.01767	0.01742	0.01713	0.01681	0.01646	0.01608
8.4	0.01743	0.01741	0.01735	0.01724	0.01708	0.01689	0.01667	0.01640	0.01611	0.01578	0.01543
8.6	0.01666	0.01664	0.01658	0.01648	0.01634	0.01616	0.01596	0.01571	0.01544	0.01514	0.01482
8.8	0.01593	0.01591	0.01586	0.01577	0.01564	0.01548	0.01529	0.01507	0.01482	0.01454	0.01424
9.0	0.01525	0.01524	0.01518	0.01510	0.01498	0.01484	0.01466	0.01446	0.01423	0.01397	0.01370
9.2	0.01461	0.01460	0.01455	0.01448	0.01437	0.01423	0.01407	0.01388	0.01367	0.01344	0.01318
9.4	0.01402	0.01400	0.01396	0.01389	0.01379	0.01367	0.01352	0.01334	0.01315	0.01293	0.01269
9.6	0.01345	0.01344	0.01340	0.01334	0.01324	0.01313	0.01299	0.01283	0.01265	0.01245	0.01223
9.8	0.01292	0.01291	0.01287	0.01281	0.01273	0.01262	0.01250	0.01235	0.01218	0.01199	0.01179
10.0	0.01242	0.01241	0.01238	0.01232	0.01225	0.01215	0.01203	0.01189	0.01174	0.01156	0.01138
10.2	0.01195	0.01194	0.01191	0.01186	0.01179	0.01170	0.01159	0.01146	0.01131	0.01115	0.01098
10.4	0.01151	0.01150	0.01147	0.01142	0.01135	0.01127	0.01117	0.01105	0.01091	0.01077	0.01060
10.6	0.01109	0.01108	0.01105	0.01101	0.01094	0.01087	0.01077	0.01066	0.01054	0.01040	0.01024
10.8	0.01069	0.01068	0.01065	0.01061	0.01056	0.01048	0.01039	0.01029	0.01017	0.01005	0.00990
11.0	0.01031	0.01030	0.01028	0.01024	0.01019	0.01012	0.01004	0.00994	0.00983	0.00971	0.00958
11.2	0.00995	0.00995	0.00992	0.00989	0.00984	0.00977	0.00970	0.00961	0.00951	0.00939	0.00927
11.4	0.00961	0.00961	0.00959	0.00955	0.00951	0.00945	0.00937	0.00929	0.00920	0.00909	0.00897
11.6	0.00929	0.00928	0.00927	0.00923	0.00919	0.00913	0.00907	0.00899	0.00890	0.00880	0.00869
11.8	0.00898	0.00898	0.00896	0.00893	0.00889	0.00884	0.00878	0.00870	0.00862	0.00853	0.00842
12.0	0.00869	0.00869	0.00867	0.00864	0.00860	0.00856	0.00850	0.00843	0.00835	0.00826	0.00817

TABLE 3

INFLUENCE VALUES OF DISTRIBUTION OF TEMPERATURE FROM HEATED STRUCTURE ON PERMAFROST, $T/T_{const} = f(Y/B)$ AND A/B = 1,000 ≈ ∞

2(A) = FOOTING LENGTH (X-DIRECTION) 2(B) = FOOTING WIDTH (Y-DIRECTION)

A/B=1000.0 X/A= 0.00

TABLE C

Z/B	Y/B										
	0.00	0.25	0.50	0.75	1.00	1.25	1.50	1.75	2.00	2.25	2.50
0.0	1.00000	1.00000	1.00000	1.00000	0.50000	0.00000	0.00000	0.00000	0.00000	0.00000	0.00000
0.1	0.93655	0.93240	0.91598	0.86071	0.48410	0.10698	0.05011	0.03062	0.02112	0.01562	0.01210
0.2	0.87433	0.86655	0.83669	0.74900	0.46827	0.18656	0.09571	0.05984	0.04164	0.03094	0.02402
0.3	0.81445	0.80390	0.76515	0.66710	0.45261	0.23667	0.13401	0.08653	0.06105	0.04568	0.03562
0.4	0.75776	0.74546	0.70227	0.60628	0.43717	0.26619	0.16427	0.10998	0.07893	0.05960	0.04673
0.5	0.70483	0.69171	0.64758	0.55900	0.42202	0.28281	0.18717	0.12992	0.09501	0.07253	0.05725
0.6	0.65596	0.64277	0.60002	0.52053	0.40723	0.29138	0.20388	0.14640	0.10919	0.08434	0.06708
0.7	0.61120	0.59848	0.55845	0.48807	0.39283	0.29480	0.21567	0.15969	0.12143	0.09497	0.07615
0.8	0.57045	0.55852	0.52185	0.45993	0.37888	0.29485	0.22361	0.17015	0.13182	0.10439	0.08443
0.9	0.53348	0.52251	0.48939	0.43504	0.36540	0.29264	0.22859	0.17818	0.14049	0.11264	0.09191
1.0	0.50000	0.49006	0.46042	0.41273	0.35242	0.28890	0.23130	0.18415	0.14758	0.11976	0.09858
1.1	0.46971	0.46077	0.43439	0.39251	0.33994	0.28412	0.23226	0.18840	0.15328	0.12583	0.10448
1.2	0.44228	0.43430	0.41089	0.37405	0.32798	0.27866	0.23188	0.19122	0.15774	0.13092	0.10964
1.3	0.41743	0.41032	0.38957	0.35710	0.31653	0.27276	0.23049	0.19287	0.16113	0.13512	0.11410
1.4	0.39486	0.38855	0.37016	0.34147	0.30560	0.26658	0.22832	0.19356	0.16358	0.13853	0.11791
1.5	0.37433	0.36873	0.35242	0.32701	0.29517	0.26026	0.22556	0.19347	0.16525	0.14122	0.12112
1.6	0.35562	0.35063	0.33615	0.31358	0.28522	0.25390	0.22237	0.19274	0.16623	0.14328	0.12378
1.7	0.33851	0.33407	0.32118	0.30109	0.27575	0.24756	0.21886	0.19150	0.16664	0.14478	0.12594
1.8	0.32283	0.31888	0.30739	0.28945	0.26674	0.24129	0.21512	0.18985	0.16656	0.14579	0.12766
1.9	0.30843	0.30490	0.29463	0.27857	0.25816	0.23514	0.21123	0.18788	0.16608	0.14638	0.12897
2.0	0.29517	0.29201	0.28281	0.26839	0.25000	0.22912	0.20724	0.18565	0.16525	0.14659	0.12992
2.1	0.28293	0.28009	0.27183	0.25886	0.24224	0.22325	0.20321	0.18322	0.16414	0.14649	0.13055
2.2	0.27160	0.26905	0.26162	0.24991	0.23485	0.21756	0.19915	0.18064	0.16279	0.14611	0.13089
2.3	0.26110	0.25880	0.25209	0.24150	0.22783	0.21204	0.19512	0.17795	0.16125	0.14550	0.13099
2.4	0.25133	0.24926	0.24319	0.23358	0.22114	0.20670	0.19112	0.17519	0.15956	0.14469	0.13086
2.5	0.24224	0.24036	0.23485	0.22613	0.21478	0.20154	0.18717	0.17237	0.15774	0.14370	0.13055
2.6	0.23375	0.23204	0.22704	0.21909	0.20871	0.19656	0.18328	0.16953	0.15582	0.14257	0.13006
2.7	0.22581	0.22426	0.21970	0.21244	0.20294	0.19175	0.17948	0.16667	0.15383	0.14133	0.12943
2.8	0.21838	0.21696	0.21280	0.20615	0.19743	0.18712	0.17575	0.16383	0.15178	0.13998	0.12867
2.9	0.21140	0.21010	0.20629	0.20020	0.19218	0.18266	0.17212	0.16099	0.14970	0.13855	0.12781
3.0	0.20483	0.20364	0.20015	0.19456	0.18717	0.17837	0.16857	0.15819	0.14758	0.13706	0.12685
3.1	0.19865	0.19756	0.19435	0.18920	0.18238	0.17423	0.16512	0.15542	0.14546	0.13551	0.12582
3.2	0.19282	0.19182	0.18886	0.18411	0.17781	0.17025	0.16177	0.15269	0.14332	0.13393	0.12472
3.3	0.18732	0.18639	0.18366	0.17927	0.17344	0.16641	0.15851	0.15001	0.14120	0.13231	0.12356
3.4	0.18211	0.18125	0.17873	0.17467	0.16925	0.16272	0.15534	0.14737	0.13908	0.13068	0.12236
3.5	0.17717	0.17638	0.17405	0.17028	0.16525	0.15916	0.15226	0.14479	0.13698	0.12903	0.12112
3.6	0.17249	0.17176	0.16959	0.16610	0.16141	0.15574	0.14928	0.14226	0.13490	0.12737	0.11985
3.7	0.16804	0.16736	0.16535	0.16210	0.15774	0.15244	0.14639	0.13979	0.13284	0.12571	0.11856
3.8	0.16382	0.16318	0.16132	0.15828	0.15421	0.14925	0.14358	0.13738	0.13081	0.12406	0.11725
3.9	0.15979	0.15920	0.15746	0.15464	0.15083	0.14619	0.14086	0.13502	0.12882	0.12241	0.11593
4.0	0.15596	0.15541	0.15378	0.15114	0.14758	0.14323	0.13822	0.13272	0.12685	0.12078	0.11461
4.2	0.14880	0.14833	0.14690	0.14459	0.14146	0.13762	0.13319	0.12828	0.12303	0.11755	0.11195
4.4	0.14227	0.14185	0.14060	0.13856	0.13680	0.13240	0.12845	0.12407	0.11935	0.11440	0.10931
4.6	0.13627	0.13590	0.13480	0.13300	0.13055	0.12752	0.12400	0.12006	0.11581	0.11133	0.10670
4.8	0.13076	0.13043	0.12945	0.12785	0.12566	0.12296	0.11981	0.11627	0.11243	0.10836	0.10413
5.0	0.12566	0.12537	0.12450	0.12307	0.12112	0.11870	0.11586	0.11267	0.10919	0.10549	0.10163
5.2	0.12095	0.12069	0.11991	0.11862	0.11687	0.11469	0.11213	0.10925	0.10609	0.10271	0.09918
5.4	0.11657	0.11633	0.11563	0.11448	0.11291	0.11094	0.10862	0.10600	0.10313	0.10004	0.09680
5.6	0.11250	0.11228	0.11165	0.11061	0.10919	0.10741	0.10531	0.10292	0.10030	0.09748	0.09450
5.8	0.10869	0.10850	0.10793	0.10699	0.10570	0.10408	0.10217	0.09999	0.09760	0.09501	0.09227
6.0	0.10514	0.10496	0.10444	0.10359	0.10241	0.10094	0.09920	0.09721	0.09501	0.09264	0.09011
6.2	0.10180	0.10164	0.10117	0.10039	0.09932	0.09798	0.09639	0.09457	0.09255	0.09036	0.08803
6.4	0.09867	0.09853	0.09810	0.09739	0.09641	0.09518	0.09372	0.09205	0.09019	0.08817	0.08601
6.6	0.09573	0.09560	0.09520	0.09455	0.09366	0.09253	0.09119	0.08965	0.08793	0.08607	0.08407
6.8	0.09295	0.09283	0.09247	0.09187	0.09105	0.09001	0.08878	0.08736	0.08578	0.08405	0.08220
7.0	0.09033	0.09022	0.08989	0.08934	0.08858	0.08763	0.08649	0.08518	0.08371	0.08211	0.08039
7.2	0.08786	0.08775	0.08745	0.08694	0.08624	0.08536	0.08431	0.08309	0.08174	0.08025	0.07865
7.4	0.08551	0.08541	0.08513	0.08467	0.08402	0.08320	0.08223	0.08110	0.07984	0.07846	0.07697
7.6	0.08329	0.08320	0.08294	0.08250	0.08191	0.08115	0.08024	0.07920	0.07803	0.07674	0.07534
7.8	0.08117	0.08109	0.08085	0.08045	0.07989	0.07919	0.07835	0.07738	0.07629	0.07508	0.07378
8.0	0.07916	0.07909	0.07886	0.07849	0.07798	0.07732	0.07654	0.07563	0.07461	0.07349	0.07227
8.2	0.07725	0.07718	0.07697	0.07663	0.07615	0.07554	0.07481	0.07396	0.07301	0.07196	0.07082
8.4	0.07543	0.07537	0.07517	0.07485	0.07440	0.07383	0.07315	0.07236	0.07147	0.07048	0.06942
8.6	0.07369	0.07363	0.07345	0.07315	0.07273	0.07220	0.07156	0.07082	0.06999	0.06906	0.06806
8.8	0.07203	0.07197	0.07180	0.07152	0.07113	0.07064	0.07004	0.06935	0.06856	0.06770	0.06675
9.0	0.07044	0.07039	0.07023	0.06997	0.06960	0.06914	0.06858	0.06793	0.06719	0.06638	0.06549
9.2	0.06892	0.06887	0.06873	0.06848	0.06813	0.06770	0.06717	0.06656	0.06587	0.06510	0.06427
9.4	0.06747	0.06742	0.06728	0.06705	0.06673	0.06632	0.06582	0.06525	0.06460	0.06387	0.06309
9.6	0.06607	0.06603	0.06590	0.06568	0.06538	0.06499	0.06453	0.06398	0.06337	0.06269	0.06194
9.8	0.06473	0.06469	0.06457	0.06436	0.06408	0.06372	0.06328	0.06277	0.06219	0.06154	0.06084
10.0	0.06345	0.06341	0.06329	0.06310	0.06283	0.06249	0.06207	0.06159	0.06105	0.06044	0.05977
10.2	0.06221	0.06218	0.06207	0.06188	0.06163	0.06131	0.06091	0.06046	0.05994	0.05937	0.05874
10.4	0.06102	0.06099	0.06088	0.06071	0.06047	0.06017	0.05980	0.05937	0.05888	0.05833	0.05773
10.6	0.05986	0.05985	0.05975	0.05958	0.05936	0.05907	0.05872	0.05831	0.05785	0.05733	0.05676
10.8	0.05878	0.05874	0.05865	0.05850	0.05828	0.05801	0.05768	0.05729	0.05685	0.05636	0.05582
11.0	0.05771	0.05768	0.05760	0.05745	0.05725	0.05699	0.05667	0.05631	0.05589	0.05542	0.05491
11.2	0.05669	0.05666	0.05658	0.05644	0.05624	0.05600	0.05570	0.05535	0.05496	0.05452	0.05403
11.4	0.05570	0.05567	0.05559	0.05546	0.05528	0.05504	0.05476	0.05443	0.05405	0.05363	0.05317
11.6	0.05474	0.05472	0.05464	0.05452	0.05434	0.05412	0.05385	0.05354	0.05318	0.05278	0.05234
11.8	0.05382	0.05379	0.05372	0.05360	0.05344	0.05323	0.05297	0.05267	0.05233	0.05195	0.05153
12.0	0.05293	0.05290	0.05283	0.05272	0.05256	0.05236	0.05212	0.05184	0.05151	0.05115	0.05075

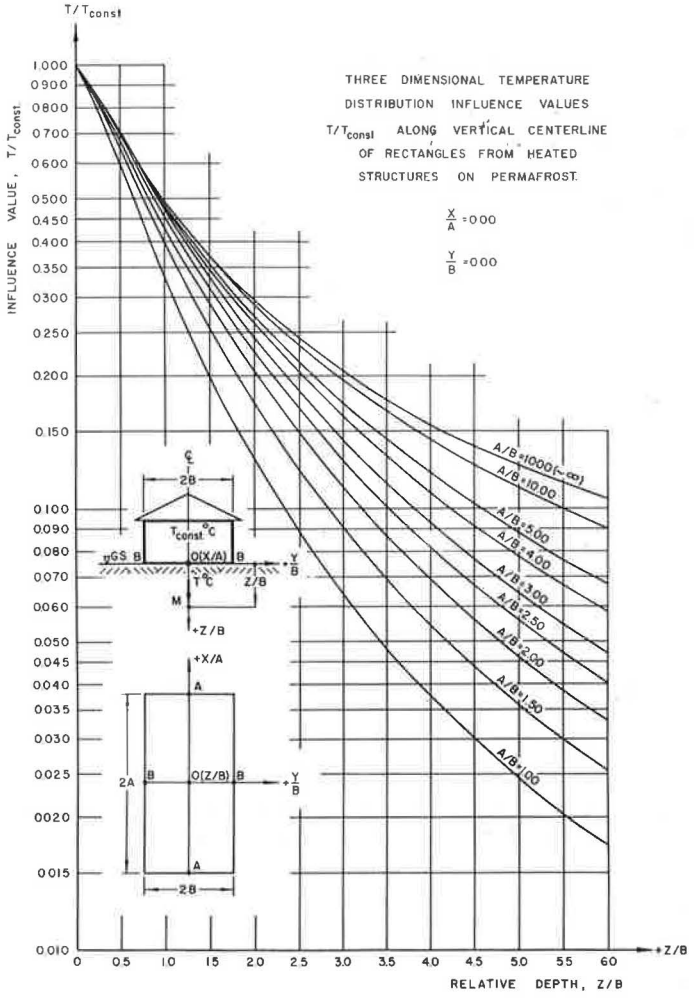

Figure 3. Influence values of distribution of temperature from heated structure on permafrost, T/T_{const} along vertical centerline of rectangles.

ACKNOWLEDGMENT

In preparing the tables, graphs, and this paper, the author acknowledges support given to him from the following persons: E. C. Easton, College of Engineering and Bureau of Engineering Research; R. C. Ahlert, Bureau of Engineering Research; M. L. Granstrom, Department of Civil and Environmental Engineering; and J. Wiesenfeld, Department of Civil and Environmental Engineering, all of Rutgers University. P. B. Singh, a graduate student in civil engineering, programmed the influence values.

REFERENCES

1. Lachenbruch, A. H. Three-Dimensional Heat Conduction in Permafrost Beneath Heated Buildings. U.S. Geological Survey, Bull. 1052-B, 1957, pp. 51-69.
2. Jumikis, A. R. Vertical Stress Distribution Influence Value Tables for Any Point in Soil Under Uniformly Distributed Loads. College of Engineering, Rutgers Univ., The State University of New Jersey, Engineering Research Publ. 52, 1971.

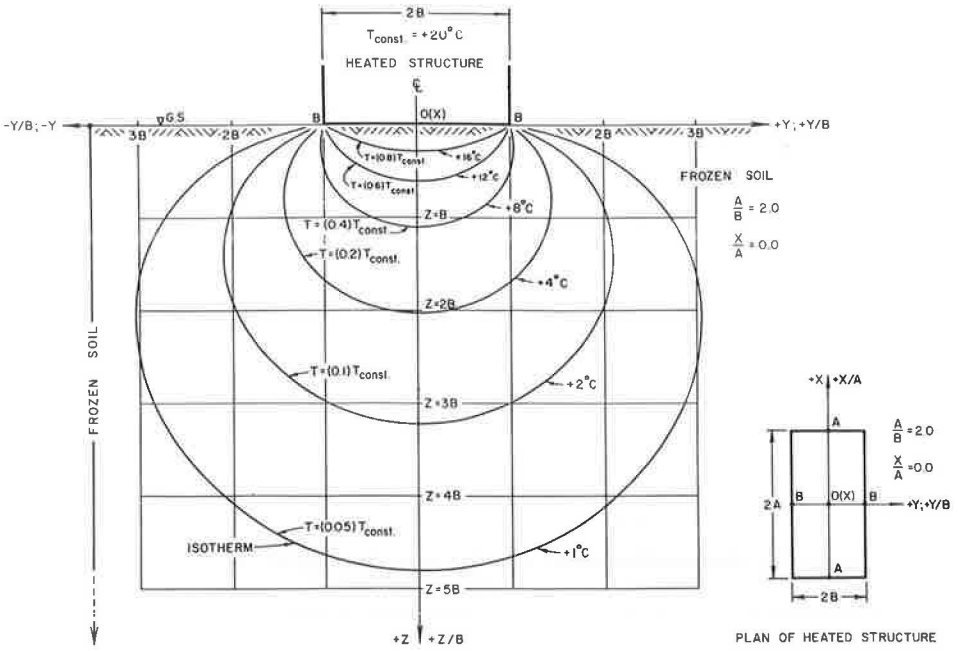

Figure 4. Disturbance temperature isotherms underneath a heated rectangular structure.

3. Porkhayev, G. V. Temperature Fields in Foundations. In Permafrost: Proc. of Internat. Conf., NAS-NRC Publ. 1287, 1966, pp. 285-291.

HIGHWAY DESIGNS TO RESIST SUBGRADE MOISTURE VARIATIONS

T. Allan Haliburton, School of Civil Engineering, Oklahoma State University

Findings, conclusions, and recommendations of a 6-year study to measure Oklahoma subgrade moisture conditions are presented. General trends in Oklahoma subgrade moisture are described, as are the effects of highway components on subgrade moisture behavior. Resistance of various highway components to subgrade moisture effects is also discussed, and specific recommendations are made for highway design and construction on expansive subgrades. Two modes of behavior, subgrade moisture accumulation and subgrade moisture variation, were found to exist under Oklahoma pavement systems. Combinations of these 2 modes also occurred. Rigid pavements were found to be extremely susceptible to cracking from vertical and lateral subgrade expansion, with resulting infiltration of water to the subgrade. However, rigid pavements performed well until upper subgrade moisture contents approached the liquid limit. Flexible pavements were more resistant to cracking from vertical and lateral subgrade expansion but were susceptible to distress when subgrade moisture contents approached the equilibrium value of 1.1 to 1.3 times the plastic limit. Recommendations include the use of a flexible and impervious base, subbase, or membrane component below the wearing surface of any pavement on expansive subgrades. Improved shoulders at least 8 ft in width are recommended, as is the establishment of equal drainage behavior on both sides of the highway section. More detailed subgrade soil testing techniques are also recommended.

•THIS PAPER summarizes findings and recommendations from a 6-year study of subgrade moisture conditions under existing Oklahoma highways. Conducted by the School of Civil Engineering at Oklahoma State University, the project was formally initiated in June 1964. After preliminary planning (1), the first of 52 field test sites was installed under existing pavement in June 1966 (2). Subgrade moisture and density data were collected periodically with nuclear depth moisture and density probes, which were calibrated for particular Oklahoma soil conditions (3, 4). In addition to subgrade moisture and density data, information concerning the following factors was compiled: precipitation, air temperature, soil type, highway design and construction history, pavement and shoulder performance, traffic, subgrade temperature, and pavement heave or settlement or both.

Data were reduced immediately on collection, and continual evaluations were carried out during the 4-year data collection phase of research. Periodically, overall evaluations were made of all data collected to date (5, 6, 7, 8, 9). Data collection was discontinued in June 1970.

SUBGRADE MOISTURE BEHAVIOR IN OKLAHOMA

This section summarizes research findings concerning subgrade moisture behavior observed under existing Oklahoma highways. More detailed analyses and data from which conclusions were drawn are available elsewhere (5, 6, 7, 8, 10, 11, 12, 13).

Sponsored by Committee on Environmental Factors Except Frost and presented at the 50th Annual Meeting.

General Conditions Existing in Oklahoma

All sites were located on existing highways in the central and north central-northeastern part of Oklahoma. Annual rainfall in this region varies between 10 and 40 in., increasing from west to east. Monthly rainfall amounts are highly seasonal; more than 12 in. may fall during the spring in the eastern part of the state, and only 2 in. or less may fall during the winter at some western locations. The average monthly mean of air temperatures range from over 80 F during July and August to approximately 30 F during January and February. In many regions of the state, the water table is located close to the surface and exhibits seasonal movement, rising during winter months and falling during summer months. A period of drought in Oklahoma ended in 1965, just before installation of the first field research sites.

Clays and clay shales often utilized as subgrade material in this portion of the state may vary somewhat, but their origins and stress histories are similar. These soils are normally classified by the AASHO system as A-6 to A-7 and by the Unified system in the upper portion of the CL range or in the CH range. The majority of cohesive soils are preconsolidated (usually by desiccation) and, after remolding, exhibit higher volume change potential than might be predicted from plasticity alone, particularly if compaction is dry of optimum.

Observed Trends in Subgrade Moisture Behavior

Data obtained from the study indicate that 2 basic types of moisture behavior, subgrade moisture accumulation and subgrade moisture variation, exist in expansive Oklahoma subgrades. Factors responsible for each type of behavior are summarized in the following sections.

Subgrade Moisture Accumulation—Subgrade moisture contents under new and relatively new construction and older existing pavements with wide improved shoulders and excellent pavement ratings tended, after a short initial period at construction moisture contents (usually below optimum compaction moisture), to increase without significant variation during an 18- to 24-month period until an equilibrium moisture content of approximately 1.1 to 1.3 times the subgrade plastic limit was reached. The word equilibrium is actually a misnomer because, in most cases, variations in moisture content begin to occur after the equilibrium point has been reached. The prime criterion for subgrade moisture accumulation without significant variation was found to be an impervious pavement system.

For these impervious pavements, moisture accumulation is thought to occur primarily from capillary sources, i.e., prevention of evaporation, but some sites obtain moisture by infiltration from outside paved shoulders. Subgrade temperature gradients were found to cause only small moisture changes (5).

Moisture accumulation noted under older construction in excellent condition probably resulted from the end of a drought cycle in 1965 just before the first research sites were installed. Increased availability of moisture from rainfall and rising water tables probably caused this behavior.

At sites with less than excellent pavement ratings (usually indicative of pervious pavement or open joints), open shoulders, or fair-to-poor drainage, subgrade moisture variations were found to occur superimposed on the overall accumulation trend. The majority of these moisture variations were caused by rainfall infiltration and evaporation, usually from outside the shoulders or through the pavement surface, but they did not appear to halt the rate of moisture accumulation, which continued in most cases until subgrade moisture contents were above the plastic limit. After reaching this equilibrium value, moisture contents at the first 2 types of sites were subject to large variations. Initial accumulation behavior noted at these sites is also thought to result from general drying of subgrade caused by the previously mentioned drought.

Subgrade Moisture Variation—At most research sites where moisture accumulation was not in progress, moisture variations were found either to occur seasonally in annual cycles (with maximum moisture contents occurring during winter months) or to be precipitation dependent. Most research sites where purely seasonal moisture variations occurred were on pavement that was rated as being excellent and impervious, and

moisture variations had little relation to measured precipitation, particularly under pavement centerlines. It was thought initially that these variations were temperature induced, but, although temperature-induced moisture migration does occur in Oklahoma subgrades, it is of relatively low magnitude, causing only a 1 or 2 percent engineering moisture content variation annually (5). In almost all cases for sites where moisture variations were seasonal and could not be related to rainfall, the great majority of moisture variation was found to be caused by seasonal water table movement, moving the zone of capillary rise, or else by delayed infiltration from areas adjacent to the pavement, caused by particular highway drainage conditions. Most seasonal variations under impervious systems did not exceed 5 percent engineering moisture content, and many were half this value.

Seasonal trends were also noted to occur at sites located on pervious pavements, but cyclic variations were affected considerably by precipitation. Precipitation-dependent variations were also noted to occur at most sites having open shoulders, despite pavement condition. Many sites where precipitation and evaporation affected subgrade soil moisture were located on rigid pavement sections modified by asphaltic concrete overlay.

As a general rule, upper subgrade moisture variations generally lagged rainfall by 6 to 8 weeks, with longer times being required for variations to occur at deeper depths. Magnitude of variations was highly dependent on overall pavement condition, whether or not sealed shoulders were present, and on type of base and subbase material used in the pavement section. The magnitude of variations caused by precipitation and evaporation was almost always higher than that of variations produced by seasonal trends. At some sites the variations exceeded 10 to 15 percent engineering moisture content during 6-month periods and produced easily noticeable changes in pavement and shoulder condition. At some sites, rainfall infiltration produced moisture contents close to the subgrade liquid limit, with resulting loss of subgrade support and rapid pavement deterioration.

Effect of Subgrade Moisture Behavior on Soil Volume Change

Oklahoma cohesive soils are particularly subject to volume change as moisture content varies. Volume change data were obtained from moisture measurements, subsurface bench marks installed at research sites (7, 11), and general observations of pavement behavior. At most research sites only the upper 5 to 7 ft of the subgrade made any large contribution to subgrade volume change; moisture contents below this level remained relatively constant. Vertical movements were not extremely large. An empirical relationship of 1 in. of pavement heave for a 10 to 12 percent increase in engineering moisture content was developed from obtained data. This correlation was extrapolated from smaller recorded measurements (1/2 to 5/8 in.) obtained at several sites on A-6 and A-7 subgrades. Moisture contents were in the vicinity of the subgrade plastic limit.

However, lateral subgrade expansion probably affects pavement performance to a larger extent than vertical swelling. The unit swelling potential of cohesive Oklahoma subgrades, compacted under normal conditions, is lower in the lateral direction than in the vertical (14). However, lateral subgrade expansion takes place over a 24- to 40-ft width, and resulting movements were found, in some cases, to exceed 3 to 5 in. Tensile stresses, produced by lateral subgrade expansion, in the pavement system caused longitudinal cracking of the subbase, base, and pavement structure. This cracking was aggravated by flexural stresses from differential vertical heaving, even though the heaving was of rather low magnitude.

Different vertical movement conditions were encountered under moderate and high fill sections. For these sections, moisture movement was downward and toward the outer edges of the fill, was caused by shoulder drying, and resulted in shoulder settlements of up to several inches in magnitude during dry periods. Some rebound was observed in succeeding wet periods.

INFLUENCE OF HIGHWAY DESIGN FACTORS ON SUBGRADE MOISTURE BEHAVIOR

Subgrade moisture behavior was definitely affected by highway design. The effects of improved shoulder width, drainage conditions, highway profile, traffic, and construction procedure are given in this section. Instances of behavior and detailed case histories substantiating these findings are given elsewhere (6, 7, 12, 13).

Improved Shoulder Width

At all research sites observed, increasing shoulder width reduced the effects of runoff infiltration. Furthermore, in impervious sections with wide improved shoulders, the wet-dry interface or distinct transition point from fluctuation to more nearly stable subgrade moisture content occurred underneath the shoulders, whereas for pavements with open shoulders or narrow improved shoulders it occurred under the pavement. Less severe differential movements from more uniform moisture content were thus expected and observed for impervious pavement with wide shoulders. The wet-dry interface was found to occur approximately 5 to 7 ft from the outside edge of a covered area. Therefore, to keep the wet-dry interface from underneath the pavement, a shoulder width of at least 8 ft is required.

Highway Drainage Conditions

Drainage conditions or rainfall infiltration tendencies or both were found to be closely related to both shoulder slope and ditch design. Steeper shoulder slopes reduced infiltration into the subgrade, and the elimination of ponding by the quick removal of surface runoff in ditches further reduced infiltration at most of the research sites where these drainage conditions existed. Gently sloping shoulder slopes were found to cause greater infiltration of runoff. However, ponding and improper ditch drainage, e.g., where ditches remained full for several days after a rain, caused measurable infiltration despite good shoulder slope conditions.

Nonuniform infiltration, producing differential moisture contents across the pavement section, was found to occur at many research sites. For undivided highways, this behavior usually occurred when the highways were constructed normal to an existing slope, with good drainage on 1 side and a tendency for ponding on the other. However, differential subgrade moisture contents from different infiltration rates were found under almost all 4-lane divided highways. It appears much more difficult to obtain good median drainage, and the median side of the divided highway usually experienced both higher maximum and average moisture contents and greater fluctuations at upper subgrade levels.

Good drainage produced lower average subgrade moisture contents at the cost of higher variation and distinct wet-dry interface behavior. Poor drainage produced higher average moisture contents but less variation.

Highway Profile

Type of highway profile also affected subgrade moisture conditions; pavements on grade or in slight cuts usually exhibit both higher pavement ratings and more nearly uniform subgrade moisture conditions, particularly in the upper subgrade levels. Fill and transition sections usually had lower pavement and shoulder ratings than other sections and also exhibited more moisture content variation, particularly at the pavement edges.

Traffic Volume

Despite several attempts during the study, significant correlations between traffic volume and subgrade moisture-related highway performance could not be established. Even when traffic volume was reduced to the general classifications of light, medium, and heavy, the only conclusion found was the obvious one that, after initial cracking or rutting or both of these rendered the pavement system pervious, higher traffic volumes

produced more rapid pavement deterioration. These data, coupled with observations that pervious bases were not usually found with degrees of saturation high enough to negate conventional wheel load distribution assumptions, form the basis for the conclusion that subgrade moisture conditions are more important than traffic volumes in determining initial (and thus, to some extent, final) pavement performance. This conclusion is also based on the assumption that at least a semirational method of considering traffic loadings and pavement stresses was used in pavement system design.

Current Oklahoma Highway Construction Procedure

Most new construction in Oklahoma is done by stage methods under a long-term planning program. Contracts for grading and drainage structures are usually let and completed, and contracts for base and surfacing are let at some later time. This construction practice results in bringing the subgrade to its approximate final level and then in leaving it for an extended period before a covering or wearing surface is applied. During the interim, several things occur. First, moisture contents in the prepared subgrade reach some equilibrium condition compatible with moisture contents in the natural subgrade below and with existing climatological conditions. This equilibrium is likely to undergo seasonal changes, becoming wetter in general during winter months and drier during summer months. Also, precipitation in Oklahoma is usually infrequent but heavy when it does occur. As a result, considerable runoff occurs across the prepared subgrade and produces erosion damage.

Another fairly common practice in Oklahoma is the use of prepared subgrades by farmers for movement of agricultural equipment either prohibited from or hazardous to on-pavement travel. If done for an extended period of time, this practice results in raveling of the subgrade during drier periods and rutting of the subgrade during wetter periods.

As a result of these factors, the original subgrade level is changed and no longer remains suitable for use as a working surface. The base-surfacing contractor is, therefore, usually required to scarify and recompact at least the upper portions of subgrade along the highway profile. Also, highway construction in Oklahoma is usually performed in warm spring and hot summer months. At this time the moisture in the uncovered subgrade is likely to be less to a considerable depth than the original compaction moisture. Compaction of cohesive subgrades in Oklahoma is usually done dry of optimum because optimum compaction moisture is either slightly below or at the plastic limit of the material. The end result is to produce a subgrade with an average moisture content in the upper portions of at least 5 percent moisture content below the subgrade plastic limit. Base and impervious (at least initially) surfacing are immediately applied over this material, and then subgrade moisture accumulation begins.

The author is not criticizing the idea of staged construction because many advantages exist for its use, particularly in Oklahoma. However, other methods of staged construction should be considered that would provide better initial subgrade moisture conditions. Current construction practice appears to be aggravating the subgrade moisture problem in Oklahoma instead of minimizing it.

EFFECTIVENESS OF HIGHWAY COMPONENTS IN PREVENTING AND RESISTING SUBGRADE MOISTURE CHANGES

This section discusses various pavement system components currently being used in Oklahoma highway construction and the resistance of components to subgrade moisture variations. Recommendations for use of certain pavement components in particular situations are also given. Additional descriptions of behavior, collected data, and case histories are given elsewhere (8, 9, 10, 11).

General Philosophy for Highway Design on Expansive Oklahoma Subgrades

Most published criteria for pavement design to resist effects of subgrade moisture are concerned with keeping moisture out of the subgrade. However, particular environmental conditions existing in the more populous areas of Oklahoma, coupled with

methods currently favored for all new construction, make it unlikely that construction moisture contents can be maintained for even short periods.

Therefore, it appears logical to develop highway designs that allow subgrade moisture contents to increase to their equilibrium condition as quickly as possible and to stay there. The system should be designed to remain impervious after differential vertical and lateral expansion associated with Oklahoma subgrade moisture accumulation has occurred. Deterioration of Oklahoma highways must be prevented by not allowing the infiltration and evaporation cycle through pervious pavement systems to begin.

Performance of Surfacing

Current Oklahoma highway design procedures involve use of both flexible and rigid pavements. Type of surfacing or surface course used was found to have little, if any, initial effect on observed subgrade moisture behavior. Of more importance was whether the surface was pervious or impervious because the wearing surface itself simply serves to keep moisture out of the subgrade or else let it infiltrate through cracks.

Rigid pavements were found to be more sensitive to longitudinal cracking than their flexible counterparts and were extremely sensitive to moisture infiltration through joints opened from thermal contraction and lateral subgrade expansion. However, rigid pavements were found to perform adequately for extended periods, after initial cracking and resulting infiltration had begun, and to maintain relatively good riding characteristics at subgrade moisture contents higher than those that were observed for flexible systems. The phenomena of pumping, widespread and severe cracking, subgrade shifting, and rapid deterioration did not usually occur until subgrade layers immediately under the pavement reached moisture contents considerably above the plastic limit and sometimes near the liquid limit.

Flexible pavements or pavement systems consisted either of asphaltic concrete surfacing over some other type of base or subbase (or both) or else asphaltic concrete surfacing over some other type of asphaltic base or subbase. In general, better performance was obtained from multilayer asphaltic systems, as opposed to asphalt over nonasphalt systems. Flexible pavements were found to be highly resistant to cracking caused by small differential vertical movements and lateral subgrade expansion, especially when more than 1 component of the system was composed of asphaltic materials. However, flexible pavements were extremely sensitive to failure by loss of subgrade support when the moisture content of the upper subgrade material approached and exceeded the plastic limit. Failure was characterized by rutting, which was followed by pavement cracking. Cracks usually extended down to the subgrade material, and infiltration and evaporation of rainfall produced further deterioration and general cracking. Better observed performance of all-asphaltic systems probably results more from a thicker layer of asphaltic material that must be cracked to allow infiltration and evaporation than from any outstanding load-bearing or distributing characteristics of the material.

Recommendations Concerning Type of Surfacing

Portland cement concrete and asphaltic concrete surfacing are the only 2 choices available to the highway engineer. When pavements are constructed on expansive subgrades, it is definitely recommended that the entire pavement system design be based on type of subgrade and other existing conditions rather than on use of a standard section.

Initial resistance to cracking from vertical and lateral subgrade expansion was lower in rigid pavements than in flexible pavements. However, rigid pavements were found to perform adequately (even though cracked) at subgrade moisture contents well above the plastic limit because of their ability to transmit wheel loadings over a wide area. The tendency of rigid pavements to crack with subgrade volume change is directly responsible for increasing moisture contents; and, once surface cracking has occurred, the deterioration of rigid pavement is only a matter of time. Therefore,

rigid pavements should not be used unless underlaid by a nonexpansive, flexible, impervious material. Load-carrying capacities of rigid pavement should be evaluated by strength tests, assuming that there is a subgrade moisture content of 1.1 to 1.3 times its plastic limit. The ability of rigid pavement to effectively carry traffic at subgrade moisture contents above the plastic limit should indicate its use in areas where poor drainage is encountered because rigid pavement normally produces higher subgrade moisture conditions. A correctly designed rigid pavement with improved shoulders over a sand-asphalt layer is probably the best design for general use on expansive subgrades.

Initial cracking from vertical and lateral subgrade expansion was resisted better by flexible pavement than by rigid pavement. However, when moisture contents approached the equilibrium value of 1.1 to 1.3 times the subgrade plastic limit, heavy traffic produced rutting and initial pavement cracking. The inability of observed flexible pavement systems to carry heavy traffic loadings at subgrade moisture contents near the plastic limit is thought not to be an indictment of this design but a reflection of the inability of current Oklahoma Department of Highways design techniques to predict subgrade strength at these moisture contents. Incorporation of revised soil-testing procedures to adequately determine subgrade strengths at moisture contents 1.1 to 1.3 times the subgrade plastic limit and to consider volume change behavior should definitely improve the chances for satisfactory long-term flexible pavement performance. Also, flexible pavement construction on expansive subgrades should definitely include the use of a nonexpansive, flexible, and impervious base, subbase, or membrane component.

Subgrade strength appears to be more important in flexible pavement design, and, therefore, these systems should give better performance where good drainage conditions are provided because they are also less susceptible to cracking from volume change produced by good drainage and would benefit materially from lower average moisture contents and resulting higher subgrade strengths.

Performance of Base Courses

Six types of base material were encountered at field research sites that are commonly used in Oklahoma base construction: sand cushion, hot sand asphalt, asphaltic black base, soil cement, stabilized aggregate, and select material. Exact definitions of these common highway materials are available elsewhere (8, 9). Sand cushion and select material were encountered as base courses for rigid pavement.

Because of observed behavior, the use of sand cushions has been deleted from Oklahoma highway design criteria. Sand cushions were found to act as water reservoirs and distribution systems, catching water that infiltrated from the shoulders and through rigid pavement cracks and joints and feeding it uniformly over the subgrade. As a result, rigid pavements on sand cushions usually experienced only small differential vertical movements. However, continued feeding of water to the subgrade resulted in lateral subgrade expansion and longitudinal pavement cracking plus upper subgrade moisture contents being at or near the subgrade liquid limit.

Hot sand asphalt was used as a base course at many highway research sites and was found to form an excellent impervious layer. The plastic properties of asphalt that were coupled with the fineness of the mineral particles allowed this material to resist the effects of lateral subgrade expansion and vertical differential movement without cracking and becoming pervious, at least better than any other type of material previously encountered.

Several research sites contained asphaltic black base underneath asphaltic concrete. Observed performance indicates that this material is probably the second-best base type tested because it is impervious and possesses good flexibility. However, its performance is not thought to be as good as that of sand asphalt because the larger size of aggregate particles used probably gives this material less flexibility and also presents the possibility of larger interconnected voids. Nevertheless, asphaltic black base was found to perform well at the majority of sites where it was encountered.

The soil-cement base courses that were encountered were used primarily in the construction of improved shoulders. Soil cement is relatively rigid compared to more flexible asphaltic materials and may suffer some initial shrinkage cracking. These cracks expand when moisture accumulation and resulting vertical and lateral subgrade expansion occur. Cracking is almost immediately reflected through the thinly surfaced shoulder, and this random cracking may be observed on almost all Oklahoma highway shoulders applied over soil-cement bases. Once the surfacing has cracked, water will enter and infiltrate through the soil cement into the subgrade, and additional volume change will occur and consequently open the joint between pavement and shoulder. The use of soil cement directly on any subgrade of even suspected expansiveness does not appear to be advantageous.

Stabilized aggregate is a mechanically stabilized material consisting of blended course aggregate, sand, mineral filler, and soil binder. The resulting product, although highly variable and depending on locally available materials, is nevertheless intended to provide a well-graded and densely compacted layer with reasonable strength properties. Stabilized aggregate base courses were found to perform satisfactorily at sites where little lateral subgrade expansion was noted to occur. At these sites, they provided (by virtue of their density and fine content) a relatively impervious barrier to infiltration, both from the shoulders and through the pavement section. However, stabilized aggregate possesses little tensile strength; and, at sites where appreciable lateral expansion was noted, this base did not stop infiltration and evaporation of water through pervious pavement surfaces.

Select material is similar to stabilized aggregate but is usually considered to be naturally occurring and is governed by somewhat different specifications. On the whole, select material was observed to behave not quite so well as stabilized aggregate but better than sand cushions.

Most of the correlations concerning base material performance are available elsewhere (8), but it should be noted that, comparing subgrade moisture contents under pavement centerlines for research site locations on more or less uniform A-6 or A-7 subgrade and on pavement rated as being excellent or good, 18 of 23 sites with pervious bases had higher moisture contents in upper subgrade levels than in lower levels. On the other hand, 7 of 11 similar pavements with impervious bases had lower subgrade moisture contents in the upper subgrade under their centerlines than at lower subgrade levels. Evaluation of amount of subgrade moisture variation under pervious and impervious bases, although subjective to some degree, nevertheless indicated that less variation with time existed in upper subgrade levels under impervious bases and that relative magnitude of variations was also lower.

The subgrade moisture contents for almost all of these sections were in the range of 1.1 to 1.3 times the plastic limit, with the upper subgrade moisture levels under the 7 impervious base sites being closer to 1.1 than to 1.3 times the plastic limit. On the other hand, average moisture content-plastic limit ratios for sites on pervious bases approached (and sometimes exceeded) the 1.3 value. These data, plus other information (8), indicate that a reasonable amount of moisture infiltrates into the subgrade from pervious base courses, even when the pavement is still in acceptable condition.

Recommendations Concerning Highway Base Courses

Base courses used in Oklahoma highway construction on expansive subgrades should, if possible, be nonexpansive, flexible, and impervious. Asphaltic types of base materials appear to provide these qualities better than any other materials encountered. If use of other base material is contemplated, the subgrade should be protected by use of a flexible, impervious subbase or else a flexible, impervious membrane located somewhere in the pavement system. If an impervious layer is provided in some other portion of the pavement system, mechanically stabilized aggregate or even select material may be used, as long as it does not become highly saturated. Soil cement should definitely not be used as a base material unless it is protected from lateral subgrade expansion by an intervening nonexpansive, flexible, and impervious layer.

Recommendations Concerning Highway Subbase Courses

Subbase components are used primarily as a means of distributing loads to the subgrade, but they can also act as barriers against water infiltration where pervious base courses are used. Oklahoma subbases are usually constructed of select material, chemically treated layers of the subgrade, or sand asphalt.

Select material subbases, when used in flexible pavement construction, obviously reduce the total required thickness of asphaltic layers. Even though economics dictates the use of locally available materials whenever possible, especially if they do not require treatment, it should be remembered that select material has minimal tensile strength and is not completely impervious. Thus, select material subbases should not be used unless some other portion of the pavement system (besides the wearing surface) contains desired nonexpansive, impervious, and flexible properties. However, the dense and relatively impervious qualities of select subbase are helpful in reducing effects of infiltration from outside the pavement system and also in protecting the base and wearing surface components from subgrade moisture and volume changes by providing a cushioning effect.

Lime-treated layers of cohesive subgrade have also been used as subbases, normally with lime contents corresponding to modification optimum for the material. The lime contents used for treatment normally result in reduction of plasticity and give an increase in soil workability. The result is to produce a treated material with properties similar to that of the select material described previously.

Sand asphalt possesses necessary imperviousness and flexibility if these qualities are desired in a subbase, and its use should allow inclusion of pervious base materials in highway design. Soil cement should not be used as a subbase if it is expected to remain reasonably impervious, and, if used, severe cracking should be expected.

Recommendations Concerning Improved Shoulders

Improved shoulders were found to provide a method for reducing infiltration of surface runoff into the base course, subbase, or subgrade or all three, particularly at pavement edges, and thus for producing more nearly uniform moisture variations over the width of the pavement. However, definite improvement in subgrade moisture conditions underneath pavement could be obtained by several modifications in shoulder design and construction technique. Because of lower traffic loadings carried by improved shoulders and also the staged construction common in Oklahoma, shoulders are often built after the pavement section has been constructed and have thinner base layers that are often of a different material. The net effect of this construction technique is to place a vertical plane of weakness between pavement and shoulder. Lateral and differential vertical expansion of cohesive subgrade tends to cause separation along this plane of weakness, provides a channel for entrance of surface runoff, and produces larger moisture variations under the pavement edge. Also, the wet-dry interface that forms under the shoulder causes shrinking and swelling of subgrade material, which develops flexural stresses along this plane of weakness.

Improved shoulders at least 8 ft in width should be constructed for all pavements on expansive subgrades. Base or subbase under the shoulders, or both of these, should be continuous with that of the pavement section and should be applied in 1 continuous shoulder-to-shoulder lift. Recommendations concerning type of base and subbase materials under shoulders are the same as for wearing surfaces.

Whatever the desired design shoulder width, shoulders on each side of the pavement section should be of equal width. If both shoulders are of equal width and the width is at least equal to 8 ft, a more nearly symmetrical subgrade moisture profile will result underneath the pavement and more nearly uniform moisture increases and decreases will occur.

Recommendations Concerning Highway Drainage Conditions

The varied topography encountered along a highway profile makes specific drainage recommendations impracticable. However, it is extremely important that existing

drainage conditions be the same on each side of a particular highway section to produce more nearly symmetrical moisture profiles, although conditions themselves may change along the profile. Special care should be given in transition sections and sections cut through slopes to provide equal drainage conditions on either side of the pavement. Also, despite numerous problems likely to be encountered, drainage conditions for 4-lane divided highways should be designed so that both the median and the outside shoulders drain. As a general rule, flexible pavements appear to be more suitable for use under good drainage conditions, whereas rigid pavements appear to be better suited for poor drainage conditions. For intermediate conditions, correctly designed pavements of either type should work satisfactorily.

Recommendations Concerning Highway Profile

The diverse topography encountered along highway profiles makes specific recommendations impractical. However, research findings definitely indicate that better highway performance is obtained in sections on grade and in slight cuts. Where possible, the highway profile on expansive subgrades should be held to these sections. Any fill or transition sections or both should be partially constructed of select material or lime-modified layers of the subgrade, such that a 5- to 7-ft depth below the bottom of the pavement system is essentially nonexpansive. An alternate procedure might be to compact the fill as closely as possible to natural moisture contents of existing soils and cover the entire fill with an asphaltic membrane. Whenever possible, high fills should be avoided, and, in any case, despite the previously mentioned treatments, shoulder settlements should be expected.

Recommendations Concerning Current Staged-Construction Procedures

If current staged-construction procedures (as described previously) are to be used, several slight modifications will improve moisture conditions in the subgrade. One method might be to compact the subgrade to a level above design final grade. This additional material will reduce subgrade drying during hotter seasons and give natural moisture contents more nearly approximating compaction specifications. In addition, this added layer will help to compensate for thickness lost through erosion and settlement. The prepared subgrade should be adequately barricaded so that agricultural traffic and other traffic may be kept off during the interim between subgrade finishing and base-surfacing application. The base-surfacing contractor could then cut the subgrade to final grade and immediately apply base and surfacing. If this procedure is not feasible, consideration should be given to provide extra rolling time (and thus money) to compact upper subgrade layers wet of optimum. However, required densities may be difficult to obtain as compaction under these conditions will normally occur at or above the plastic limit. Nevertheless, higher initial moisture contents and a clay particle orientation less conducive to volume change would result and may be worth the additional effort.

Another alternative procedure would be to cover the prepared subgrade with an asphaltic membrane and allow it to reach equilibrium moisture conditions over a 2-year period or longer between subgrade completion and base-surfacing application. Still another alternative procedure would be the use of the deep-plow lime treatment of upper subgrade layers to produce a less expansive buffer layer, which would maintain more nearly constant moisture conditions in lower portions of the subgrade. This procedure has been attempted experimentally by the Research and Development Division, Oklahoma Department of Highways (15).

Recommendations Concerning Revised Staged-Construction Procedures

Some thought should also be given to a more radical revision of the staged-construction process to ensure better long-term subgrade moisture conditions. The philosophy and methods by which current Oklahoma highways are constructed dictate that the entire base and surfacing courses be applied at one time. However, the ultimate traffic loading for the pavement system is not usually encountered until late in its

design life. Initially, traffic is likely to be substantially below expected maximum values, and the section is perhaps overdesigned. The possibility of traffic considered in design being greater than that during initial years after construction and establishment of subgrade moisture equilibrium suggests that alternative methods of staged construction be used.

One method would be to divide construction into 3 stages. Initially, the subgrade would be prepared in a manner recommended previously. Then, after the normal time lag, base material would be applied, but only part of the total surfacing thickness would be applied. Surfacing applied at this time should be adequate to carry current traffic but should be less than the ultimate surfacing thickness recommended for the section. Within a reasonable length of time after initial surfacing is applied and the section is opened to traffic, moisture equilibrium should occur underneath the pavement system, and its subgrade will be just beginning to start the infiltration and evaporation cycle through the now pervious pavement structure. At this time, usually somewhere between 2 and 5 years after initial construction, the final surfacing course should be applied to bring the pavement section up to design thickness and effectively seal the surface from infiltration and evaporation. Moisture equilibrium should have been achieved by this time, and, as the accumulation phase is completed, sections should be produced where adverse moisture variations would be minimized. If subgrade soil conditions at moisture equilibrium values have been correctly anticipated, excellent highway performance should be achieved, and future maintenance costs should be markedly reduced. During the design life of the highway, at least 1 less overlay should be needed, and this in itself would reduce total highway cost.

An alternate procedure would be to use current staged-construction methods but then to apply surfacing in 2 stages. This procedure should cause more initial moisture accumulation and relative movement and might require the final surfacing course earlier than the procedure mentioned previously. However, it should also increase subgrade moisture resistance of the final section.

Still a third alternate might be to extend the initial staged-construction phase to include base and temporary surfacing, with intermediate or final surfacing courses or both courses to be applied at later dates. This technique might be applicable when turnkey or non-staged-construction projects are anticipated because of considerations dictating rapid availability of the highway to traffic. The sections could be completed quickly, but provision would be available to counteract adverse subgrade moisture conditions, which would of necessity be built into a turnkey project.

SUMMARY

This paper has described subgrade moisture conditions in Oklahoma as determined by a 6-year research study. Effectiveness of various highway components in preventing and resisting adverse subgrade moisture conditions was also discussed. Recommendations concerning the need for more comprehensive subgrade soil-testing procedures, for use of certain pavement components in particular situations, and for revision of current construction practice to enhance subgrade moisture resistance of pavement systems have also been described. It is suggested that, whenever possible, recommendations made here be applied in routine design and construction of highways on expansive Oklahoma soils.

ACKNOWLEDGMENT

Support for this study was provided by the Oklahoma Department of Highways, in cooperation with the Federal Highway Administration. The opinions, findings, and conclusions expressed in this paper are those of the author and not necessarily those of the Oklahoma Department of Highways or the Federal Highway Administration.

REFERENCES

1. Haliburton, T. A. Interim Report I: Preliminary Planning. Subgrade Moisture Variations Research Project, School of Civil Eng., Oklahoma State Univ., Stillwater, June 1966.
2. Heiliger, W. L., and Haliburton, T. A. Interim Report II: Access Tube Installation. Subgrade Moisture Variations Research Project, School of Civil Eng., Oklahoma State Univ., Stillwater, January 1967.
3. Manke, P. G., and LeFevre, E. W. Interim Report III: A Preliminary Standardization and Calibration Procedure for Nuclear Moisture/Density Gages. Subgrade Moisture Variations Research Project, School of Civil Eng., Oklahoma State Univ., Stillwater, May 1967.
4. Moore, R. K., and Haliburton, T. A. Interim Report IV: Suggested Nuclear Depth Gage Calibration Procedures. Subgrade Moisture Variations Research Project, School of Civil Eng., Oklahoma State Univ., Stillwater, Jan. 1968.
5. Osterhout, R., and Haliburton, T. A. Interim Report VII: Subgrade Temperature Measurement. Subgrade Moisture Variations Research Project, School of Civil Eng., Oklahoma State Univ., Stillwater, May 1969.
6. Marks, B. D., III, and Haliburton, T. A. Interim Report VI: Evaluation of Collected Data 1966-1967, Subgrade Moisture Variations Research Project, School of Civil Eng., Oklahoma State Univ., Stillwater, May 1968.
7. Shaw, L. K., and Haliburton, T. A. Interim Report VIII: Evaluation of Collected Data 1966-1969. Subgrade Moisture Variations Research Project, School of Civil Eng., Oklahoma State Univ., Stillwater, Jan. 1970.
8. Snethen, D. R., and Haliburton, T. A. Interim Report IX: Effectiveness of Existing Highway Designs. Subgrade Moisture Variations Research Project, School of Civil Eng., Oklahoma State Univ., Stillwater, Aug. 1970.
9. Haliburton, T. A. Final Report. Subgrade Moisture Variations Research Project, School of Civil Eng., Oklahoma State Univ., Stillwater, Aug. 1970.
10. Haliburton, T. A. Interim Report V: Data Summary 1966-1967. Subgrade Moisture Variations Research Project, School of Civil Eng., Oklahoma State Univ., Stillwater, April 1968.
11. Haliburton, T. A. Interim Report X: Summary of Collected Data. Subgrade Moisture Variations Research Project, School of Civil Eng., Oklahoma State Univ., Stillwater, Aug. 1970.
12. Marks, B. D., III, and Haliburton, T. A. Subgrade Moisture Variations Studied With Nuclear Depth Gages. Highway Research Record 276, 1969, pp. 14-24.
13. Haliburton, T. A., and Marks, B. D., III. Subgrade Moisture Variations in Expansive Soils. Proc., 2nd Conf. on Expansive Clay Soils, Texas A&M University, College Station, Aug. 18-20, 1969.
14. Srinivasan, V. Aniosotropic Swelling Characteristics of Compacted Clay. Oklahoma State Univ., Stillwater, PhD dissertation, July 1970.
15. Hartronft, B. C., Buie, L. D., and Hicks, F. P. A Study of Lime Treatment of Subgrades to Depths of Two Feet. Research and Development Division, Oklahoma Department of Highways, Oklahoma City, 1969.

PREFABRICATED SUBSURFACE DRAINS

Kent A. Healy and Richard P. Long, Department of Civil Engineering,
University of Connecticut

The design of a prefabricated subsurface drain system based on well screen criteria is presented. This drain is fabricated by using synthetic cloth and a channelized core that ensures proper filtration and permeability. Laboratory and full-scale field test results are given and show the prefabricated subsurface drains to be an effective substitute for conventional mineral aggregate subsurface drains. Mineral aggregate filters are reviewed. The difficulties inherent in their design and construction and the advantages of prefabricated subsurface drains are discussed.

•SUBSURFACE DRAINS have been used for many years to remove excess water from the ground to improve crop growth, strengthen pavement foundations, stabilize slopes, and reduce water pressure against retaining walls. The water is often carried away from a site by a perforated pipe, and a filter material must be provided between the soil and the pipe that will retain the soil while allowing the free flow of water into the pipe. The conventional subsurface drain uses a filter of mineral aggregate that has been graded to match the soil (1). This type of filter performs satisfactorily only if designed and constructed carefully.

A subsurface drain system that uses synthetic materials and that fulfills the requirements of filtration and water flow has been developed. Because this system can be prefabricated in lengths that are easily handled and installed in the field, many of the construction problems of mineral aggregate drains are eliminated.

DESCRIPTION OF PREFABRICATED SUBSURFACE DRAINS

The prefabricated drain is shown in Figure 1 and consists of a slotted pipe, a channelized vertical core inserted into the pipe slot, and a fine-mesh filter cloth enclosing the pipe and the core. The cloth retains the soil and keeps the core channels open. The groundwater drains through the cloth, down the channels, into the pipe, and away from the site.

The selection of the filter cloth is based on criteria established in the 1930's for well screens (2). A properly designed well screen retains only the coarsest particles of a soil; these particles will retain the finer particles.

The openings in the screen should be just small enough to retain the coarsest 20 percent of the particles (D_{80}) in a well-graded soil and the coarsest 40 percent (D_{60}) in a uniform soil (3). The percentage of open area of the screen should be approximately the same as the porosity of the soil to prevent restriction of water flow. Well screens meeting these criteria have remained effective for many years in soils ranging from fine sand to gravel.

The filter cloth used on the prefabricated drains functions in the same way as a well screen. An advantage of using cloth as a filter is its high permeability even with small openings. Cloth with mesh openings between 0.075 and 0.150 mm and a minimum 15 percent open area will retain most soils that can be effectively drained by gravity and will not restrict the flow of water from the soil.

Sponsored by Committee on Subsurface Drainage and presented at the 50th Annual Meeting.

Materials Used

The materials used in the prefabricated surface drains are given as follows:

1. Filter cloth—Two types of cloth have been tested and used as filters—a nylon chiffon and a polyester butterfly (Fig. 2). Both materials have good tensile strength and resist decomposition in the ground. The chiffon has a mesh opening of 0.15 mm and a 45 percent open area. The butterfly has a mesh opening of 0.075 mm and a 15 percent open area. Long-term model tests have shown that both cloths will filter soils ranging from a fine silty sand to a glacial till with no sign of soil erosion or clogging. The butterfly cloth with 15 percent open area has adequate permeability for soils containing silt. The chiffon having a greater percent of open area is preferable for draining more permeable soil. Both cloths are more permeable than a 2-in. layer of coarse gravel. The gradation of particle sizes and permeability of soils successfully filtered by nylon chiffon cloth are shown in Figure 3. These soils, ranging from a medium sand to a glacial till with a high percentage of silt, were tested in the laboratory under a hydraulic gradient much higher than that occurring in the field.

2. Core—The core must support the cloth and provide channels large enough to carry the water into the pipe as quickly as it flows from the soil. The following materials have been used as cores in field-test installations and are shown in Figure 4: Type 1, expanded aluminum sheet, purchased from U.S. Steel, having the commercial name Armorweave; and Type 2, vinyl tube fencing, purchased from Sears, Roebuck and Co. The core materials were tested for crushing strength and water-carrying ability. The expanded aluminum showed little deformation under a pressure of 200 lb/sq in., and the vinyl tube fencing had a crushing strength of 160 lb/sq in. Intrusion of the cloth into the channels decreases the area through which the water can flow and is a possible source of malfunction. Tests with the vinyl tube fencing showed that, under an earth pressure of 4.0 kip/sq ft, the cloth intruded less than 0.025 in. and that a 1-ft wide

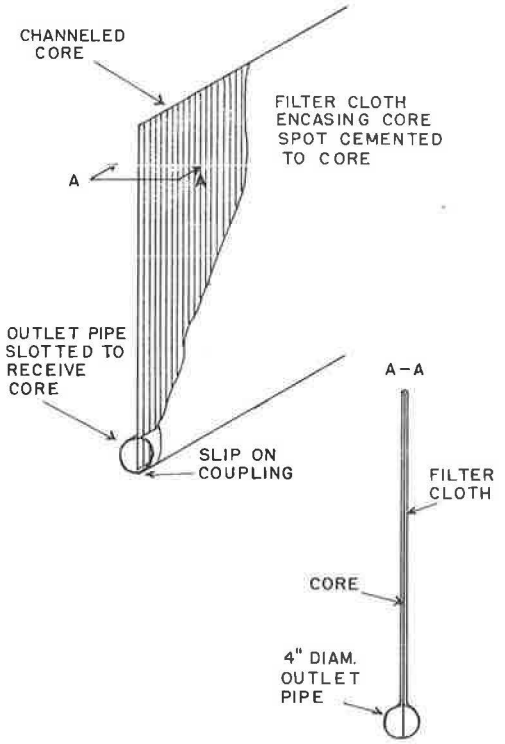

Figure 1. Basic design of prefabricated subsurface drains.

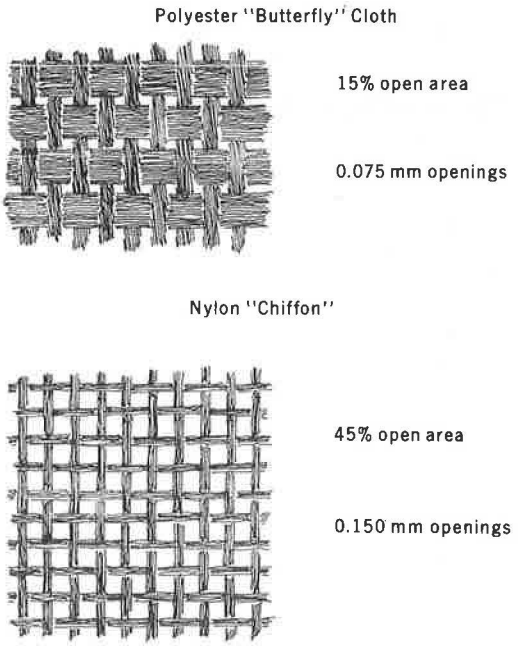

Figure 2. Weave characteristics and porosity of cloth used.

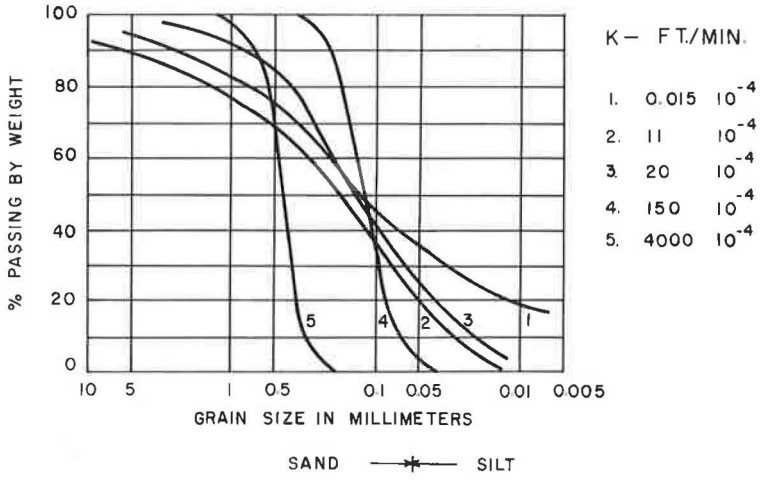

Figure 3. Soils successfully filtered by nylon chiffon.

section of the drain, when vertical, could carry 2.5 gal/min. This is sufficient to drain a soil with a permeability of 5×10^{-2} ft/min. Tests on the expanded aluminum core showed similar flow characteristics under stress.

3. Pipe—A hard plastic pipe with a 4-in. diameter and a 1/8-in. wall thickness has been used for the field sections. The slot was cut on a table saw. This pipe is available in 10-ft lengths from building supply companies and has a crushing strength of 0.9 kip/ft.

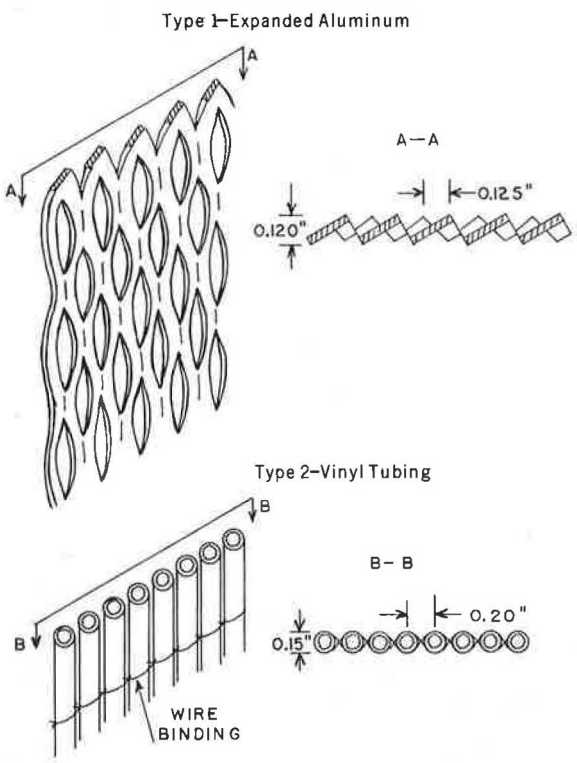

Figure 4. Core configuration.

Installation Methods

Prefabricated drains are easily installed on slopes or in trenches, as shown in Figure 5. Drain sections 10 ft long weigh less than 20 lb and can be placed and connected with slip couplings from the ground surface. Trenches need be only wide enough to receive the drain, thereby making attractive the use of trenching machines in suitable soil.

The core is flexible enough to be pressed tightly against 1 face of the exposed natural soil, as shown in Figure 5. In this manner the more permeable strata in the native soil can be drained quickly. The type of backfill depends on the drainage desired at the site. If most of the water enters the drain from 1 side, as on a slope, the native soil may be used as backfill against the opposite face. When the drain receives water from both sides, sand may be used as backfill. This ensures that the natural

drainage channels in the soil are not blocked and makes the compaction easier in a trench section. The short flow path through the sand to the core of the drain will not impede the free movement of water.

The prefabrication of the drain sections ensures proper operation even when installed by people who are unfamiliar with filter principles. The drain sections can be fabricated in any height and length to suit the installation.

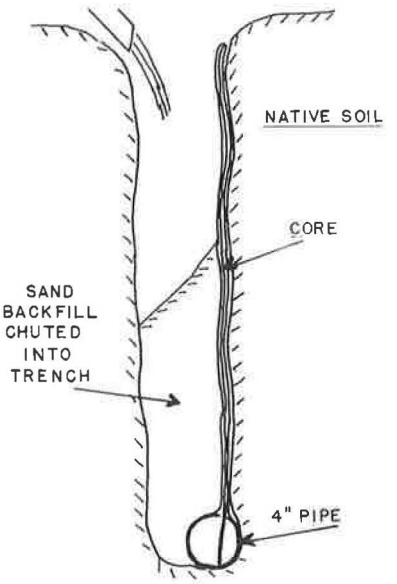

Figure 5. Prefabricated drain installed in trench.

FIELD TESTS

Sites

Prefabricated drains were installed in 2 small wet areas in 1968 and performed well. In the spring of 1969, 600 ft of drain were installed to stabilize a cut slope that was sloughing because of excess water. This installation is described in detail in this paper.

During the late summer and early fall of 1970, installations were made at 3 other sites. These 3 installations are mentioned especially to illustrate other applications for the prefabricated underdrains. Field measurements on them are continuing. One installation surrounds a septic system leach field to control the groundwater in the vicinity. Another installation was placed to intercept the groundwater flowing into a lot on which a home is to be built. The third installation was placed beside a road to control frost heave by lowering the local groundwater table.

Description of Unstable Slope

The slope, a plan of which is shown in Figure 6, is the northwest side of a drumlin, located on the University of Connecticut campus and formed when the hill was cut back from a natural slope of 1 on 3.3 (17 deg) to a 1 on 2 slope to allow the placement of a sanitary line and sidewalk. The slope started sloughing after the first heavy rain, and it was a continual maintenance problem to keep the walk clear of mud in the spring and ice in the winter. The soil in its natural state is a dense, well-graded glacial till with particles varying from cobbles to clay size. Disturbed samples of the soil have a permeability of approximately 1×10^{-6} ft/min, as measured by a falling head permeameter. Slow direct shear tests showed an effective stress friction angle of 41 deg. The natural undisturbed soil is slightly cemented and contains numerous small channels parallel to the surface that seep water below the water table in an open cut.

Installation

In July 1969, 2 lines of prefabricated drains with type 1 core and butterfly cloth were installed along the slope, as shown in Figure 6. It had originally been planned to install the upper drain line by cutting a berm with a bulldozer. However, at the time of installation the slope was too wet, and a berm had to be dug by backhoe from below. Figure 7 shows a typical cross section and the method used to place the drains. A trench was dug for the lower drain and was backfilled with sand for ease of compaction. In the very wet areas, the upper drain sections were partially backfilled with the backhoe immediately after placement to prevent local sliding. Figure 8 shows the upper drain partially backfilled. Final backfilling and grading were completed by a bulldozer, as shown in Figure 9. The lower trench installation is shown in Figure 10.

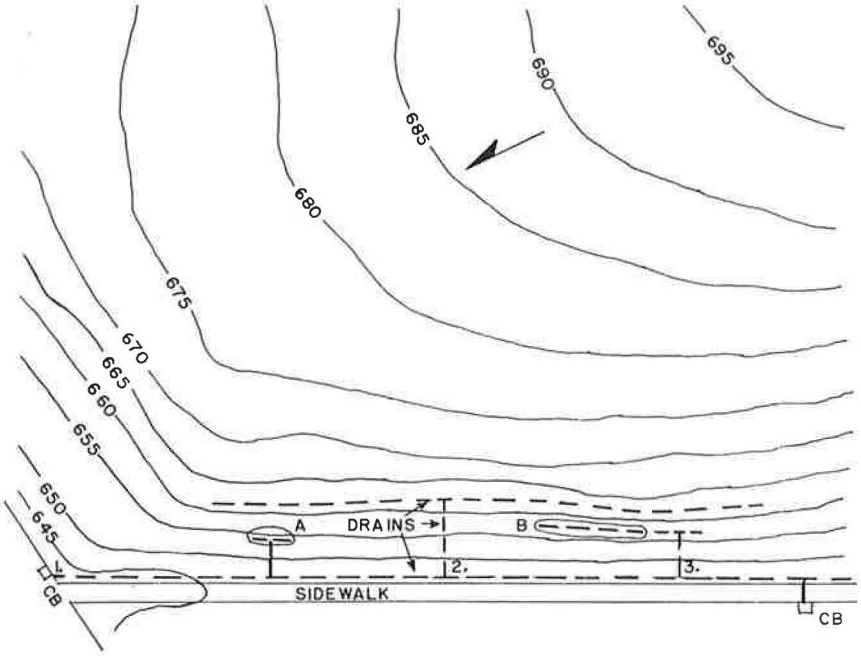

Figure 6. Plan of field installation.

In the fall of 1969, heavy rains caused surface erosion, and in 2 areas, marked A and B in Figure 6, the natural drainage channels were such that water was exiting under the upper drain, causing sloughing below. An additional 20-ft length of drain was installed by hand at the south end of the area B halfway up the slope, and this portion was

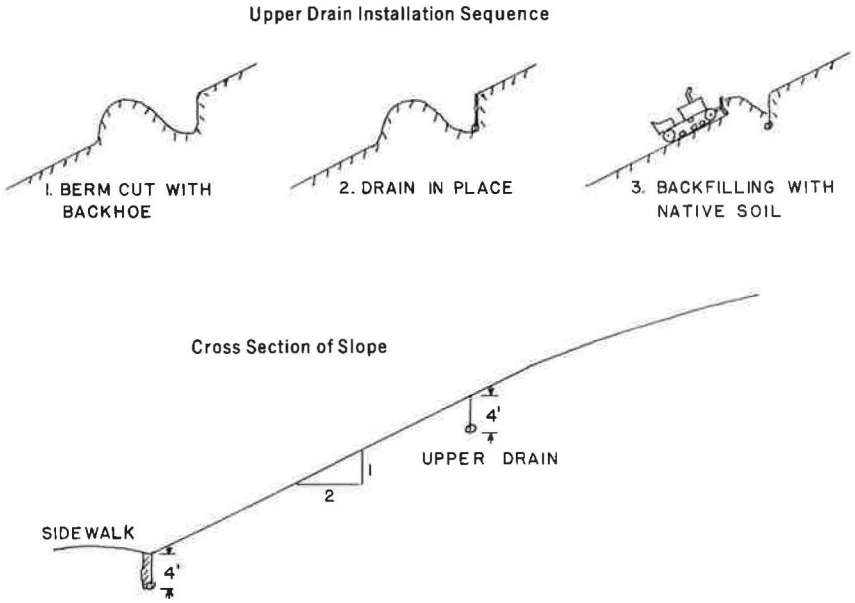

Figure 7. Cross section of field installation.

stabilized. In the spring of 1970, 90 ft of drain with type 2 core and chiffon filter cloth was installed with a backhoe and bulldozer in the remaining portion of area B, and 20 ft of drain was installed in area A. Observation pipes were installed at points marked 1, 2, and 3 in Figure 6, and the water flow in the drain pipes can be measured at these points by using calibrated probes.

Figure 8. Upper drain partially backfilled.

Evaluation of Field Installation

Some piezometers were installed, but they did not reflect apparent water conditions accurately. This may be due to the nonhomogeneous permeability characteristics of the soil. The evaluation of the field installation has therefore, been based on the overall stability of the slope and measurements of water flow out of the drains.

The slope, which was unstable over essentially its whole length, has been stabilized. Surface seeping has been almost eliminated, and the slope surface drys up within a few days after a heavy rain.

Water flow from the drains has been monitored continually since installation. The 250-ft upper drain removes water from the soil at a rate of 2 gal/min during wet periods. Calculations, assuming a hydraulic gradient in the soil of 0.2, show the field permeability to be 1.6×10^{-3} ft/min. This increase of 1,000 times over the permeability from lab tests on disturbed samples may be due to the natural channels occurring in the deposit. There has been no indication of fines being removed from the soil by the drain, indicating that the cloth is filtering properly.

Costs

The upper drain was installed where it would have been nearly impossible to install a conventional trench drain, so that cost comparisons are difficult to make, but the prefabricated drains appear to be competitive with conventional drain systems. The material cost of the prefabricated drain using vinyl tube core and chiffon is less than $1.35/ft for a 4-ft deep section. The main drainage core can be provided in almost any height and length at a cost of approximately $0.25/sq ft.

COMPARISON OF MINERAL AGGREGATE AND PREFABRICATED SUBSURFACE DRAINS

Most subsurface drains are constructed from mineral aggregates, and a comparison with prefabricated drains is appropriate.

Figure 9. Dozer backfilling upper drain.

Figure 10. Installing lower drain in trench.

Filter Requirements

Tests run by Bertram in 1940 (4) and at the U.S. Army Engineer Waterways Experiment Station (5) resulted in the development of the following criteria for mineral aggregate filters:

1. Preventing continuous movement of soil particles requires that the effective pore size (assumed to be 1/5 D_{15} of the filter) be smaller than the coarsest 15 percent (D_{85}) of the soil being drained. This is normally expressed as

$$\frac{D_{15}\ (\text{filter})}{D_{85}\ (\text{soil})} \leq 5$$

$$\frac{D_{50}\ (\text{filter})}{D_{50}\ (\text{soil})} \leq 25$$

2. Preventing restriction of water flow by the filter requires

$$\frac{D_{15}\ (\text{filter})}{D_{15}\ (\text{soil})} > 4 \text{ to } 5$$

Preventing movement of the filter particles into the pipe, if a perforated pipe is used to remove the water from the filter, requires

$$\frac{D_{85}\ (\text{filter})}{\text{pipe-opening size}} > 1$$

In the prefabricated subsurface drain, all filtration is accomplished by the cloth with openings constituting at least 15 percent of the area and having a size between 0.075 and 0.150 mm.

Design and Construction

In many situations the criteria for mineral aggregate filters must be applied with great care. The Vicksburg criteria implicitly assume well-graded soil (1). If the soil to be filtered and drained is gap-graded, the number of large particles may be insufficient to prevent movement of the smaller particles, and the filter must be designed to retain a size smaller than the coarsest 15 percent of the soil particles.

Filters placed against soil deposits, whose gradation varies from point to point, must be designed to hold the finest particles in place, and a graded mineral aggregate filter may be required to allow free drainage.

Some of the important points (1) in constructing the mineral aggregate filter are as follows:

1. Filter materials must be handled and placed with care to avoid segregation and contamination;
2. The filter must be well compacted to reduce the possibility of dropping fines of the filter through void spaces; and
3. A single improperly constructed portion of the filter can lead to failure of the drainage system.

Construction control for the prefabricated subsurface drain is less demanding. The prefabrication ensures that the system can be easily and correctly installed by personnel unfamiliar with filter criteria.

CONCLUSIONS

Laboratory and field tests have indicated the following:

1. A fine mesh cloth is suitable as an effective filter for a wide range of soil types;
2. A thin channelized core allows free movement of water into the outlet pipe;
3. Prefabricated subsurface drains are easily handled and installed in the field and allow placement where conventional drains would be difficult to construct; and
4. Prefabricated subsurface drains are economically competitive with conventional mineral aggregate systems.

ACKNOWLEDGMENT

This research was carried out in the Civil Engineering Department of the University of Connecticut and was sponsored by the Joint Highway Research Advisory Council of the University of Connecticut and the Connecticut Department of Transportation, the Connecticut Public Works Department, and the University of Connecticut Physical Plant Department.

REFERENCES

1. Cedergren, H. R. Seepage, Drainage, and Flow Nets. Wiley and Sons, New York, 1967, Chap. 5.
2. Tolman, C. F. Ground Water. McGraw-Hill, New York, 1937, p. 410.
3. Bennison, E. W. Ground Water, Its Development and Uses. Edward F. Johnson, Inc., St. Paul, Minn., 1947, p. 190.
4. Investigation of Filter Requirements for Underdrains. U.S. Army Engineer Waterways Experiment Station, Corps of Engineers, Vicksburg, Miss., Tech. Memo. 183-, Nov. 1941, revised Dec. 1941.

GRAVITY FLOW TO EXCAVATIONS AND DRAINAGE TRENCHES IN LAYERED AQUIFERS

Francis G. McLean, Westenhoff and Novick, Inc., Chicago; and
Raymond J. Krizek, The Technological Institute, Northwestern University

The finite-element method is used to analyze the problem of steady-state gravity flow to typical excavations and drainage trenches in layered aquifers. Dimensionless flow quantities and information on the location of the phreatic surface are presented as functions of the relative material permeabilities and the geometric configuration of the soil profile and excavation size or drainage trench position. These results are then applied to an example problem to select a satisfactory configuration of subsurface drains for an actual depressed highway profile.

•ALTHOUGH the topic of plane flow through layered systems has been investigated extensively by workers in the field of agricultural drainage (12), a large portion of the effort has been directed toward the solution of confined flow problems (9, 12, 13, 14). Relatively little attention has been given to gravity flow systems (such as flow to excavations and drainage trenches), which are commonly encountered in civil engineering practice in general and in highway engineering in particular. Accordingly, the multiple aquifer systems shown in Figure 1 were studied to gain insight regarding the interaction effects of the various layers when subjected to conditions of steady-state gravity flow. The single excavation without drains (Fig. 1a) is typical of a general system with wide application on construction sites or in highway cuts, whereas the configuration with drains (Fig. 1b), although broad in use, is limited for illustrative purposes to a particular combination of material permeabilities that are representative of those found in a portion of a large highway project. The latter more specialized situation is used to test the concepts developed during the more general study of the single excavation. Because the combination of a permeable boundary at the trench side walls, the free surface, and the layered materials (with the resulting complex configuration of the free surface) makes these problems very difficult and generally tedious to solve by ordinary methods, the finite-element method (4, 6, 17, 20, 21, 22) was chosen for use in this investigation.

EVALUATION OF FINITE-ELEMENT METHOD

The advantages and disadvantages, as well as the accuracy, of the finite-element method has been well documented by workers in the area of structural analysis. Some typical studies include the consideration of various formulations (5, 8) and the description of various structural systems by different types of discrete elements (15, 21). Much has been published about the methods for obtaining solutions to the associated system of simultaneous equations, the conditioning thereof, and accuracy and error analysis of the procedures and answers. Results obtained by the finite-element method, as applied to the "quasi-harmonic" problem (which includes seepage), have been shown (19, 20, 21) to be comparable with those obtained by finite-difference methods and closed-form solutions. Also, a comparison has been made (6, 17) between results obtained by a finite-element analysis and those obtained by Casagrande

Sponsored by Committee on Subsurface Drainage.

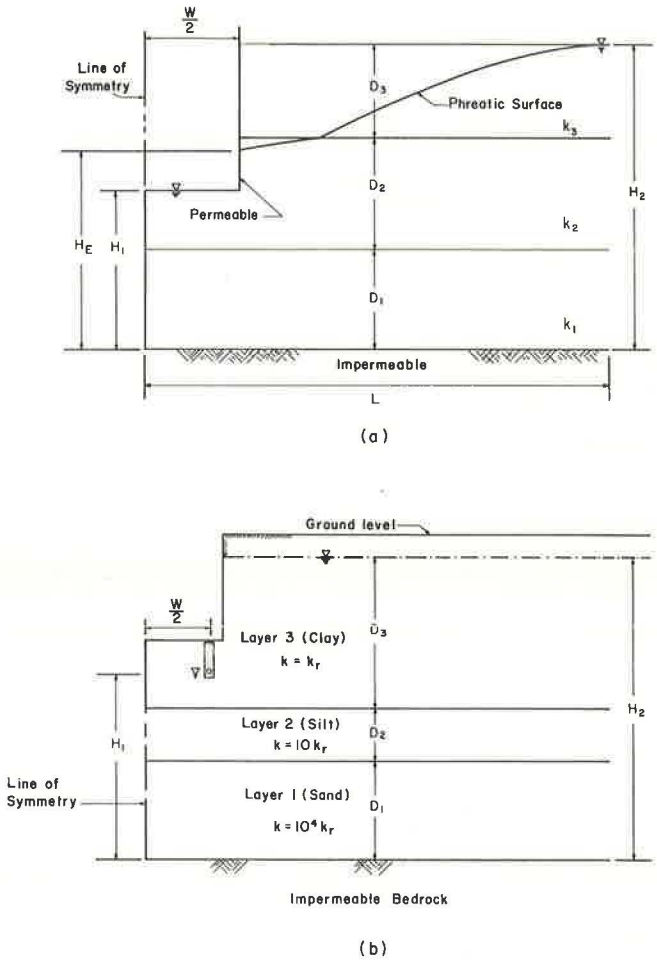

Figure 1. Typical geometric configurations considered.

(2) for the location of the free surface and the exit point for steady-state flow through a dam that rests on an impermeable base. The effect of mesh size on the solution for a geometrically simple, confined-flow problem has also been reported elsewhere (11).

The accuracy of the finite-element program (essentially that described by Taylor and Brown, 17) used in this study was ascertained by making several checks of flow quantities, seepage pressures, and free surface locations for various axisymmetric and plane flow cases. In the first case, an electric analog model of a trench, which partially penetrates a homogeneous, isotropic aquifer, was used (18) to check the flow quantity and potential distribution obtained by the finite-element method. The results shown in Figure 2 indicate very good agreement. In another comparison, 3 cases of a well, which partially penetrates an unconfined, homogeneous, isotropic aquifer underlaid by an impermeable stratum, were analyzed by the finite-element method. Results in all cases differed by less than 10 percent from those obtained (1) by relaxation and the methods of Kozeny and Forchheimer.

The problem of gravity flow through a dam on an impermeable base has been studied by relaxation (16), by the hodograph method (13), by an iteration scheme (7), and by use of a flow model (3). Hence, this problem affords an excellent opportunity for comparison of solutions.

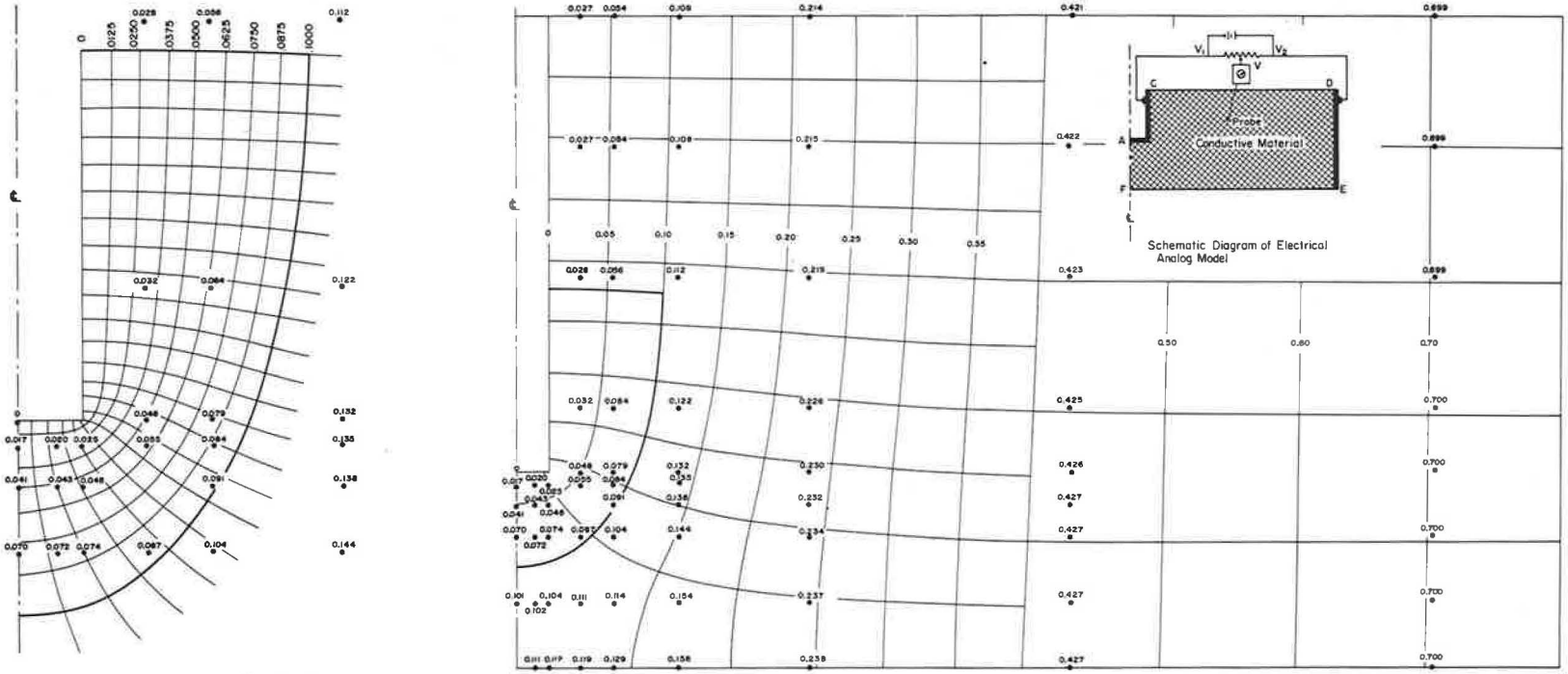

(a) Detailed Portion of General Model

(b) General Model

Figure 2. Comparison of potential values obtained for an electric analog and the finite-element method.

Figure 3a shows the finite-element mesh that was constructed to describe this problem, and Table 1 gives the geometric information and the resulting flow and pressure characteristics for the specific cases considered. The maximum number of iterations allowed for each case was 15, and, if completed, they required about 200 sec of central processor time on a CDC 6400 computer. The specified beta quantity is used in the program as an under-relaxation factor for free-surface adjustments between iterations, and the maximum pressure variation (associated with particular values of beta and tolerance) for the nodes along the free surface is given in Table 1. Also shown are the dimensionless flow parameters calculated from the finite-element analysis and the Dupuit assumption, which, according to Muskat (13), yields values almost identical to those obtained by the hodograph method. The first trial and final locations for the free surface in each case are shown in Figure 3b, and Figure 3c shows the results for a problem whose geometry was chosen to compare with that of the experimental model investigated by Chapman (3). The solution obtained (10) by the method of finite differences is also shown. Because of the excessive computer time required, the finite-element solution was not allowed to attain the best possible free-surface location, nor was a better first-trial free surface tried; however, all points that lie between the solution curves were moving upward when the solution was terminated. The single point lying above the Chapman curve near the tail water was observed to be essentially stable during the last 2 iterations.

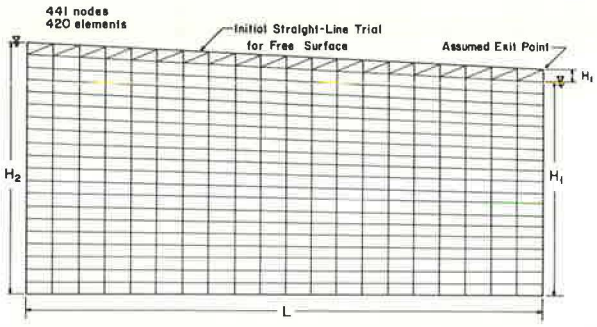

(a) Finite Element Mesh for Flow Through a Vertical-faced Dam

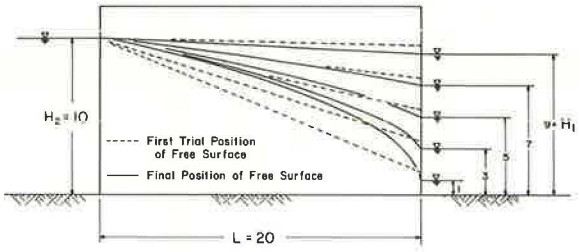

(b) First Trial and Final Positions of Free Surface for Various Head Differences

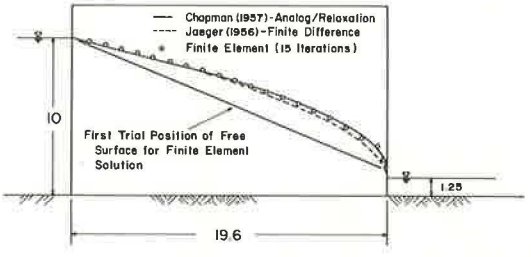

(c) Comparison of Free Surface Positions as Caculated by Various Methods

Figure 3. Flow through a dam with vertical faces.

For the cases considered here, the convergence of the solution determined by the finite-element idealization and the convergence of the free-surface iterative procedure are of concern. The latter may be evaluated for each specific solution by observing the residual pressures calculated for the free-surface nodes, whereas the former may be assessed by comparing results obtained from several different idealizations for any given problem. In general, as the size of the elements becomes small and the number of elements becomes large, convergence is ensured for most conditions (21). For the several hundred computer solutions performed during the course of this and associated studies, satisfactory convergence was obtained through the exercise of reasonable care and judgment in the apportionment and placement of elements, even with seemingly rather coarse configurations. Although no comprehensive rules can be established with regard to the size and number of elements used in any given case, satisfactory convergence was obtained for the problems considered here by idealizations ranging from 125 nodes and

TABLE 1

COMPARISON OF FLOW PARAMETERS FOR SEEPAGE THROUGH A RECTANGULAR DAM WITH VERTICAL FACES

H_1/H_2	L	Number of Iterations	Maximum Variation in Free Surface Pressure	H_s/H_1		Q/kH_2	
				FEM	Polubarinova-Kochina	FEM	Dupuit
0.100	20.0	15	$+7 \times 10^{-3}$	0.1680	0.1143	0.2475	0.2475
0.125	19.6	15	$+6 \times 10^{-3}$	0.2821	—	0.2511	0.2511
0.300	20.0	14	$+3 \times 10^{-4}$	0.0002	0.0003	0.2275	0.2275
0.500	20.0	8	$\pm 7 \times 10^{-5}$	0	0	0.1875	0.1875
0.700	20.0	6	$\pm 7 \times 10^{-5}$	0	0	0.1275	0.1275
0.900	20.0	5	$+2 \times 10^{-6}$	0	0	0.0475	0.0475

Note: H_2 = 10.0; k = 1.0; maximum iterations = 15; beta = 0.9; and tolerance = 0.001.

101 elements to 461 nodes and 447 elements, and the number of iterations required to locate the free surface varied from 3 to 10.

FLOW TO AN EXCAVATION IN A LAYERED AQUIFER SYSTEM

For the case of flow to the type of excavation shown in Figure 1a, the following boundary conditions were used with the finite-element idealization. Zero normal flow conditions were imposed along the line of symmetry, the phreatic surface, and the impermeable lower boundary; the boundary nodes at distance L were subjected to a hydrostatic pressure distribution; zero pressure was specified at the nodes that describe the lower boundary of the excavation; and flow was allowed to occur through the excavation side wall. Finite-element meshes ranged in size from 125 nodes and 101 elements for the narrow trench with deep penetration to 236 nodes and 215 elements for the wide trench with shallow penetration. Relatively small, nearly square elements (2.5:2 units) were used in areas of rapidly changing pressures, whereas larger rectangular elements (60:30 units) were used in areas with small pressure changes. Various sizes of rectangular elements were used in the transition regions. Because of the complex free-surface configurations that resulted from the various layered systems and permeability ratios, 15 different meshes were used for this problem.

The number of variables needed to characterize the excavation problem shown in Figure 1a was reduced as follows: (a) the layer thicknesses D, were assigned a value of $H_2/3$ equal to 30 units; (b) the effective length L of the domain was taken to be 1,000 units; (c) the depth of penetration of the trench $(H_2 - H_1)/H_2$ was chosen to be $H_2/6$, $H_2/2$, and $5H_2/6$; (d) the width W of the excavation was given values of 80 units and 4 units to obtain information on width effects; (e) the excavation was assumed to be dewatered and to have permeable side walls; and (f) the relative permeability values (ratio of variable permeability k_v to reference permeability k_r) were taken to be 0.01, 0.1, 1, 10, and 100. Each layer, in turn, was considered to be the variable layer (whereas the permeability of the other 2 layers was held constant), and its relative permeability was allowed to traverse the full range of assumed values, thus yielding a 2- or 3-layer system composed of 2 materials. This was done for each combination of excavation width and penetration, and information regarding the exit point on the seepage face and the flow quantity is given in Table 2.

Interpretation of Results

The location of the exit point varies as a function of the confined nature of the system, the exit point being higher when the uppermost layer (or layers) is less permeable than the underlying layer (or layers). This effect is present, to a degree, whether or not the excavation extends into the more pervious underlying layer, and it may also be observed when the layer that contains the bottom of the excavation is least permeable and the overlying layers are more permeable. In addition, for these same situations,

TABLE 2

SUMMARY OF SEEPAGE CHARACTERISTICS FOR AN EXCAVATION

Penetration Ratio	Relative Permeability of Layer			Exit Point of Phreatic Surface		Flow Parameter	
	k_1/k_r	k_2/k_r	k_3/k_r	4-Unit Width	80-Unit Width	4-Unit Width	80-Unit Width
1/6	1.00	1.00	1.00	0.83	0.83	0.169	0.184
	1.00	1.00	0.01	0.90	0.87	0.016	0.046
	1.00	1.00	0.10	0.85	0.83	0.076	0.116
	1.00	1.00	10.00	0.83	0.83	0.643	0.654
	1.00	1.00	100.00	0.83	0.83	5.288	5.336
	1.00	0.01	1.00	0.83	0.83	0.089	0.094
	1.00	0.10	1.00	0.83	0.83	0.111	0.118
	1.00	10.00	1.00	0.84	0.83	0.541	0.724
	1.00	100.00	1.00	0.89	0.85	1.436	3.450
	0.01	1.00	1.00	0.83	0.83	0.115	0.120
	0.10	1.00	1.00	0.83	0.83	0.120	0.126
	10.00	1.00	1.00	0.84	0.83	0.475	0.647
	100.00	1.00	1.00	0.86	0.84	0.995	2.080
1/2	1.00	1.00	1.00	0.50	0.50	0.149	0.156
	1.00	1.00	0.01	0.50	0.50	0.126	0.131
	1.00	1.00	0.10	0.50	0.50	0.128	0.133
	1.00	1.00	10.00	0.51	0.50	0.314	0.341
	1.00	1.00	100.00	0.89	0.85	1.404	1.721
	1.00	0.01	1.00	0.93	0.83	0.019	0.045
	1.00	0.10	1.00	0.53	0.50	0.071	0.089
	1.00	10.00	1.00	0.50	0.50	0.720	0.728
	1.00	100.00	1.00	0.50	0.50	6.416	6.466
	0.01	1.00	1.00	0.50	0.50	0.086	0.086
	0.10	1.00	1.00	0.50	0.50	0.092	0.093
	10.00	1.00	1.00	0.58	0.51	0.530	0.702
	100.00	1.00	1.00	0.77	0.63	1.534	3.327
5/6	1.00	1.00	1.00	0.17	0.17	0.119	0.119
	1.00	1.00	0.01	0.17	0.17	0.105	0.105
	1.00	1.00	0.10	0.17	0.17	0.106	0.107
	1.00	1.00	10.00	0.17	0.17	0.196	0.198
	1.00	1.00	100.00	0.86	0.85	0.996	1.071
	1.00	0.01	1.00	0.17	0.17	0.077	0.078
	1.00	0.10	1.00	0.17	0.17	0.082	0.083
	1.00	10.00	1.00	0.31	0.30	0.442	0.445
	1.00	100.00	1.00	0.84	0.83	1.372	1.517
	0.01	1.00	1.00	0.91	0.90	0.015	0.017
	0.10	1.00	1.00	0.45	0.42	0.060	0.062
	10.00	1.00	1.00	0.17	0.17	0.714	0.714
	100.00	1.00	1.00	0.17	0.17	6.650	6.654

the case with the narrower excavation width indicates consistently higher values for the exit point elevation.

For a penetration ratio, $(H_2 - H_1)/H_2$, of 1/6, the results of which are shown in Figures 4a and 4b, the relative permeability of layer 3 exerts the most influence on the flow quantity, and little variation in flow quantity is caused by changes in k_1 and k_2 when their relative permeability values are approximately less than 1. In addition, the effect of the excavation width can be evaluated by comparing the 2 sets of curves. In the case of the wide excavation, there is very little variation in flow quantity with a variation in any of the layer relative permeabilities, except for the very high or very low relative permeability values; whereas, in the case of the narrow excavation, the influence of layer 3 manifests itself more readily. Another quantitative appraisal of excavation width can be obtained by comparing the flow quantities for a given set of permeability conditions; the difference between any two such values essentially represents the additional quantity of flow that is passing through the bottom of the excavation. The curves for layer 1 indicate that it exerts the least influence on the flow characteristics of the system.

As the depth of the excavation extends into layer 2, that layer exerts the largest influence on the flow in the system, and these effects are shown in Figures 4c and 4d for the different excavation widths. Figure 4c shows that the underlying layer (layer 1) has a dominant influence in the relative permeability range from 1 to 10, even though

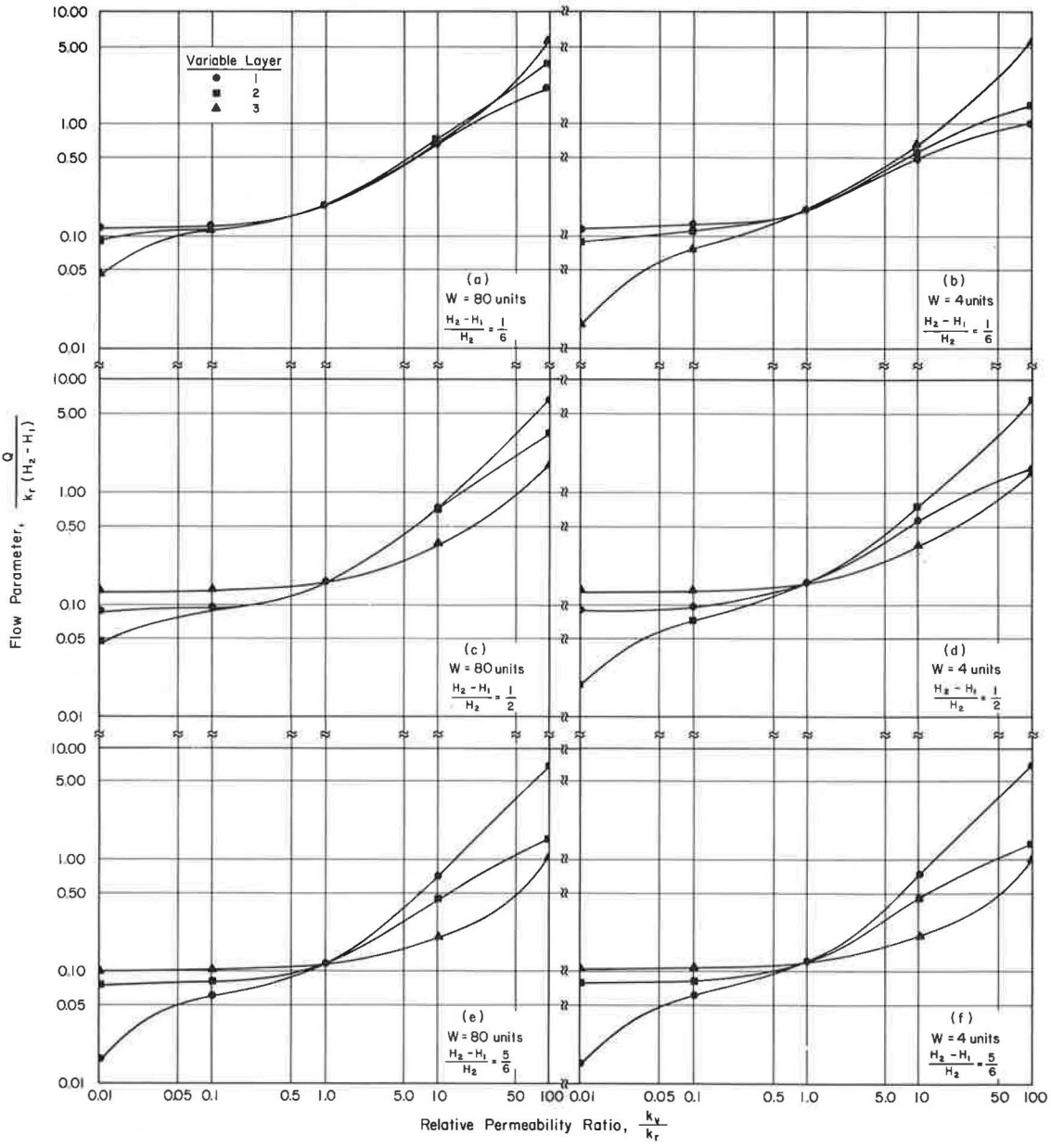

Figure 4. Flow parameter versus relative permeability ratio for various conditions of excavation width and penetration depth.

it has not been penetrated. Also, a reduction in the influence of layers 1 and 3 may be observed for relative permeabilities of more than 1, and an increase in the influence of layer 2 for relative permeabilities of less than 1 is apparent; these changes are attributable to excavation width.

Figures 4e and 4f show the results for the case where the excavation penetrates the bottom layer. For this situation, layer 1 exerts the major effect on the flow quantity. A comparison of these results shows very little change in flow due to excavation width because the underlying layer is impermeable.

Conclusions

Several qualitative conclusions may be drawn from the results of flow studies. For the geometrical configuration studied, it is apparent that the layer containing the bottom of the excavation manifests the dominant influence on the flow quantity. Where the excavation is wide and an underlying layer is relatively permeable, the underlying layer may, for a certain range of relative permeabilities, contribute more to the flow quantity than the layer that contains the bottom of the excavation. The exit point of the phreatic surface may be expected to assume a location that is a function of the degree to which the system is confined. In particular, there are certain commonly encountered field conditions that make it difficult to lower the free surface.

SUBDRAINS IN LAYERED AQUIFERS

In a more specific application of the preceding concept, the cross sections shown in Figure 1b were considered (18), and the effect of varying the thickness of layer 2 on the flow characteristics for several subdrain penetration depths was investigated. Although this case represents a subdrain system that is quite general in nature, the particular combination of soil profile, varying layer thicknesses, and relative permeabilities is felt to typify a portion of the proposed Crosstown Expressway in Chicago. Before the specific results obtained in this phase of the study are considered, several deductions may be made from the preceding results. First of all, for the particular combination of relative permeabilities shown, it should prove difficult to lower the phreatic surface sufficiently unless the silt-sand layer is tapped directly by the drains. Second, changes in the spacing of the subdrains will probably have little effect on the resulting flow quantities (analogous to the width effect for the excavation) because most practical spacings for highway drains will approximate a wide excavation. Third, changes in the thickness of the silt layer will probably not have a significant effect on the quantity of flow until the subdrains tap the silt layer or until it becomes very thick (i.e., the sand layer will maintain an almost constant pressure on the lower interface of the silt layer).

With the foregoing thoughts in mind, we obtained solutions for drain spacing widths W of 50 units and 200 units and for penetration ratios of 1/6, 1/3, 1/2, and 1, where the water level in the drains was assumed to be at the penetration depth. Portions of the resulting data are given in Table 3 and shown in Figure 5. Table 3 gives information that indicates the position of the phreatic surface (offset values from the original water table are shown for various points along the effective length L of the domain). The value for L was 10 times the penetration ratio $(H_2 - H_1)$, each drain was 2 units wide, the thickness D_2 of the silt layer was set at 0, 1/3, 2/3, and 1 times D_3 whereas D_3 was a constant 30 units, and H_2 was held constant at 60 units.

For the purpose of this study, the absolute magnitudes of the flow quantities were considered to be of little concern. The major interest centered around the effect of the thickness of layer 2 on the relative flow quantities and the location of the free surface. Thus, the case where D_2 equals zero was selected as a reference case for each different drain penetration, and the flow quantity Q for various values of D_2 is divided by the flow quantity Q_r to form a dimensionless flow parameter Q/Q_r, which is shown in Figure 5 as a function of the thickness ratio D_2/D_3 and the depth of penetration parameter $(H_2 - H_1)/H_2$. When D_2/D_3 is zero, the bottom layer is all sand, and the corresponding value of Q/Q_r is 1 for all cases. When D_2/D_3 equals 1, the bottom layer is all silt, and appropriate values for Q/Q_r are shown in Figure 5.

TABLE 3

LOCATION OF PHREATIC SURFACE FOR FLOW TO DRAINAGE TRENCHES

Penetration Ratio	Layer Thickness Ratio	50-Unit Width					200-Unit Width				
		Line of Symmetry	1 Unit Left	1 Unit Right	0.05 L Right	0.40 L Right	Line of Symmetry	1 Unit Left	1 Unit Right	0.05 L Right	0.40 L Right
1/6	1	5.25	9.80	9.00	7.10	2.27	3.16	8.60	8.70	7.12	2.30
	2/3	3.83	8.05	8.05	6.24	0.96	0.12	8.05	8.20	6.22	0.95
	1/3	3.71	8.00	8.00	6.18	0.89	0.09	8.00	8.10	6.16	0.88
	0	3.58	8.00	8.00	6.11	0.83	0.07	8.00	8.10	6.11	0.83
1/3	1	12.89	17.70	17.20	13.37	6.67	11.27	17.50	17.40	13.41	6.66
	2/3	7.13	13.10	11.60	7.80	0.29	0.26	11.30	11.60	7.79	0.29
	1/3	6.75	12.80	11.50	7.53	0.22	0.17	11.00	11.20	7.54	0.22
	0	6.38	12.10	11.10	7.28	0.18	0.13	10.80	10.80	7.28	0.18
1/2	1	28.44	29.90	29.60	26.97	16.10	28.28	29.80	29.60	26.98	16.51
	2/3	12.77	18.50	17.00	9.35	0.72	1.49	12.00	14.00	9.37	0.34
	1/3	9.05	13.80	13.70	7.02	0.49	0.94	13.50	12.80	7.04	0.49
	0	28.47	30.00	29.50	27.06	16.83	28.31	30.00	30.00	27.07	16.83
1	1	60.00	60.00	57.30	48.22	26.51	60.00	60.00	57.30	48.22	26.51
	2/3	60.00	60.00	57.40	50.04	30.00	60.00	60.00	57.40	50.04	30.00
	1/3	60.00	60.00	57.60	52.51	34.00	60.00	60.00	57.60	52.51	34.00
	0	60.00	60.00	57.10	48.43	27.31	60.00	60.00	57.10	48.43	27.31

The data given in Table 3 show that the spacing of the drains has little effect on the position of that portion of the free surface located outside the drains. However, the extent of the drawdown between the drains is significantly affected when the underlying layers are a combination of sand and silt but not when only 1 material is present for a penetration ratio of 1/2. The effect of drain spacing on flow quantity is negligible for all cases, and the curves shown in Figure 5 represent both values of W. Although the thickness of the silt layer has relatively little effect on flow quantity when the drains do not tap that layer, a large effect is observed when the drains do tap the silt layer. However, full penetration of the drainage trenches reduces the effect of the silt layer, because the sand aquifer contributes the major portion of the flow quantity for all cases.

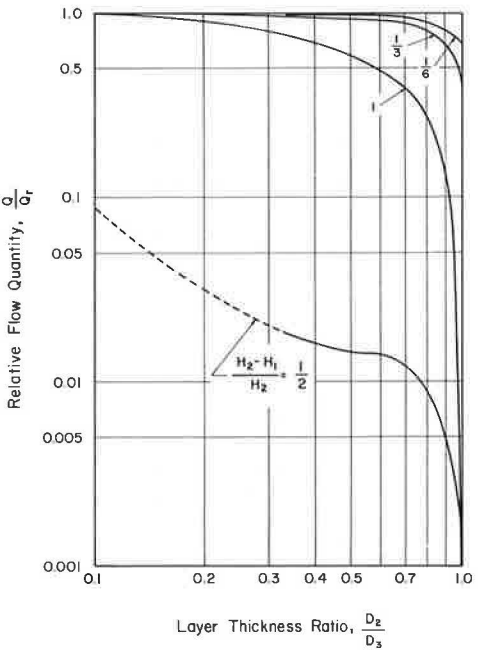

Figure 5. Relative flow quantity versus layer thickness ratio for various drain penetrations.

Results of Subdrain Studies

Although the spacing of drains in an open cut has been shown to have little effect on flow quantities and on the position of that portion of the free surface located outside of the drains, it does exert a substantial influence on the drawdown between the drains. However, under certain conditions the thickness of an intermediate silt layer, typical of a situation encountered along a portion of a proposed highway cut in the Chicago area, was found to affect significantly the seepage characteristics of the system. The results obtained from this latter, more specific study are qualitatively consistent with those that were deduced from the preceding, more general study of flow into an excavation.

APPLICATION OF QUALITATIVE RESULTS TO AN EXAMPLE PROBLEM

The area to be traversed by the proposed Crosstown Expressway in Chicago consists of various surficial soils, lacustrine sands and silts, glacial till sheets, pockets of dense granular soils, and bedrock. Conditions are quite variable, and the water table is approximately 5 to 10 ft beneath the existing ground surface in most places. Accordingly, depressed sections of the roadway will generally be located in soil profiles very similar to those considered in the previous sections of this study. As a particular example, consider the typical soil profile (obtained for the preliminary subdrain study) shown in Figure 6a with its representative permeability values. Because a depressed roadway is to be constructed in this profile, it is necessary to specify the type and placement of permanent drains to maintain satisfactory dewatering and free-surface location.

Based on the preceding study, the system appears to display "confined flow" characteristics, and hence the free surface will be difficult to lower. Narrow drainage trenches will probably be used, and therefore no increase in flow quantity should be expected for each drain because of width effect. However, the use of multiple trenches will create a pseudo-wide-trench response, and disproportional amounts of water will be drawn from the underlying strata by creating a large region in which vertical flow

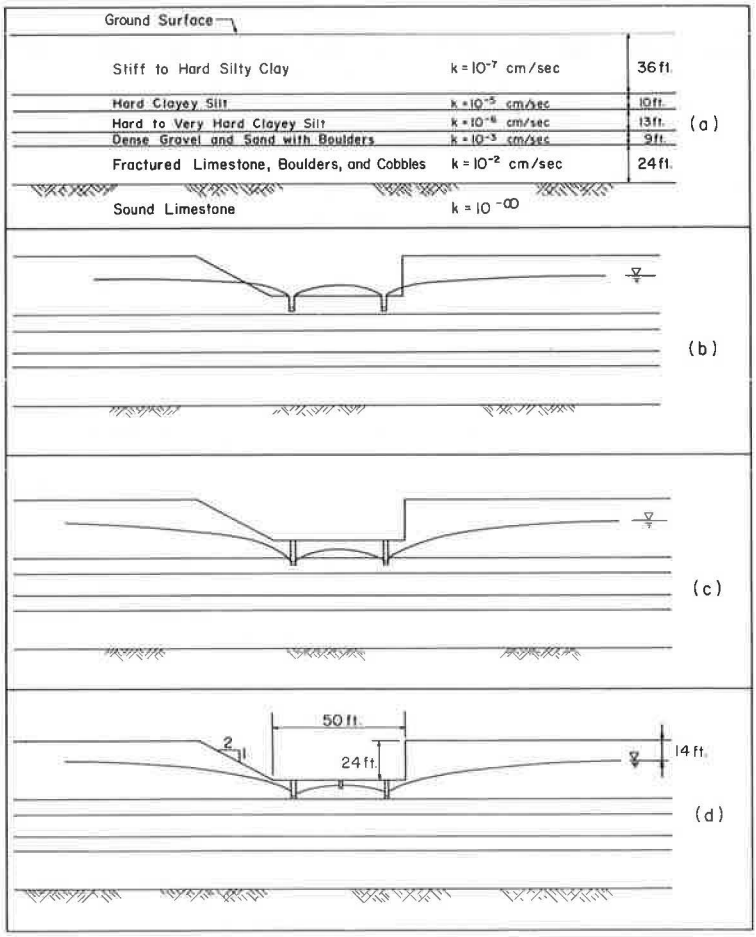

Figure 6. Typical soil profile and drainage systems for a roadway cut in the Chicago Crosstown Expressway.

predominates. Furthermore, it would appear that at least 2 drains are necessary, one on either side of the roadway, and that they must penetrate the layer that has a 10^{-5} cm/sec permeability to lower the free surface. Also, these drains should be spaced as close together as possible to maximize the drawdown between the drains.

The preceding qualitative deductions were checked by studying 4 different drain configurations by means of the finite-element method. Idealizations involving from 236 nodes and 223 elements to 265 nodes and 252 elements were used, and between 3 and 7 iterations were needed to obtain the free-surface location. Although Figure 6b shows what might be a first intuitive selection of drain penetration, the results of the earlier studies presented here have demonstrated that a configuration of this type cannot provide satisfactory drainage. This conclusion was verified by the finite-element solution, which is shown in Figure 6b. As can readily be seen, the phreatic surface is totally unsatisfactory; and problems with slope stability, subbase and retaining wall drainage, and excess pressures on the pavement will be encountered if no supplementary drains are supplied.

Extension of the drains into the more pervious silt layer, the next logical choice in light of the general study, yields the satisfactory solution shown in Figure 6c, as long as a minimum spacing of drains is maintained. According to the preceding study, just tapping the silt layer will give essentially the same position for that portion of the free surface outside the drains and the same flow quantity into the drains. However, the position of the free surface between the drains will need to be controlled by use of a third or centerline drain, as shown in Figure 6d. This latter solution, which was verified by a finite-element computation, has the advantage of requiring smaller quantities of excavation and filter materials.

In each of these cases, no special provision for drainage of the retaining wall was considered. The calculated seepage quantity for the final drainage system shown was less than 2 cu ft per day per foot of length for each drain, with the bottom layer contributing approximately 96 percent of this quantity. Thus, the qualitative predictions, based on the results of previous studies, for the seepage characteristics of a typical depressed roadway in a layered system provided a reasonably accurate description of the results that were obtained from a finite-element analysis.

SUMMARY

The qualitative concepts developed for the general case of an excavation in a layered aquifer are shown to apply to more specific field problems that involve the installation of subdrains. These data aid in understanding the complex interaction that occurs in plane flow through systems of layered aquifers, and they allow a more direct and logical approach to the design of highway drainage systems.

ACKNOWLEDGMENTS

The computer time used for this investigation was supplied by the Vogelback Computing Center at Northwestern University. The authors are grateful to Crosstown Associates, Chicago, Illinois, for permission to use data obtained from the Preliminary Boring Program and Preliminary Underdrainage Study for the proposed Crosstown Expressway.

REFERENCES

1. Boreli, M. Free-Surface Flow Toward Partially Penetrating Wells. Trans. American Geophysical Union, Vol. 36, No. 4, 1955, pp. 664-672.
2. Casagrande, A. Seepage Through Dams. Harvard Graduate School, Eng. Publ. No. 209, 1937; Boston Society of Civil Engineers, Contributions to Soil Mechanics 1925-1940.
3. Chapman, T. G. Two-Dimensional Ground-Water Flow Through a Bank With Vertical Faces. Geotechnique, Vol. 7, No. 1, 1957, pp. 35-40.
4. Clough, R. W. The Finite Element Method in Structural Mechanics. In Stress Analysis (Zienkiewicz, O. C., and Holister, G. S., eds.), John Wiley and Sons, New York, 1965, Chap. 7.

5. deVeubeke, B. F., ed. Matrix Methods of Structural Analysis. Pergamon Press, New York, 1964.
6. Finn, W. D. L. Finite-Element Analysis of Seepage Through Dams. Journ. Soil Mech. and Found. Div., Proc. ASCE, Vol. 93, No. SM6, 1967, pp. 41-48.
7. Finnemore, E. J. and Perry, B. Seepage Through an Earth Dam Computed by the Relaxation Technique. Water Resources Research, Vol. 4, No. 5, 1968, pp. 1059-1066.
8. Gallagher, R. H., Rattinger, I., and Archer, J. S. A Correlation Study of Methods of Matrix Structural Analysis. Pergamon Press, New York, 1964.
9. Harr, M. E. Groundwater and Seepage. McGraw-Hill, Inc., New York, 1962.
10. Jaeger, C. E. Engineering Fluid Mechanics. Blackie, Ltd., London, 1956.
11. Javandel, I., and Witherspoon, P. A. Analysis of Transient Fluid Flow in Multi-Layered Systems. Water Resources Center, Dept of Civil Eng., Univ. of California, Berkeley, Contribution No. 124, 1968.
12. Luthin, J. N., ed. Drainage of Agricultural Lands. American Society of Agronomy, Madison, Wisconsin, 1957.
13. Muskat, M. The Flow of Homogeneous Fluids Through Porous Media. McGraw-Hill, New York, 1937; reprinted by Edwards Brothers, Ann Arbor, Mich., 1948.
14. Polubarinova-Kochina, P. Y. Theory of Ground Water Movement. DeWiest, J. M., tr., Princeton Univ. Press, N. J., 1962.
15. Przemieniecki, J. S. Theory of Matrix Structural Analysis. McGraw-Hill, New York, 1968.
16. Shaw, F. S. An Introduction to Relaxation Methods. Dover Publications, New York, 1953.
17. Taylor, R. L., and Brown, C. B. Darcy Flow Solutions with a Free Surface. Jour. Hydraulics Div., Proc. ASCE, Vol. 93, No. HY2, 1967, pp. 25-33.
18. Volovisky, E. S. Finite Element Solution for Underdrain Seepage Characteristics of a Layered Porous Medium. Northwestern Univ., Evanston, Ill., unpublished master's thesis, 1969.
19. Wilson, E. L., and Nickell, R. E. Application of the Finite Element Method to Heat Conduction Analysis. In Nuclear Engineering and Design, North-Holland Publishing Company, Amsterdam, No. 4, 1966, pp. 276-297.
20. Zienkiewicz, O. C., and Cheung, Y. K. Finite Elements in the Solution of Field Problems. The Engineer, The Institution of Civil Engineers, London, Vol. 220, No. 5722, 1965, pp. 507-510.
21. Zienkiewicz, O. C., and Cheung, Y. K. The Finite Element Method in Structural and Continuum Mechanics. McGraw-Hill, New York, 1967.
22. Zienkiewicz, O. C., Mayer, P., and Cheung, Y. K. Solution of Anisotropic Seepage by Finite Elements. Jour. Eng. Mech. Div., Proc. ASCE, Vol. 92, No. EM1, 1966, pp. 111-120.